2006-12-15

Mechanisms of Endocytic Sorting: A Dissertation

Deborah Marie Leonard
University of Massachusetts Medical School

MECHANISMS OF ENDOCYTIC SORTING

A Dissertation Presented

By

Deborah Marie Leonard

Submitted to the Faculty of the

University of Massachusetts Graduate School of Biomedical Sciences, Worcester

In partial fulfillment of the requirements for the degree of

DOCTOR OF PHILOSOPHY

December 15, 2006

Biomedical Sciences

Copyright Notice

Approval Page

MECHANISMS OF ENDOCYTIC SORTING

A Dissertation Presented

By

Deborah Marie Leonard

Approved as to style and content by:

David Lambright, Ph.D.	Chair of Committee
Mitsuo Ikebe, Ph.D.	Member of Committee
Mary Munson, Ph.D.	Member of Committee
Janet Stein, Ph.D.	Member of Committee
Marianne Wessling-Resnick, Ph.D.	Member of Committee
Silvia Corvera, M.D.	Thesis Advisor
Anthony Carruthers, Ph.D.	Dean of the Graduate School of Biomedical Sciences

Interdisciplinary Graduate Program
December 15, 2006

DEDICATION

This dissertation is dedicated to my husband Jack and my family for their encouragement and support while I pursued my dream. I cannot begin to thank you for the sacrifices that you made or for the love and encourage that you gave me to help me complete this work. It is said that a good scientist loves his/her's work, but it takes a loving family to allow the scientist time for his/her work.

ACKNOWLEDGEMENTS

I would like to thank the department of Molecular Medicine and Physiology for their generous support of my work.

I would like to thank my committee members.

I would like to especially thank Dr. Silvia Corvera. She has generously shared her time and experiences so that I could develop as a scientist. She has instilled in me a passion for imaging and cell biology that will forever be a part of me and I look forward to working with her in the future.

I would like to acknowledge members of the Corvera laboratory both past and present. Dr. Akira Hayakawa, Dr. Anil Chawla, Dr. Olga Gealikman, Alison Burkart, My Chouinard, Xiarong Shi, and James Young for their helpful assistance during my five years as a member of the laboratory. I would also like to thank Dr. Deirdra Lawe and Dr. Varsha Patki for their helpful discussions and support and although they are no longer in the laboratory our work will forever be tied together. I would also like to thank Dr. Susan Hayes, who performed the FYVE domain siRNA screen in *C. elegans.*

I would like to acknowledge members of the Imaging Core, Kevin Fogarty, Dr. Clive Standley, Dr. Karl Bellve, Dr. Lawrence Lifshitz and Dr. Richard Tuff for their assistance with the live imaging and 3-D restorations used in this work.

I would like to thank Craig Mellow and members of his laboratory for their assistance with the *C. elegans* screen.

I also thank David Lambright and his laboratory for their expertise that help support my work with the Rab GTPases.

To my friends both inside and outside the UMass community, your support and encouragement has seen my through this process, thank you.

Serving as a source of determination, I would like to thank my parents, Shirley and Robert Nichols who have supported and encourage me unconditionally for as long as I can remember.

Finally, my source of inspiration, I would like to thank my family. My husband Jack has been there assisting and encouraging me during each step of my graduate training. I also thank my children Ryan and Caitlyn, and step-children James and Justin, who have sacrificed my time and extended encouragement so that I could complete this work. I look forward to what the future holds for all of us.

ABSTRACT

Endocytosis is important for the regulation of signal transduction and for the movement of essential cellular components from outside the cell to their appropriate intracellular compartment(s). Two established mechanisms of endocytosis are clathrin-mediated (CME) and clathrin-independent endocytosis, and they are responsible for internalization of different ligands. In this study, the newly established technique of total internal reflection fluorescent microscopy (TIRF-M) was used, along with standard biochemical and molecular biological tools, to systematically study the sorting and early trafficking of two established ligands of endocytosis, transferrin (Tf) and epidermal growth factor (EGF).

TIRF-M studies revealed that Tf binds its receptor that is located in large clathrin arrays positioned just below the surface of the cell and that these large clathrin platforms serves as the major site of CME at the plasma membrane. EGF endocytosis is very different and occurs as follows 1) the liganded EGFR recruits Rab5 to the plasma membrane, 2) Rab5 concentrates around vesicles containing liganded EGFR and 3) these vesicles co-localize with EEA1 enriched endosomes. EEA1 was shown to play a pivotal role in EGF endocytosis, establishing a new role for EEA1 in vesicle trafficking in addition to its role in tethering and fusion. Finally, WDFY2, a new FYVE domain protein was shown to decorate a specific subset of vesicles, upstream of the EEA1 vesicle pool that appear to participate in Tf endocytosis. These studies establish new functions and components of endocytosis that enhances our understanding of this complex process.

TABLE OF CONTENTS

LIST OF FIGURES

LIST OF TABLES

LIST OF ABBREVIATIONS

AP-1-4 adaptor proteins 1-4
AP180 assembly protein 180
CALM clathrin assembly lymphoid myeloid leukemia protein
Cbl casitas B-lineage lymphoma
CCP clathrin-coated pit
CCV clathrin-coated vesicle
CIN85 Cbl interacting protein of 85 kDa
CME clathrin mediated endocytosis
EEA1 early endosome antigen 1
EF evanescent field
EGF epidermal growth factor
EGFR epidermal growth factor receptor
Eps15 EGFR-pathway substrate-15
ERC endocytic recycling compartment
ESCRT endosomal sorting complex required for transport –I, -II, -III
FYVE Fab1, YOTB, Vac1, EEA1
GAP GTPase-activating protein
GED GTPase effector domain
GERL Golgi, endoplasmic reticulum, and lysosomes
GFP green fluorescent protein
GLUT4 – glucose transporter 4
GPCR G-protein coupled receptor
Grb2 growth factor receptor-bound protein
HB-EGF heparin-binding EGF-like growth factor
HIV human immunodeficiency virus
Hrs hepatocyte growth factor regulated tyrosine kinase substrate
Lamp lysosomal-associated membrane protein
LDL low-density lipoprotein
LDLR low-density lipoprotein receptor
M6PR mannose-6-phosphate receptor
MAPK mitogen-activated protein kinase
MVB multivesicular body
PI phosphoinositide
PI(3)P phosphatidylinositide-3-phosphate
RFP red fluorescent protein
RME receptor mediated endocytosis
RNA ribonucleic acid
RTK receptor tyrosine kinase
siRNA small interfering RNA
SOS Son-of-sevenless
STAM signal transducing adaptor molecule
Tf transferrin

TfR transferrin receptor
TGF-α transforming growth factor-α
TIRF-M total internal reflection fluorescent microscopy
Tsg101 Tumor-susceptibility gene-101
TTP transferrin receptor trafficking protein
UBPY Ub isopepitdase Y
UIM ubiquitin-interacting motif
USP8 ubiquitin-specific processing protease

CHAPTER I

Endocytosis is important to all eukaryotic cells for the regulation of signal transduction and for the movement of essential cellular components from outside the cell to the appropriate intracellular compartment(s). There are several mechanisms of endocytosis, including phagocytosis, macropinocytosis, clathrin-mediated endocytosis (CME), caveolae-mediated endocytosis, clathrin-and caveolae-independent endocytosis and these mechanisms have been extensively studied [1].

Transferrin (Tf) and epidermal growth factor (EGF) are commonly used markers for receptor-mediated endocytosis (RME)—more commonly known as CME—that differ only in sorting; Tf and its receptor recycles to the cell surface, while EGF and the epidermal growth factor receptor (EGFR) are processed through the degradative pathway to its final destination in the lysosome. However, recent knockdown studies of established components of these mechanisms and preliminary work presented here, suggest discrepancies in these presumed models.

MOLECULAR DETAILS OF CLATHRIN-MEDIATED ENDOCYTOSIS

The best understood mechanism of internalization; CME is responsible for the continuous uptake of essential nutrients, such as low density lipoprotein (LDL) and iron-loaded Tf. CME is the process of internalization of receptors and their bound ligands by clathrin-coated pits (CCPs) which are formed by the assembly of a scaffold of cytosolic coat proteins, with clathrin as the primary structural unit [2]. CCPs invaginate and pinch off to form endocytic vesicles that carry the receptor-ligand complex into the cell.

Endocytosis through CCPs requires an internalization signal in the cytoplasmic domain. Two types of internalization signals have been identified, the tyrosine based motif and the dileucine motif. The tyrosine based motif has a tyrosine as the critical residue (YXXϕ or NPXY, where X is any amino acid and ϕ is a hydrophobic residue), while the dileucine motif uses either two consecutive leucines or an isoleucine and leucine for signaling [3]. Receptor competition and over-expression studies using the Tf receptor (TfR), the LDL receptor (LDLR) and the epidermal growth factor receptor (EGFR) imply that there is little, if any, competition between these receptors for access to the CME machinery, although the entry of each receptor into CCPs is limited by receptor density [4, 5].

Different receptors use different mechanisms for uptake into clathrin-coated vesicles (CCVs). For example, the endocytic sorting motif of the TfR is Yxψϕ, where x is any amino acid, ψ a bulky hydrophilic residue and ϕ a hydrophobic residue. This sequence is recognized by the μ2 subunit of the adaptor protein 2 (AP-2) complex. The LDLR uses a different sorting motif, FxNPxY that is recognized by Dab-2 which also binds AP-2 and can mediate clathrin assembly. The leucine-based motif, (DE)xxx(LL)I, where position four and occasionally position five from the first leucine are usually acidic and the second leucine can be replaced by isoleucine, serves as an internalization signal in many single- and multi-spanning transmembrane proteins [1, 6].

The basic unit of the clathrin-coat is a triskelion formed by the tight association of three clathrin (180 kDa) heavy chains with three clathrin (30-35 kDa) light chains. This three legged polymer assembles into a lattice of hexagons and pentagons. In addition to clathrin, the clathrin-cage contains additional assembly proteins, such as adaptor protein

180 (AP180) and AP-1 through AP-4 [4, 7]. Importantly, AP-2 links the clathrin lattice to the plasma membrane for CCV formation [8]. AP-2 is composed of two large, structurally related subunits, α– and β2-adaptins, a medium sized subunit, μ2 and a small subunit σ2. The α-adaptin subunit of AP-2 interacts with the plasma membrane and directs clathrin assembly to that site. The β-subunits of AP-2 also interact with clathrin; the μ2-subunit of AP-2 binds tyrosine-based internalization motifs on the cytoplasmic domain of liganded receptors and leads to receptor accumulation in the CCPs. Phosphoinositides with a phosphate at the D-3 position of the inositol ring (PI) increase the affinity of the AP-2 complex for activated receptors, suggesting that the action of AP-2 may be modulated by phosphatidylinositol 3-phosphate (PI(3)P) [9]. In neurons, the recovery of "spent" synaptic vesicles uses a neuron-specific form of a monomeric adaptor protein, AP180, to stimulate clathrin assembly [10].

Rappoport and co-workers proposed that there are two functionally distinct populations of clathrin at the plasma membrane, a dynamic population and a static population; only the latter population is associated with AP-2. They also proposed that although co-localization of clathrin and AP-2 marks the site of CCP formation, AP-2 does not seem to remain with the CCV when it starts to move [11].

CME is spatially organized at endocytic hot-spots, presumably constrained by the cortical actin cytoskeleton and by regional distribution of signaling networks. Scaffolding molecules connect the endocytic machinery to the actin cytoskeleton by a variety of protein-protein and/or protein-lipid interactions. For example, amphiphysin

serves as a membrane bound platform that binds AP-2, clathrin and dynamin and is thought to target dynamin to the CCPs [1].

AP-2 is also recruited to the plasma membrane by epidermal growth factor pathway substrate 15 (Eps15), epsin and clathrin assembly lymphoid myeloid leukemia protein (CALM) to initiate CCP formation. The dynamin-interacting proteins, such as intersectin, amphiphysin and endophilin then target dynamin to the CCPs and work as co-factors to form CCVs. Amphiphysin and endophilin are thought to have a function in CCP invagination; endophilin directs the fission reaction through its lipid modifying activity [11, 12].

Dynamin is a GTPase that mediates fission by constriction of the thin neck of the CCP. This is done by creating a GTP-dependent conformational change that generates the force used to separate the CCV from the plasma membrane. Dynamin encodes its own GTPase-activating protein (GAP) and self-assembles into helical rings and stacks that can induce a 100-fold GTPase effector domain (GED)-mediated stimulation of GTPase activity [1]. During this last step of CCV formation, dynamin appears to self-assemble into a collar at the neck of the invaginated CCP. This large, modular GTPase also has domains that support $PI(4,5)P_2$ binding, self-assembly and interaction with other endocytic components. The last step of vesicle fission is for the newly formed CCV to move away from the plasma membrane in an actin dependent manner [13].

Currently there are two models to explain dynamin's ability to cleave the lipid bilayer. One model suggests that dynamin functions as a mechano-chemical enzyme to physically drive membrane vesicle formation [1]. The other model suggests that

dynamin functions as a regulatory molecule to recruit and/or to activate downstream effectors in CCV formation. Thus, CCP-associated proteins, such as intersectin, syndapin and N-Wasp work with dynamin to regulate actin polymerization and to push the CCP away from the membrane until the "stretched neck" snaps and the newly formed CCV is carried into the cytosol [13].

Newly released CCVs quickly shed their clathrin coats and the newly formed endosomes fuse with one another and/or pre-existing sorting endosomes. These vesicles then translocate along microtubules, stop fusing with newly endocytosed vesicles and become more acidic. In as little as 5-10 minutes, the incoming vesicles localize with the sorting endosomes, which are tubular-vesicular structures with an internal pH of ~6.0. ATP-driven proton pumps on the endosome help to maintain the acidic environment of these organelles. In the sorting endosome, as the name implies, cargo is sorted into one of three possible destinations, the plasma membrane, late endosome or the endocytic recycling compartment [14, 15].

The size of the cargo appears to determine the size of the CCV, and also the time it takes to achieve its final form. The CCV then undergoes a directed motion away from the budding point, presumably along a cytoskeletal track. Ehrlich and co-workers proposed that assembly of the clathrin-based endocytotic machinery is a random process that occurs where the cytoskeleton and the plasma membrane meet [16]. This is in contrast to the model set forth by Gaidarov and colleagues, who proposed that the plasma membrane is composed of preferential sites of CCP formation, suggesting that CCP assembly and function is spatially regulated [17]. This later hypothesis is supported by

the work of Rappoport and Simon, who used total internal reflection fluorescent microscopy (TIRF-M) to track Tf through CCPs and found that Tf did not distribute into all the CCPs suggesting that the cargo within each CCP might not be identical [18].

As seen in Figure 1, almost immediately upon cargo entry into the cell, a complicated sorting process begins that escorts this new cellular component to its final intracellular destination. The vesicles then choose one of several routes into the cell, although the molecular events that mediate this selection process are not fully understood. Clearly, the early endosome, marked by early endosomes antigen 1 (EEA1)

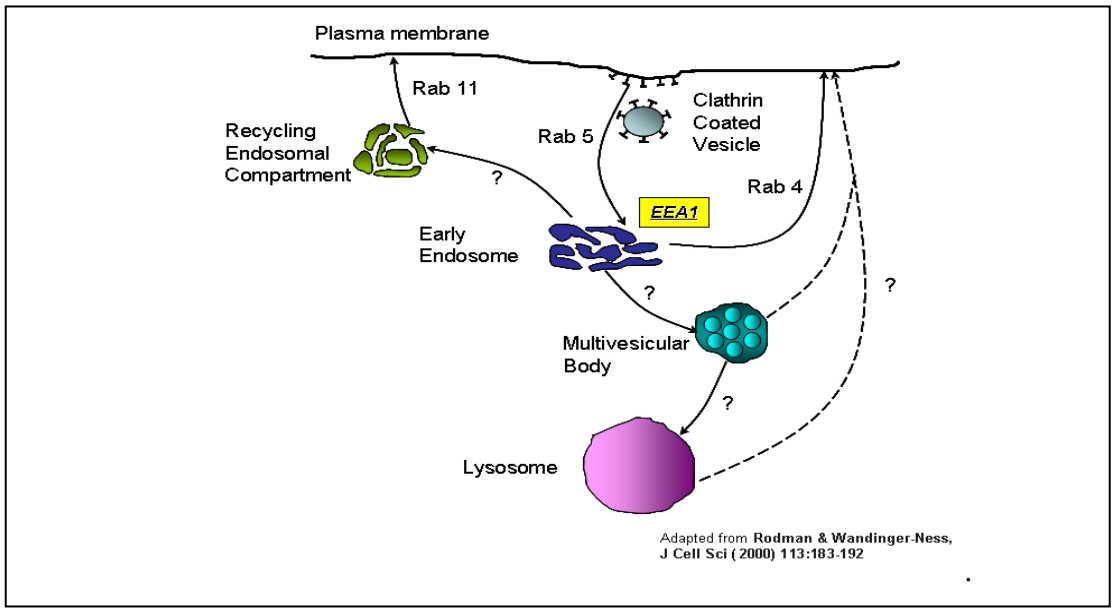

Figure 1. Current model of Clathrin Mediated Endocytosis. Signaling molecules to be identified are indicated by question marks.

is one of the earliest destinations and pathways appear to branch from this “organizing center" to other intracellular locations, such as the lysosome for degradation, or the recycling endosomal compartment for return to the plasma membrane; while other cargoes are returned to the plasma membrane without being process through the recycling

endosomal compartment. This recycling pathway is composed of morphologically heterogeneous vesicles with varying rates of flux and is uncomplicated by internal signal-dependent sorting mechanisms. For cargo to exit from the recycling pathway and move towards the lysosome, or to a new domain on the cell surface (as seen in transcytosis) requires a more selective routing process involving specific sorting signals [19].

The Early Endosome

Early endosomes harbor specific cellular markers, such as the GTPases Rab4 and Rab5 and are also thought to exist in two distinct populations. There is a dynamic population of early endosomes that are highly mobile and rapidly proceed to the late endosomes and a second population of early endosomes that matures more slowly [4]. Using Tf as a marker of endocytosis and GFP-tagged Rab proteins, Sonnichesen and co-workers showed by fluorescent microscopy and electron microscopy that within the vesicle, cargo moved through distinct microdomains in the endosome lumen and that these domains are delineated by clusters of like, membrane bound Rab proteins. Three major populations of microdomains on the endosomal membrane were observed: one that only contained Rab5, another population that contained Rab4 and Rab5 and the last population that contained Rab4 and Rab11. It is generally believed that this mosaic arrangement of Rab family members is organized through the recruitment of specific effector proteins that act cooperatively to generate these membrane micro-environments [20].

Rab4, Rab5 and Rab11 are well accepted regulators of the endocytic/recycling pathway, where they function as regulators of targeting/docking/fusion processes [20]. Cargo enters the cell mainly through the Rab5-containing endosome. Rab5 regulates homotypic endosome fusion and incoming vesicle traffic. Fast recycling is achieved by the rapid sorting from Rab5 structures into the Rab4/Rab5 positive microdomains in the same endosome [21]. Once Tf enters the Rab4/Rab11 microdomain, recycling slows down [22]. In polarized MDCK cells, Rab11 appears to play a role in endosome recycling at the apical membrane; in contrast, in non-polarized cells Rab 11 participates in perinuclear recycling. Rab11 has also been proposed to be involved with endosomal traffic from the trans-Golgi network to the plasma membrane. Rab4, the second marker of this microdomain, has also been reported to be associated with the Golgi, so it is possible that not all of the Rab4 and Rab11 compartmental interactions are involved in slow recycling, but may have a role in the transport of protein from the Golgi compartment [23].

Cargo/Receptor Sorting

In the period of time before the maturing sorting endosome translocates to the center of the cell, most recycled molecules are rapidly and efficiently removed. Molecules to be recycled are sorted from soluble molecules in the sorting endosomes, the tubular portion of the endosome pinches off from the vesicular portion to preferentially separate recycled membrane from the soluble molecules. As a result, in the absence of specific targeting information, a membrane protein that has been internalized into the

endosome will be transported back to the plasma membrane, while proteins with specific targeting information will be transported to the late endosome. Based on analysis of TfRs and fluorescent lipid analogues, it has been shown that exit from the sorting endosomes occurs within 4 minutes or less, and that more than 95 - 99% of the cargo, Tf, and its receptor, TfR, are removed from the sorting endosomes before they mature [14].

Endosomes carrying cargo destined for degradation begin to accumulate Rab7—a late endosome marker, along with Rab9 and the lysosomal-associated membrane protein, (Lamp) [22]. Eventually these endosomes lose Rab5 as they mature into late endosomes. Analysis of the life cycle of Semliki Forest virus showed that it is internalized by CME and transported by early endosomes to late endosomes and lysosomes. The virus progresses from Rab5 positive, early endosomes to a small population of early endosomes (approximately 10% of the total) that contain Rab5 and Rab7. The Rab7 domain sequesters the virus destined for release and the virus laden endosome is transported along microtubules to the late endosomes [24].

At this point of endosome maturation, another sorting step occurs. Vesicles with Rab4/Rab5 lose Rab5 and become part of the cell's perinuclear recycling compartment, where slower recycling takes place. This compartment is composed of a network of tubules that contain recycling molecules, these structures are usually less acidic than the early endosome and are usually concentrated in the perinuclear area. Vesicles that have matured into late endosomes will next develop into multi-vesicular bodies (MVBs) and it is at this step that Tf and EGF internalization is thought to differ [19, 25].

Receptor Recycling

There are two main routes back to the plasma membrane from the sorting endosomes. Some recycling molecules are delivered directly to the plasma membrane (rapid recycling), while other recycling receptors are delivered to the endocytic recycling compartment (ERC) (slow recycling). Rapid recycling occurs in 4 minutes or less, while slow recycling has been reported to take from 12 to 20 minutes to be completed. The ERC is a collection of microtubule associated, tubular organelles with an estimated diameter of 60 nm. ERC distribution varies with different cell types and in most cells the ERC tubules are widely distributed throughout the cytoplasm; intracellular location of the ERC does not appear to effect recycling [14].

During this recycling process many of the internalized ligands are subsequently degraded in the lysosome, while many of the receptors are recycled to the cell surface for reuse. In addition, endosome trafficking can be altered in response to signaling mechanisms that can increase or decrease the number of receptors at the cell surface. For example, a cell's response to insulin is to increase the amount of glucose transporter 4 (GLUT4) on the cell surface, while cells will decrease the number of EGFR on the cell surface in response to EGF signaling.

Transferrin Receptor Recycling

The TfR is a disulfide-linked homodimer made up of two 760 amino-acid subunits that span the lipid bilayer and binds the serum iron transport protein, Tf [26-28]. The transmembrane domain of the TfR, residues 62 – 89, serves as an internal signal peptide

[29]. Each subunit is palmitoylated at the junction of the transmembrane domain and the bilipid layer, and this fatty acid modification appears to play a role in membrane localization [27]. TfRs do not actively recruit adaptor proteins to the plasma membrane; instead TfRs diffuse to and/or aggregate at pre-existing CCPs [5]. Importantly, TfR, and other constitutively endocytosed protein receptors, like LDLR, are internalized due to their constitutive binding to the AP-2 complex and are recruited to the CCP [30].

The transferrin receptor trafficking protein (TTP) is a SH3 containing protein that specifically regulates the internalization of the TfR. TTP localizes in CCPs and CCVs and its SH3 domain binds dynamin. Over-expression of TTP inhibits TfR internalization and causes morphologically abnormal CCPs; however, this defect can be overcome by the over-expression of dynamin. Tosoni has suggested two possible ways that TTP functions in TfR endocytosis [31]. According to her "adaptor" hypothesis, TTP acts as a scaffold coordinator that connects the hardware of the CCP to the fission machinery. Her "vesicle loading" hypothesis, takes advantage of the observation that TfR has a 10-fold lower affinity than dynamin for the SH3 domain of TTP. In this scenario, TfR accumulates in the CCP until it reaches a critical threshold concentration, at which time it breaks the TTP-dynamin interaction by mass action and the liberated dynamin initiates the fission of the CCV. Importantly, these two models are not mutually exclusive.

Tf is an 80 kDa glycoprotein with two homologous iron-binding domains at the N- and C-termini [32]. In humans, the serum concentration of Tf is 15-25 μM, more than three orders of magnitude greater than its K_D of 5.1 nM for the TfR; as a result the TfR is saturated by Tf under normal physiological conditions. Trischler and co-workers showed

that endocytosed Tf moves sequentially through Rab5 coated compartments to the Rab11 coated compartments and Rab4 is found in both of these compartments. They also showed that Tf containing vesicles decorated with Rab5 had little, if any, Rab11; while Tf loaded, Rab11 decorated vesicles lacked Rab5 [33].

At pH 7.0, iron-loaded Tf (diferric Tf) has the same affinity for the TfR as the iron-depleted, apo-Tf at the intralumenal pH of 5.4. Importantly, at pH 7.0 apo-Tf quickly dissociates from the TfR. With this in mind, Tf cycling is fairly simple; diferric-Tf loads the TfR at the plasma membrane and is endocytosed. The pH of the endocytic vesicle drops to 5.5 or lower, which causes the dissociation of the iron from the Tf:TfR complex. The iron remains within the cell and the apo-Tf:TfR complex is recycled back to the plasma membrane, where the apo-Tf dissociates from the cell surface because of the neutral pH of the interstitial space. Tf is then reloaded with iron in the serum and the "unloaded" TfR is ready for another round of Tf transport. Once the iron dissociates from Tf, it binds to a low molecular weight carrier protein in the cytoplasm on its way to the mitochondria for heme-biosysnthesis or storage as ferritin [30, 34].

The lifecycle of TfR is dynamic. Within 2 to 6 minutes of binding the Tf:TfR complex moves to an acidic non-lysosomal compartment, the iron is released and by 14 minutes the recycled TfR is returned to the cell surface. TfR recycling differs from other receptor-mediated models; unlike insulin receptors and LDLRs, where ligands are transported in vesicles destined for the lysosome and the "empty" receptors are recycled back to the plasma membrane, Tf does not dissociate from its receptor until the apo-Tf:TfR complex is returned to the cell surface [34, 35].

Receptor Degradation

Termination of signaling receptors is usually accomplished by 1) pH dependent dissociation of the activated ligand and 2) targeting the receptors to the late endosomes/lysosomes for degradation. The first step in targeting a signaling receptor for down-regulation is often the ubiquination (see below) of its cytoplasmic domain, which then functions as a signal for delivery of the tagged protein to the invaginated membrane in the late endosomes/lysosomes [4, 14].

The MVB, rich in the lysophosphatide, lyso-bisphosphatidic acid, is an intermediate compartment formed when the limiting membrane of the endosome invaginates and buds into its lumen. The FYVE domain protein (FYVE domain proteins are usually involved in membrane trafficking), hepatocyte growth factor regulated tyrosine kinase substrate (Hrs), along with the endosomal sorting complex required for transport (ESCRT) complexes, are required for formation of the MVB and for the budding of certain enveloped RNA viruses, such as human immunodeficiency virus, HIV. Hrs and ESCRT-I, -II, and –III, are also necessary for the endosomal sorting of membrane bound proteins into MVBs [36, 37]. MVBs are structurally distinct organelles that do not contain early endosome specific proteins or recycling receptors, These organelles move on microtubules to deliver their contents to the lysosome where MVB proteins are either recycled or delivered for degradation [38]. Non-ubiquitinated cell surface receptors are recycled, while ubiquitinated receptors are passed on to the lysosome/vacuole for degradation (down-regulation).

Lysosomes are dense, Lamp-1 positive and mannose-6-phosphate receptor (M6PR) negative structures that contain the acid-dependent hydrolases responsible for the degradation of internalized and endogenous macromolecules. Lysosomes function in both a cell's endocytic and bio-degradation pathways. According to Kornfeld and Mellman lysosomes can be morphologically heterogeneous and because of its variations in content(s), "this has resulted in a rich and complex terminology for lysosomes, including the terms, residual bodies, MVBs, autophagosomes, GERL (Golgi, endoplasmic reticulum and lysosomes), primary and secondary lysosomes" [39].

EGFR Downregulation

The receptor tyrosine kinase (RTK) family of cell surface receptors controls cell proliferation, differentiation, cell survival, cell migration and adhesion [40]. EGF and its cognate receptor, EGFR, is a frequently used model of this class of ligand regulated receptors. EGF binding to the extracellular ligand binding domain of EGFR induces receptor dimerization by direct receptor:receptor interactions, in which a protruding β-hairpin arm of each domain II holds the body of the other [41]. Dimerization triggers the *trans*-autophosphorylation of tyrosine residues on the cytosolic tail of EGFR. This sets up the formation of docking sites for SH2 or phosphotyrosine-binding domain containing downstream effector proteins [42, 43]. For example, the autophosphorylation sites on the EGFR act as binding sites for growth factor receptor bound protein (Grb2) which complexes with son-of-sevenless (SOS) to activate Ras [42]. Ras activates Raf-1 which phosphorylates and activates mitogen-activated protein kinase (MAPK) [44].

EGFRs are found in caveolae and lipid rafts, with as much as 60% of the EGFR localized to lipid rafts [40]. The EGFR family consists of four RTKs, EGFR or ErbB1, ErbB2, ErbB3 and ErbB4 and has several ligands, such as EGF, transforming growth factor α (TGFα), and heparin binding EGF-like growth factor (HB-EGF). The ligand for ErbB2 is unknown; however, ErbB2 can be activated by heterodimerization with an EGF activated EGFR [43, 45].

EGF binding to the EGFR recruits c-casitas B-linage lymphoma (Cbl) to phosphotyrosine 1045 and promotes sustained multiubiquination of the receptor, thereby regulating EGFR degradation. Multiubiquination targets the endocytosed EGFR to the MVB. Cbl interacts with CIN85 and endophilin to increase membrane curvature and promotes fission of CCVs. The ability of c-Cbl to transiently associate with ErbB1 in the endosome, tags the endosome for ubiquitination and subsequent degradation. On the other hand, v-Cbl shunts receptors to a default recycling pathway that allows the recycling vesicles to return the EGFR to the plasma membrane. C-Cbl-mediated ubiquitination provides the ligand-dependent internalization signal that recruits the activated EGFRs into CCPs and then into the clathrin-mediated pathway of endocytosis [46, 47].

Internalized EGFRs move into early endosomes to be sorted to the recycling endosome or to the lysosome for degradation. The dileucine motif L^{679} and L^{680} of the EGFR is involved in endosomal sorting to the lysosome [48, 49]. The activated and phosphorylated EGFR complex interacts with Eps15, signal transducing adaptor molecule (STAM) and Hrs, which direct the EGFR vesicle to Tsg101 and the ESCRT

complexes on the MVBs to terminate signaling. EGF binding to the EGFR leads to the rapid down-regulation of the receptor at the plasma membrane and thereby acts like an "on/off" switch for mitogens-activated protein kinase (MAPK) signaling cascade. The magnitude and kinetics of signal activation is important in cancer, thus integrating endocytosis and signaling [40, 50].

There are two classes of EGFRs, a high-affinity class with an apparent K_D of ~8 pM and the low-affinity class with an apparent K_D of ~400 pM. The intracellular domain of EGFR controls ligand affinity. Cells expressing a truncated EGFR that lack the entire intracellular domain or just the C-terminal 63 residues have only low-affinity receptors. On the other hand, phosphorylation of the intracellular domain of EGFR by phorbol ester activates phosphotyrosine kinase C to convert high-affinity receptors to low-affinity receptors [51].

Clathrin Mediated EGFR Internalization

It is generally accepted that EGF binding to EGFR initiates clathrin assembly. The phosphorylation of Eps15 by activated EGFR is essential for receptor internalization. While Eps15 is a target for EGFR phosphorylation and is required for down-regulation, Eps15 does not directly bind to the receptor but binds AP-2 and clathrin. The redistribution of activated EGFR from caveolae to CCPs appears to be mediated by receptor mediated phosphorylation of c-Src. The EGFR activated c-Src then phosphorylates the clathrin heavy chain at T^{1477} leading to a redistribution of clathrin to

the CCP [52]. However, siRNA knockdown of clathrin light chains A and B (90-95% knockdown of both clathrins) does not appear to alter EGFR endocytosis [53].

While the loss of clathrin light chains did not alter EGFR endocytosis, other participants in CME appear to influence EGFR endocytosis. Knockdown of CALM—a major component of the AP-2 complex—inhibits EGFR internalization. The Grb2 adaptor protein couples EGFR to dynamin through its SH2 and SH3 domains, respectively; and Grb2 knockdown reduces EGFR endocytosis. These data suggest that CALM and Grb2 participate in EGFR internalization through CME [53]. In support of this hypothesis, potassium depletion reversibly halts CCP formation and aborts EGF endocytosis, suggesting that CME and EGF endocytosis are similarly affected by metabolic inhibitors [54].

Caveolae/Lipid Raft Interactions with EGFR

While CME is the generally accepted mechanism of EGFR endocytosis, recent work has suggested that caveolae and lipid rafts also interact with EGFR. Caveolae are flask-shaped invaginations of the plasma membrane made of cholesterol- and sphingolipid-rich microdomains that concentrate many signaling molecules and membrane receptors [1]. These organelles are sometimes called detergent-resistant liquid-ordered domains because of their resistance to detergent solubilization. This is thought to be due to the liquid-ordered phase created by their cholesterol and sphingolipid content. The shape and structural organization of caveolae is dictated by caveolin, a dimeric 16-25 kDa protein that binds cholesterol and attaches to the inner

leaflet of the plasma membrane [1]. Caveolae (~50-100 nm in diameter) can be attached or detached from the plasma membrane and have been shown to fuse into grape-like structures and tubules with sizes significantly larger than 100 nm. The actin cross-linking protein, filamin, has been shown to associate with caveolin-1 most likely by interaction with the caveolin scaffolding domain, a 20 amino acid sequence in the N-terminal portion of caveolin-1 [55]. Interaction of caveolin-1 with the cortical actin cytoskeleton implicates caveolae in clathrin-independent endocytosis and in turn, could be important for initiating signal transduction network(s) [21, 56].

Caveolae are abundant in endothelial cells, adipocytes and lung epithelial cells. Caveolin-1 expression is highest in white adipose and lung tissue and is down-regulated in fibroblasts upon oncogenic transformation [57]. Under normal cell culture conditions, caveolae represent a largely immobile plasma membrane compartment and are not involved in constitutive endocytosis. The immobility of the caveolae depends on interactions with an intact actin cytoskeleton [56]. Under physiological conditions, stable caveolae at the plasma membrane may serve different functions: 1) as key sensors and regulators of cholesterol homeostasis; 2) as specialized platforms facilitating the protein-protein interactions required for signaling, or 3) for the sequestration of inactive receptors. Caveolae mediate the entry of proteins such as albumin, bacterial toxins, folate receptors and viruses; Le Lay and co-workers have suggested that caveolin is required for maintenance of cholesterol in the lipid droplets of adipocytes [1, 21, 57].

In addition to the caveolae, lipid rafts are caveolin-free, cholesterol-rich microdomains on the plasma membrane that diffuse freely in the membrane bilayer. The

unique lipid composition of these small structures (40-50 nm in diameter) provides a physical basis for the specific sorting of specific membrane proteins and glycolipids, based on their membrane spanning domains. The high degree of saturation of the hydrocarbon chains in sphingolipids allows for cholesterol to be tightly intercalated, forming a liquid-ordered domain that floats in the less-ordered liquid domains of the plasma membrane [58, 59].

Caveolae and lipid rafts concentrate signal tranducers and these pre-assembled signaling complexes serve as molecular switches. While the ability to identify lipid rafts in intact cells is controversial, there is a large body of evidence that suggests that G-protein-coupled receptors (GPCRs), RTKs, components of the Ras-mitogen-activated protein kinase pathway, and Src family of tyrosine kinases are all found in caveolae and lipid rafts. Caveolae internalization is initiated by a signaling event that results in tyrosine phosphorylation of caveolae components. Glebov and co-workers showed that flotillin-1 (also called reggie-2) can be used to identify both caveolae and lipid rafts and appears to be a component of a clathrin-independent endocytotic pathway. However, flotillin-1 has also been reported to reside in lysosomes, as well as, other endocytic compartments, including the nucleus, and therefore, raises concerns about the utility of this protein as a marker for caveolae and lipid rafts [1, 4, 21, 58-61].

Caveolae and lipid rafts are best identified by the two-component bacterial endotoxin, cholera toxin. First, the B subunit of cholera toxin binds to the glycosphingolipid, GM_1 that is concentrated in caveolae and lipid rafts. Next, the A subunit of cholera toxin binds to the anchored B subunit, and traverses the membrane,

where it then ADP-ribosylates $G\alpha_s$, a heterotrimeric G protein concentrated on the cytoplasmic surface of the caveolae. The ADP-ribosylation of $G\alpha_s$ results in constitutive activation of $G\alpha_s$, which activates adenylyl cyclase and produces cyclic AMP. Thus, cholera toxin serves as an excellent example of the dual role that caveolae and lipid rafts may play in both endocytosis and signal transduction [58].

Couet and co-workers showed that EGFR directly interacts with the caveolin scaffolding domain by a conserved caveolin binding motif located within the EGFR kinase domain. They suggested that the binding of caveolin to EGFR inhibits EGF signaling by stabilizing the inactive conformation of the EGFR kinase or by steric hindrance that prevents receptor dimerization and subsequent *trans*-phosphorylation [62]. When rafts are disrupted by cholesterol sequestration, EGFR rearranges into large clusters that contain high concentrations of activated EGFR presumably due to spontaneous activation as a result of receptor packing [63]. Conversely, cholesterol loading reduces EGF binding to its receptor [40].

The changes in EGFR signaling seen with cholesterol manipulation are due to a change in the number of EGFR (approximately 40% increase on the cell surface) not due to its binding affinity [64]. While EGFR autophosphorylation increases with cholesterol depletion, the rate of dephosphorylation is unchanged. Once the EGFR is stimulated the level of EGFR decreases in the lipid rafts. Cholesterol depletion releases EGFR from lipid rafts, relieving the functional inhibition of the receptor. Cholesterol depletion also inhibits receptor internalization and down-regulation and this probably contributes to the

enhanced ability of EGF to activate MAPKs and other downstream signaling pathways [50].

The prevailing view is that the major route of EGFR endocytosis is through CME. Concentrated unoccupied receptors reside in caveolae and lipid rafts, but upon ligand binding and kinase activation these receptors translocate out of the caveolae. In addition to serving as a reservoir for EGFR, caveolae are the site where multiple signaling pathways meet.

Lipid rafts act as platforms to concentrate receptors and assemble the signal transduction machinery. In the case of the EGFR, the lipid rafts serves both functions. EGFR and endocytic proteins are enriched by EGF stimulation and that the activated EGFR containing rafts are incorporated into emerging coated pits. On the other hand, it is possible that EGFR containing rafts do not use the clathrin pathway, but upon EGF stimulation, the activated EGFR may trigger its own clathrin independent endocytosis. Ubiquination has been shown to preferentially couple EGFR to the clathrin independent pathway [44]. Puri and co-workers suggest that at low concentrations of EGF, the EGFR is tyrosine phosphorylated and is ready for signaling, but is not ubiquitinated and therefore is internalized through CCPs; however, at high concentration of EGF the EGFR is ubiquitinated and shows substantial endocytosis through the clathrin-independent pathway [65].

Lipid rafts can also serve as signaling platforms. When EGFR moves into a caveolae and EGF is present, resident Ras-mediated signaling is initiated. From its

location in the caveolae, the EGFR can also interact with other resident transducing molecules to initiate a complex pattern of signal transduction networks [65].

Trafficking of the Endocytosed EGFR

Ligand binding to the EGFR quickly induces Rab5 activation and recruits EEA1 from the cytosol to the plasma membrane [66, 67]. Rab5 activation is most likely due to action of Rabex-5 binding to ubiquitinated EGFR, through its ubiquitin-interacting motif (UIM). Thus, it seems likely that activated EGFR recruits Rabex-5 to the plasma membrane or early endosome to facilitate GDP:GTP exchange on Rab5. Rin1 has also been proposed to function in a similar manner to recruit proteins to the plasma membrane or the early endosome. It is possible that Rabex-5 and Rin1 could have redundant functions even though they are activated by different post-translational modifications of the EGFR and may represent two different pathways for signaling and down-regulation [68].

Down-regulation of the EGFR utilizes receptor ubiquitination as a sorting signal for its processing to the lysosome. Cbl down-regulates tyrosine kinases by controlling ubiquitination and degradation [69]. De-ubiquination, on the other hand, is also an important regulator of EGFR down-regulation. Over-expression of the de-ubiquinating enzyme Ub isopeptidase Y (UBPY)/ubiquitin-specific processing protease (USP8) decreased the amount of ubiquinated EGFR and delayed its degradation in EGF stimulated cells. Depletion of UBPY by RNA interference caused an increase in ubiquinated EGFR and accelerates degradation in EGF stimulated cells. These

observations suggest that UBPY/USP8 de-ubiquinates ligand-activated EGFR and negatively regulates its rate of down-regulation [70].

CONTEMPORY TOOLS TO STUDY EARLY EVENTS OF ENDOCYTOSIS

One of the primary tools used to study vesicle trafficking is fluorescence microscopy. Fluorescently tagged ligands or fusion proteins are used to identify the components of the vesicular pathway being studied and until recently epifluorescent microscopy was the method of choice. In this optical approach the fluorescently tagged molecules throughout the cell are excited by specific wavelengths of light. Because of the 3-dimensional nature of the cell and the inability to limit reporter excitation to a specific cellular location, use of this method for regional deistribution studies, especially for vesicle trafficking is limited.

More recently, the ability to selectively excite reporter molecules in a defined region of the cell has provided a significant improvement in the ability to observe event at or near the plasma membrane. Total internal reflection fluorescence microscopy (TIRF-M), sometimes called evanescent wave microscopy, selectively excites fluorophores in an aqueous or cellular environment within 100 nm of a solid surface without exciting fluorophores residing beyond the evanescent field. A thin zone of electromagnetic energy (evanescent field) is used to excite fluorescent molecules within this limited field; and yields images with very low background fluorescence and little, if any, out-of-focus fluorescence. TIRF-M also limits the exposure to light to all other

planes in the sample. These unique characteristics of TIRF-M make it an ideal tool for applications in biochemistry and cell biology [71].

The evanescent field (EF) is generated when a beam of light travels in a medium of high refractive index, such as adjoining water or an adherent cell, and strikes an interface with a medium of lower refractive index, such as the coverslip (Fig. 2). When the angle of incidence α of the beam of light exceeds its "critical angle", then the beam of light undergoes total internal reflection. This electro-magnetic wave can not simply disappear and this propagates a thin layer of energy in the water or cell that selectively excites fluorescent molecules near the interface that exponentially dissipates with distance away from the coverslip. Fluorescent molecules located beyond the 100 nm of the EF remain unexcited. Reporter molecules closest to the coverslip are the brightest. In addition, since the EF illumination leads to less bleaching per photon collected, hundreds of images can be collected from a single cell.

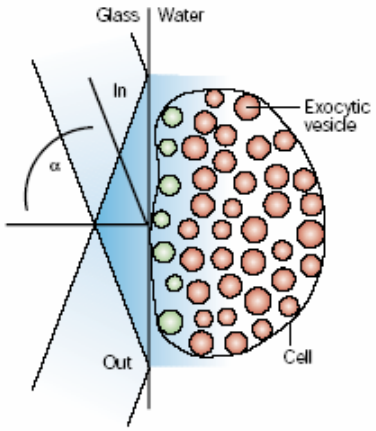

Figure 2. Evanescent Field. When a parallel beam of light in a medium of high refractive index strikes an interface with a medium of lower refractive index, it suffers total internal reflection creating the Evanescent Field. Steyer and Almers, Nat Rev Mol Cell Biol, 2001, 2:268-275.

There are two common types of TIRF microscopes, the prism-type microscope and through-the-lens microscope. The prism-type microscope uses a prism to direct light into a coverslip and the excited fluorescence is collected opposite the reflecting interface, whether

with an objective dipping into an open chamber or with an oil immersion objective if the chamber is covered by a coverslip. These microscopes allow for larger field illumination and are used to image several cells or a larger single cell. The background is darker with the prism-type microscope; however, the cells are sandwiched in a narrow space limiting access to the cells while imaging. This method is also limited because the variation in brightness due to distance from the interface is reduced and this can be a disadvantage when trying to evaluate movement of molecules in real time. The through-the-lens microscopes allow open access to the cells, are more efficient in collecting fluorescent light from object near the interface and have higher image quality and spatial resolution. Through-the-lens microscopes generate the EF with light transmitted through the microscope objective (Fig 3). The light diverging from a point source can be made parallel by placing the point source in the focal plane of an objective lens and the focal plane at the back of the objective. The further off axis the point source the larger the angle at which the parallel beam leaves the objective. Most of the early work using TIRF-M used prism-type microscopes; however, today most work is done with through-the-lens microscopes due to the availability of commercial attachments and lens [71, 72].

For these studies, I used a through-the-lens system that uses coherent Innova 70C lasers; one an argon ion laser that produces light with a wavelength of 488 nm and the other, is an argon-krypton laser that produces light with a wavelength of 568 nm. A KineFLEX fiber coupler is used to couple the two beams into a single mode fiber (the point source). An Olympus IX81 inverted microscope (contained in a 35°C chamber) was modified with a TIRF fiber illuminator and a Plan APO 60X objective with a numerical aperture of 1.45. TIRF illumination was introduced through the edge of the objective at an angle set between 65 and 68 degrees, producing a penetration depth of 90-121 nm at 488 nm and 105-141 nm at 568 nm. Light from the fluorophores are collected and relayed onto a 640 X 448 pixel charge-coupled device camera developed by Lincoln Laboratory (MIT) and a Physik Instruments PIFOC was used for fine focus control.

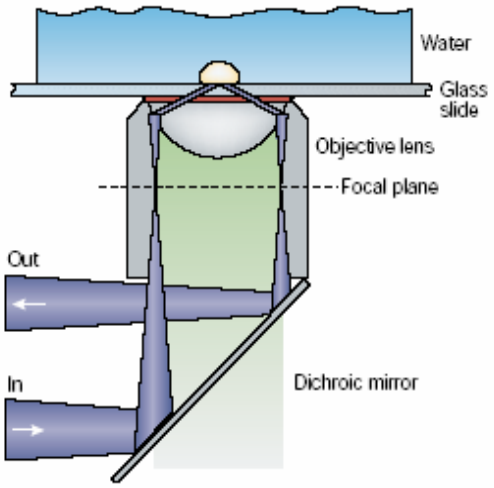

Figure 3. **Through-the-lens microscope.** The Evanescent Field is generated by diverting light from its point source in the focal plane of an objective. Steyer and Almers, Nat Rev Mol Cell Biol, 2001, 2:268-275.

SPECIFIC AIMS

The goal of this body of work is to characterize the early steps in cargo sorting during endocytosis. While CME is thought to mediate both EGFR and TfR endocytosis, recent work by Huang and co-workers showed that these two RTKs used very different endocytic pathways. SiRNA mediated knockdown of CALM inhibited EGFR endocytosis, but not that of TfR endocytosis [53]. On the other hand, clathrin depletion and/or α-adaptin knockdown inhibited Tf uptake, but had no affect on EGF endocytosis [73].

Preliminary studies of the role of EEA1 in protein sorting/vesicle fusion raised serious concerns about many of the assumptions regarding the early steps of endocytosis. I found that endocytosed TfR did not co-localize with EEA1, while the liganded EGFR was strongly associated with EEA1-tagged vesicles. Using the recently developed TIRF-M approach to examine the earliest steps in the endocytotic process, I confirmed that the TfR did not co-localize with EEA1, but was strongly associated with static patches of clathrin. Conversely, TIRF-M revealed that the EGFR was strongly associated with EEA1, and poorly associated with the clathrin patches in COS cells. These differences in endocytic behavior of two widely used models of endocytosis only became unambiguous using TIRF-M and clearly indicate that the early steps of endocytosis need to be reexamined. Thus, the specific aims of this study are:

1. To define the role of the static, concentrated clathrin-patches in CME.

2. To examine ligand induced early endocytic remodeling for EGF internalization.

3. To evaluate the role of a new FYVE domain protein (WDFY2) in endocytosis.

CHAPTER II

PLASMA MEMBRANE DOMAINS SPECIALIZED FOR CLATHRIN-MEDIATED ENDOCYTOSIS IN PRIMARY CELLS

This chapter is in the format that it was published in the J. Biol. Chem. (2006), 281:16139-16146, as written by the authors, Bellve KD, **Leonard D**, Standley C, Lifshitz LM, Tuft RA, Hayakawa A, Corvera S, and Fogarty KE.

The TIRF microscope and attached camera was purchased and assembled by the Biomedical Imaging Facility at UMASS Medical School under the direction of Clive Standley and Richard Tuft. The imaging software was designed by Karl Bellve, Lawrence Lifshitz and Kevin Fogarty. Computer modeling was performed by Kevin Fogarty. The FRAP experiment was a joint effort between the Biomedical Imaging Group, and myself. I was responsible for the cell preparation; photobleaching, data analysis; modeling was done by the Imaging Group. Primary adipocytes were prepared by My Chouinard and Alison Burkart. All transfections and imaging were done by me and I was responsible for the image restoration and figure preparation.

Summary

Clathrin distribution at the cell surface varies from diffuse spots to larger clusters or patches of clathrin. Since the large clathrin patches are prominent in cultured cells, they are thought to represent either clathrin nucleation sites or artifacts of cell adhesion in culture dish. We used TIRF-M to examine early endocytic events that occur within 100 nm of the plasma membrane. To mark the events of early endocytosis we used Tf, a commonly used ligand for the study of endocytosis. Upon the addition of Tf to the cell media, Tf rapidly diffuses over the surface of the cell and within minutes congregates into larger clusters similar to that observed with clathrin; co-expression experiments showed that TfR co-localizes with clathrin in these larger clathrin arrays. This raises the possibility that Tf enters the cell via the larger clathrin patches.

To eliminate any adhesion artifacts due to cell culture, we used primary adipose cells isolated from mice to examine clathrin function and organization. Primary adipocytes are naturally buoyant and are unable to attach to the surface of a coverslip or tissue culture dish. The majority of the clathrin (>60%) was organized into large clathrin patches that displayed no lateral mobility in the adipocyte membrane and persisted for several minutes. A smaller number of small spots were also observed to quickly appear and disappear from the plane of focus. Direct visualization of Tf showed that Tf bound to the clathrin patches and internalized through vesicles that emerged from these domains. Using high resolution imaging (50 images/s) to observe changes in intensity fluctuations from the static clathrin patches, we found that the changes in Tf intensity are consistent with the formation and detachment of CCVs from the clathrin patch.

These data suggest that the large clathrin patches serve as active sites of Tf endocytosis. This leads to a model of clathrin organization that includes a small group (<20%) of transient events that appear to be randomly initiated, and a larger group (50-80%) that occurs on larger, defined regions of the plasma membrane. These regions appear to consist of flat lattices that give rise to individual coated vesicles or clusters of individual pits that form repeatedly on the same regions of the membrane.

Introduction

Clathrin assembly at the plasma membrane is required for the endocytosis of many receptors and transmembrane proteins. Insight into the mechanism of clathrin assembly and coated vesicle formation was obtained initially from electron microscopy and biochemical studies. This information formed the basis for a well accepted model in which individual clathrin-coated pits form on the plasma membrane, grow and invaginate by progressive association of coat subunits, and detach to form free, short-lived vesicles enriched in endocytic cargo [6, 74-78].

The availability of fluorescent derivatives of clathrin provided the opportunity to test this model in live cells. The first visualization of fluorescent clathrin generated several surprising findings, among which was the perception that clathrin-coated vesicles were produced recurrently from specific sites within the plasma membrane. In addition, many of these sites displayed a gradual loss of fluorescence, not a sudden catastrophic disappearance, suggesting that individual coated pits could form from within an expansive clathrin patch. Results consistent with the existence of large clathrin lattices harboring invaginated structures have also been captured by electron microscopy [76].

The use of total internal reflection fluorescence microscopy (TIRF-M) has provided the additional technical advantage over confocal microscopy of being able to specifically see events occurring within 100 nm of the plasma membrane [71, 79]. Images derived from TIRF-M of clathrin are consistent among many groups using either dsRed-clathrin or enhanced green fluorescent protein (EGFP)-clathrin, in stable or transiently transfected cells, and also have provided unexpected results. Foremost among

these findings is that the vast majority (80%) of the clathrin signal on the plasma membrane is present as a population that is static during the average period of observation, typically 60 s. Only a small population of clathrin (10–20%) is present as small, rapidly disappearing structures, which would be the ones expected to predominate if the earlier model of clathrin-mediated endocytosis were occurring in live cells [2, 11, 15, 18, 80-83]. Although these observations have been reported repeatedly, the significance of this organization has remained unclear, and the possibility has been suggested that it may represent an artifact of cell adherence in culture [16].

To better define the physiological significance of these observations, we have analyzed the dynamics of clathrin assembly using three novel approaches. First, we visualized clathrin dynamics in primary adipose cells isolated from mouse epididymal fat. Isolated adipocytes float in culture medium because of the buoyancy conferred by their lipid content, and therefore artifacts due to adherence onto glass or plastic are eliminated. Moreover, this cell type has been used in studies of endocytic trafficking of GLUT4, a transmembrane transporter known to internalize through a clathrin-mediated mechanism [84, 85]. Second, we have used algorithms that incorporate the signal detected throughout the whole adherent surface of the cells, avoiding the potential bias introduced by the selection of single events for analysis. Third, we have developed an imaging platform consisting of a TIRF microscope equipped with two lasers and a highly sensitive, high speed camera that allows the capture of images at rates up to 50 Hz (50 images/s). Our results indicate that apparently static clathrin patches display small subregional intensity changes consistent with the formation of clathrin-coated pits from

within these patches. Moreover, simultaneous imaging of transferrin and clathrin demonstrates that ligands are internalized from large clathrin patches. These results suggest a model in which defined regions of the plasma membrane are specialized for the assembly of large clathrin assemblies that functionally support endocytosis.

Experimental Procedures

Optical System: Coherent Innova 70C lasers were used (argon ion and an argon-krypton ion) to produce the 488 and 568 nm light, respectively. The combined beams were coupled into a single mode fiber using a KineFLEX fiber coupler (Point Source). A modified Olympus IX81 inverted microscope, TIRF fiber illuminator, and Plan APO 60x objective with a numerical aperture of 1.45 were used. TIRF illumination was introduced through the edge of the objective at an angle set between 65 and 68 degrees, giving a penetration depth of 90–121 nm at 488 nm and 105–141 nm at 568 nm. Light was collimated through the objective and a layer of immersion oil onto the coverslip. The quality of the collimation was set halfway between the best qualities for 488 and 568 nm. Light from the fluorophores was collected and relayed onto a 640 x 448-pixel charge-coupled device camera developed by Lincoln Laboratory (MIT). A Physik Instruments PIFOC was used for fine focus control. The entire microscope was contained in a heated chamber held at 35 °C.

Imaging Hardware and Software: The acquisition system uses the following components: Intel L440GX+ server motherboard with dual peripheral component interconnect (PCI) buses; two 800-MHz Pentium III processors with 2 gigabytes of RAM; Instrutech ITC-18 data acquisition system; Bitflow Roadrunner differential camera interface; ATTO UL3D Ultra160 SCSI Raid controller and four Seagate Cheetah 18-gigabyte Ultra 160 SCSI drives (model ST318351LW). The Bitflow Roadrunner uses a 66-mHz PCI slot. The other components use the 33-Mhz PCI bus. The four Seagate

Cheetah drives are in a Raid-0 configuration. Two drives are attached to each of the two controllers on the ATTO UL3D. Sustained read and write speeds are over 100 megabytes/s. The acquisition software, called ScratchNG, is a custom multi-threaded Windows application designed for sustained image capture to RAM, a RAID disk, or both. The Roadrunner streams incoming images into a primary double buffer in system memory. Although one buffer is being addressed by the Roadrunner, the image from the other buffer is copied into a secondary buffer. The secondary buffer can vary in size, depending upon the number of images that need to be captured or whether the images are to be transferred directly to the RAID device. The software image capture capability is only limited by the size of the RAID device, which is 72 gigabytes currently. ScratchNG uses the Instrutech ITC-18 to generate camera read pulses, shutter openings, filter wheel changes, and focus changes. Interactive three-dimensional and four-dimensional (3D+time) visualization and co-localization analysis was performed using Data Analysis and Visualization Environment software [86]. Curve fitting was done using Origin (Origin Labs Corp., Northampton, MA).

Fluorescent Probes and Cells: Alexa568-transferrin (Molecular Probes) was applied to the cells at 20 µg/ml. GFP-clathrin represents a N-terminal fusion of GFP with clathrin light chain A, generated and generously provided by J. H. Keen [87]. In the experiments described herein, COS cells were transfected with 1–4 µg of plasmid DNA using calcium phosphate transfection. For primary fat cell isolation, epididymal fat pads from 10-week-old male C57BL6 mice were weighed and cut into 0.03-cm^3 pieces with scissors and then resuspended in KRH (NaCl 125 mM), KCl 5 mM, $CaCl_2$ 1.3 mM, $MgSO_4$

1.2 mM, HEPES, pH 7.4, 25 mM, sodium pyruvate 2 mM, and 2.5% bovine serum albumin containing 1 mg/ml collagenase (Worthington). The fat pads were digested for 30–45 min at 37 °C in an orbital bath with shaking at 100 rpm. The digested samples were squeezed through chiffon and the isolated cells and washed three times in KRH buffer, pH 7.4, plus 0.5% bovine serum albumin and immediately transfected by electroporation. Cells were then placed in Dulbecco's modified Eagle's medium supplemented with 10% fetal bovine serum and visualized 18 h later.

Results

Isolated adipocytes transfected with GFP-clathrin were visualized by epifluorescence and TIRF-M. To enable contact between the adipocytes (which float) and the bottom coverslip, a 15-mm coverslip was placed over a 15-µl volume of the cell suspension, trapping the cells in the 84-µm space between the two coverslips (Fig. 4, *diagrams above panels A–C*). GFP-clathrin was seen in epifluorescence as a bright rim surrounding the single large lipid droplet. As the objective was lowered, a small adherent region could be visualized (Fig. 4, *A–C*). When visualized by TIRF-M the same region appeared smaller in diameter (Fig. 4, compare *D* and *F*) because of the illumination of only 100 nm from the surface of the coverslip. Images were then acquired at 0.5 Hz (one image every 2 s) for a duration of 10–20 min.

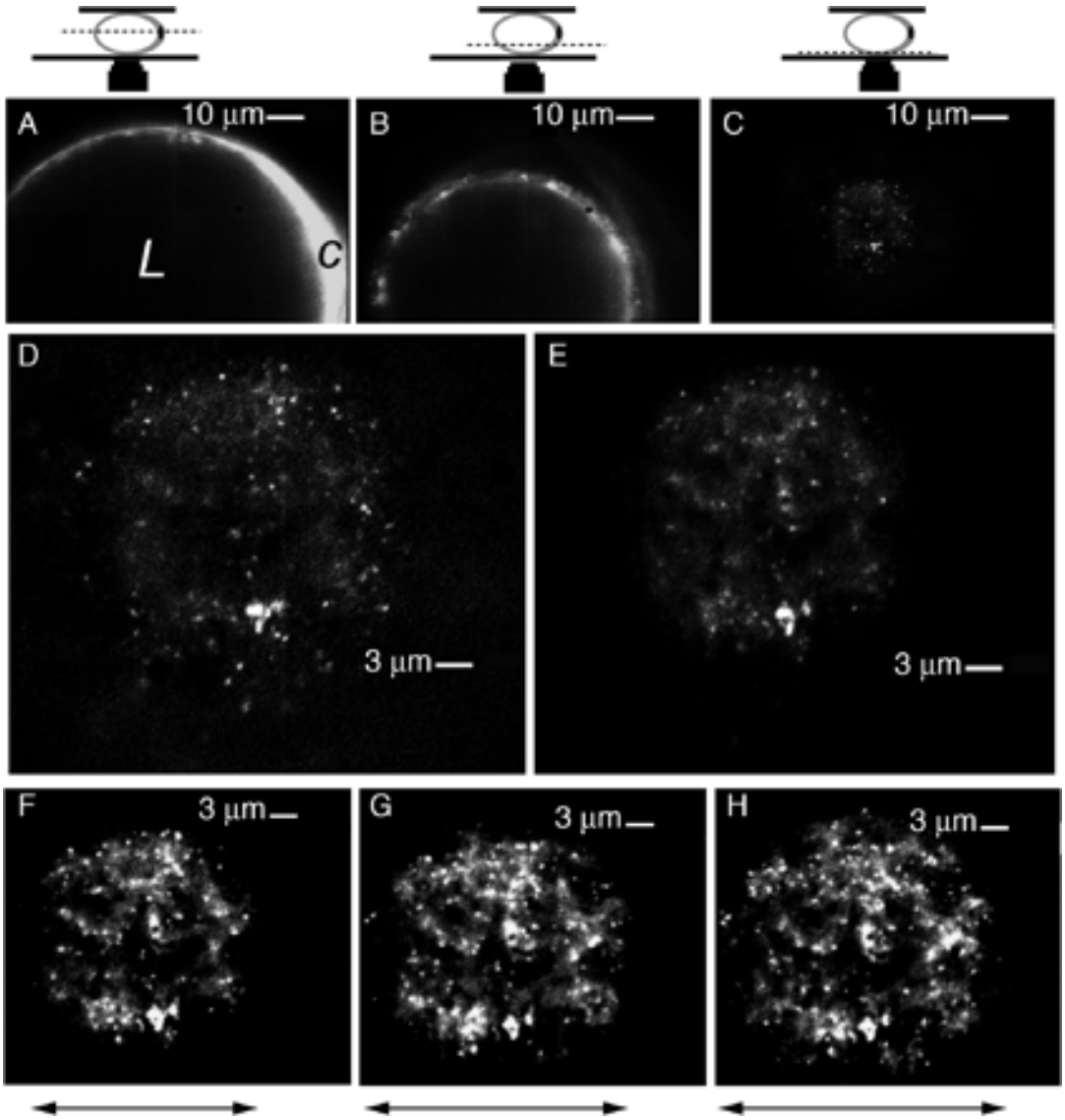

Figure 4. Clathrin domains on the plasma membrane of primary adipocytes. Primary adipocytes were placed on a 25-mm coverslip and overlaid with a smaller coverslip, as depicted in the diagrams *above* each panel. Images were acquired immediately. In epifluorescent mode, images were taken through the middle of the cell (*A*) and progressively toward the bottom (*B*) until the lowest in-focus plane was reached (*C* and *D*). The single lipid droplet (*L*) and thin cytoplasmic rim (*c*) characteristic of the primary white adipocyte are clearly apparent. The laser was then switched to TIRF mode (*E*), and images were obtained every 2 s for a period of 20 min (*F–H*). The diameter of the cell footprint increased slightly during this period of acquisition (*double arrows under panels F–H*), possibly because of slight evaporation of the buffer between the two coverslips during this period.

GFP-clathrin was observed in regions of heterogeneous size and intensity. To analyze quantitatively the distribution of clathrin within these regions, we used the following strategy. First, raw images were corrected by subtracting the background fluorescence outside the cell (Fig. 5*a, panel A*). Second, a running average of three time points in all each comprising a 4-s interval was generated, which removed slight speckling due to camera noise but had a negligible effect on the data (Fig. 5*a, panel B*). Third, to generate images in which structured fluorescence (*i.e.* pits and patches) could be quantitatively analyzed without interference from background diffuse fluorescence, images were smoothed by convolving with a small, two-dimensional Gaussian spot (s = 160 nm), which preserved the mean intensity. In order to be able to separate the clathrin spots from the background based on their intensity, the local background was estimated by convolving with a larger, two-dimensional Gaussian (s = 320 nm) and subtracting this from the smoothed images. From this we generated a binary masking image by setting the intensity of all positively valued pixels to 1 and all other pixels to zero (Fig. 5*a, panel C*). We then multiplied the mask by the original image (Fig. 5*a, panel D*) to display areas in the image with intensity exceeding the average local background. The masked images could then be used to measure the size and intensity of clathrin pits or patches over the entire adherent surface of the cell. They could also be used to measure the average persistence of these regions over time, as well as their co-localization with cargo (see below).

To estimate the size distribution of clathrin assemblies, histograms of images from 16 time points/cell for four independent cells were averaged (shown in). A peak

comprising small, diffraction-limited regions 360 nm in diameter was seen. 30% of total fluorescence was derived from regions smaller than 360 nm in diameter, 60% from regions 360–700 nm in diameter, and 10% from regions larger than 700 nm in diameter. The resolution of the TIRF system was measured by imaging a 190-nm fluorescent green bead three dimensionally with 100-nm z-steps to obtain the best focal plane, and then switched to TIRF. The full width of the image obtained was 376 nm. Because single pits would be expected to have a real diameter of ~50–100 nm and thus be visualized in TIRF as regions of <376 nm, we concluded that in primary cells, the majority of clathrin is distributed in assemblies larger than those attributed to individual clathrin-coated pits. This distribution of clathrin regions is similar to that observed by others in either stably or transiently transfected cell lines [11, 15, 18, 80, 82].

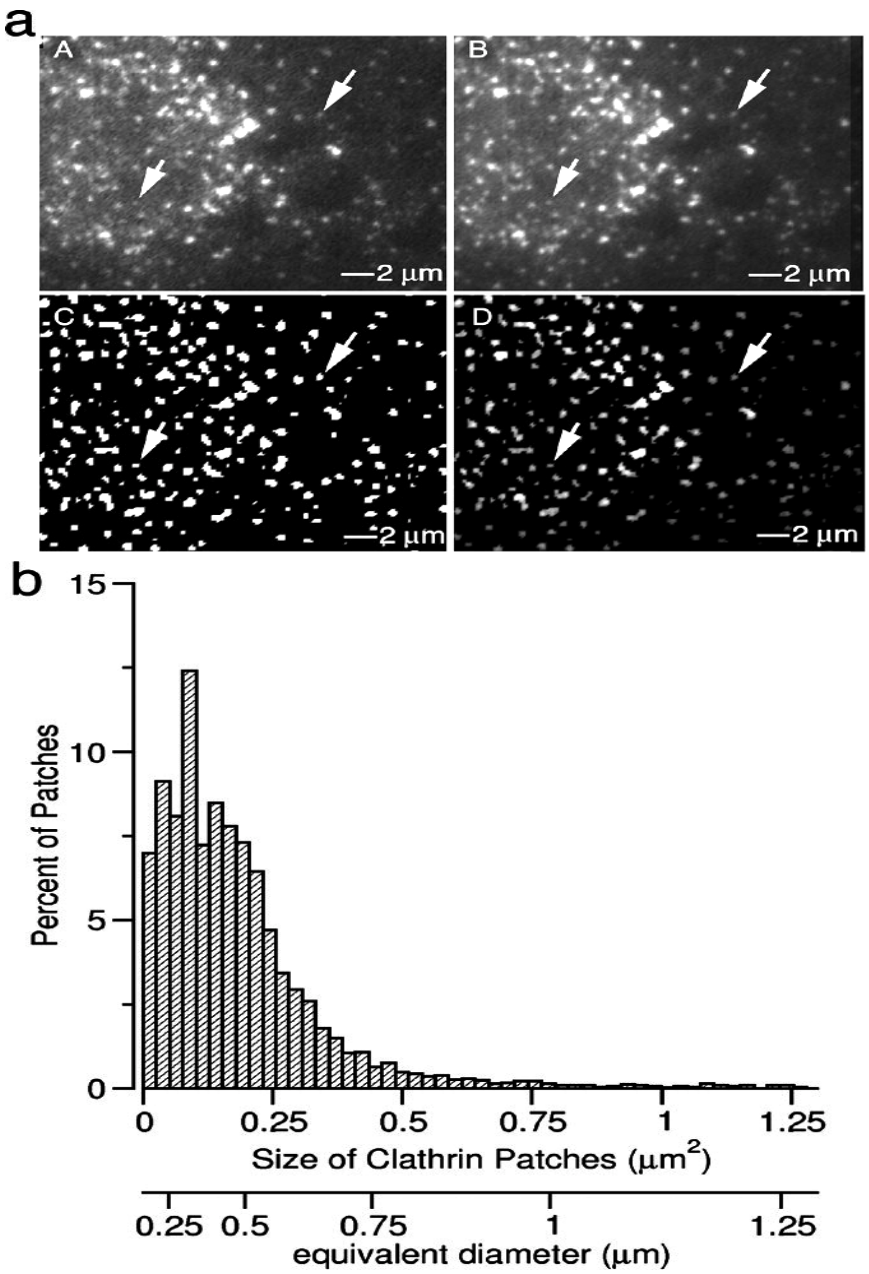

Figure 5. Size distribution of clathrin regions in primary adipocytes.
a, analysis steps. Regions of high intensity of varied size and shape (*arrows*) can be seen over the diffuse background of variable intensity in the images even after subtraction of the background outside the cell *(A)*. An image was subjected to a 3-image running average *(B)*. A binary mask was generated by deconvolution *(C)*. The product of the original data and the binary mask is shown *(D)*. *b*, size distribution. A histogram of the size distribution of clathrin regions is defined by the binary mask. Shown is an average histogram from 18 images/cell from four independent cells, which is similar to individual histograms before averaging.

The behavior of these regions over time was quantified by the following procedure. First, the time series was projected as a three-dimensional image, with the TIRF image defined by *X* and *Y* and time defined by *Z*. Clathrin "objects" were defined as contiguous voxels in this three-dimensional space (Fig. 6*A*). Second, for each time point in the series, the regions corresponding to objects present because $t = 0$ were labeled as "persistent," whereas those appearing *de novo* were labeled as "new" (Fig. 6*B*). Third, the total amount of fluorescence in persistent or new regions at each time point was recorded (Fig. 6*C*). This provided a measurement of how much clathrin was present in rapidly disappearing *versus* persistent regions throughout the whole adherent surface.

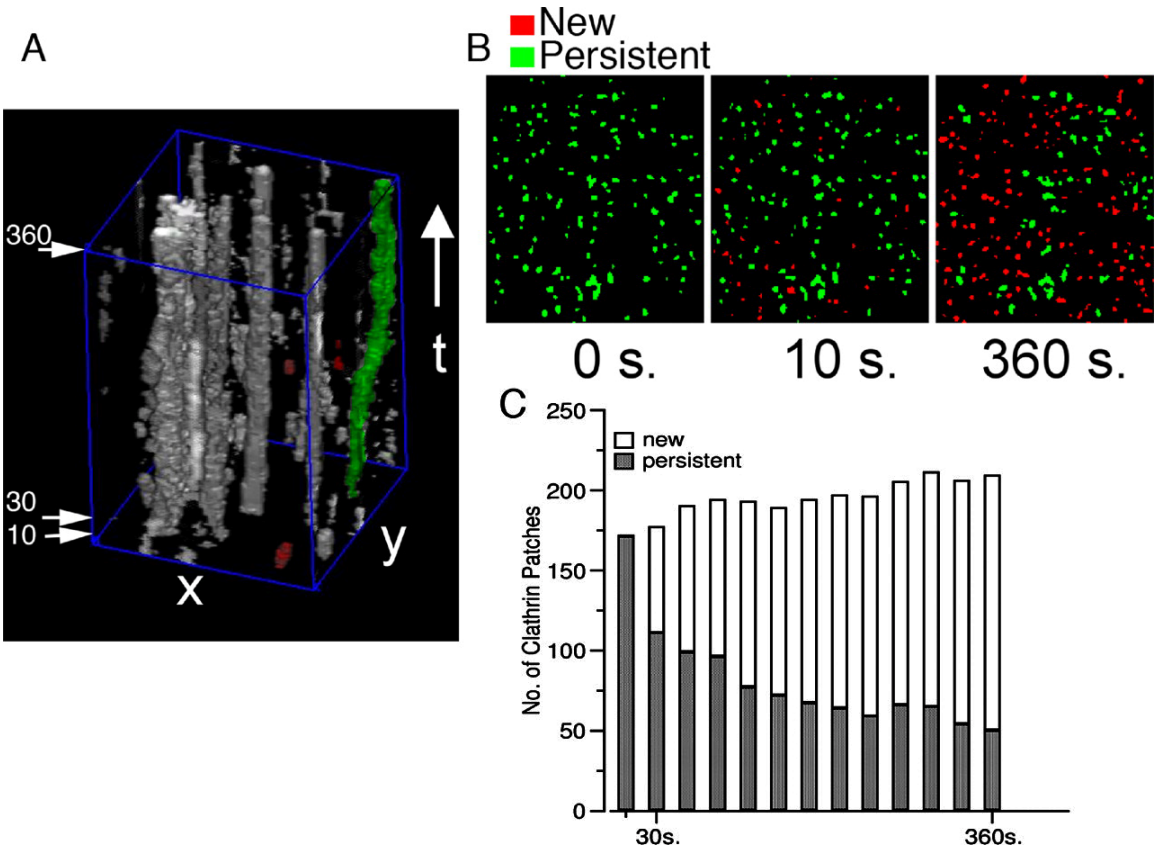

Figure 6. Persistence of clathrin regions over time.
A, time series are rendered in three-dimensional space, and sets of contiguous voxels are identified as objects. A clathrin object persistent throughout the 360-s time series is pseudocolored *green*, and several rapidly appearing and disappearing objects are pseudocolored *red*. *B*, the population of objects present at $t = 0$ and persistent after 10 or 360 s is depicted in *green*; those present at 10 or 360 s that were absent at $t = 0$ are depicted in *red* in three cross-sections corresponding to the position of the *horizontal arrows* in A, which represent three selected time points. *C*, the number of new or persistent regions found at each time point is plotted.

When the plot was fitted with the sum of two exponentials, a fast time constant of 24.0 ± 16.4 s (95% confidence interval) was observed, which accounted for 40% of the regions. A slow time constant of 537 ± 222 s (95% confidence interval) accounted for the remaining 60% of the regions. Thus, more than half of the clathrin regions in the cell are long-lived. A complementary measurement of the persistence of clathrin regions is shown in (Fig. 7*A*), in which the degree of co-localization of an image ($t = 0$, displayed in *green*) with subsequent images ($t = n$, displayed in *red*) is quantified. Co-localized spots are displayed in *white*, and *red* and *green* voxels represent regions that appeared or disappeared outside the more stable areas, which remain *white* (Fig. 7*A*). For quantification, the loss of co-localization was measured as the percent of red voxels co-localized with green voxels over the whole adherent surface of the cell, using images acquired at 2-s intervals over a 2.5-min period (Fig. 7*B*). When these plots were fitted with the sum of two exponentials, fast and slow time constants of 8.4 ± 0.87 and 157 ± 5 s (95% confidence interval), accounting for 43 and 57% of the regions, were observed. These time constants are slightly faster than those derived from the procedure shown in Figure 6, probably because of the fact that this alternative method does not account for cell shape changes that would lead to an artificial decorrelation of persistent regions. Nevertheless, the proportion of long-lived clathrin-coated regions was still estimated to be higher than 50%.

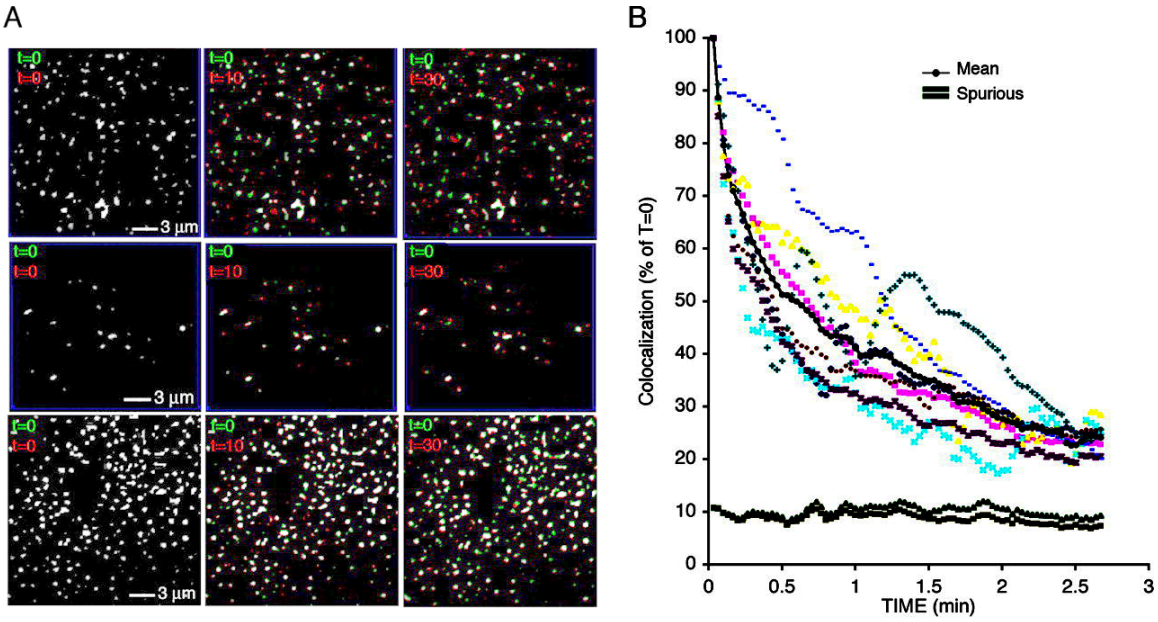

Figure 7. **Persistence of clathrin domains over time is independent of expression levels.**

A, *upper*, *middle*, and *bottom rows* exemplify cells expressing total clathrin concentrations within a 10-fold range (evaluated by the total intensity of the signal in both TIRF and epifluorescence). For each cell, an image obtained at $t = 0$(*green*) is overlaid with images of subsequent time points (*red*) as indicated in the *upper left corner of each panel*. Voxels co-localized between the two time points are displayed in *white*. *B*, co-localization of clathrin over the entire adherent surface over a 2.5-min period. Images were acquired every 2 s, and the co-localization between $t = 0$ and $t = 2$ s is arbitrarily assigned the maximal value of 100%. Plotted are the results from eight measurements from four independent cells (one measurement is the co-localization of $t = 0$ with $t = n$; the second is the co-localization of $t = n$ with $t = 0$), the mean value of which is depicted in *black*. Spurious co-localization in a high and a low expressing cell were calculated using the $t = 0$ image flipped along the x axis

A similar behavior was observed in cultured cell types, including differentiated 3T3-L1 adipocytes (not illustrated) and COS cells (Fig. 8). To estimate the size distribution of clathrin images, histograms from 18 images/cell from three independent cells were averaged. As in primary cells, a peak around the equivalent diameter of 360 nm is seen, which possibly corresponds to single pits (Fig. 8*A*). Regions smaller than 360 nm (between 361 and 700 nm) and larger than 700 nm accounted for 20, 60, and 20% of the total fluorescence, respectively. Analysis of the persistence of objects in time also corresponded well with that observed for primary cells (Fig. 8*B*). When the loss of co-localization over time was measured (Fig. 8, *C* and *D*) fast and slow time constants of 11.6 ± 1.1 and 376 ± 6 s (95% confidence interval) accounting for 40 and 60% of the regions were observed. Thus in both primary and cultured cells, the majority of clathrin was found in large assemblies that persisted in the same region for prolonged periods of time.

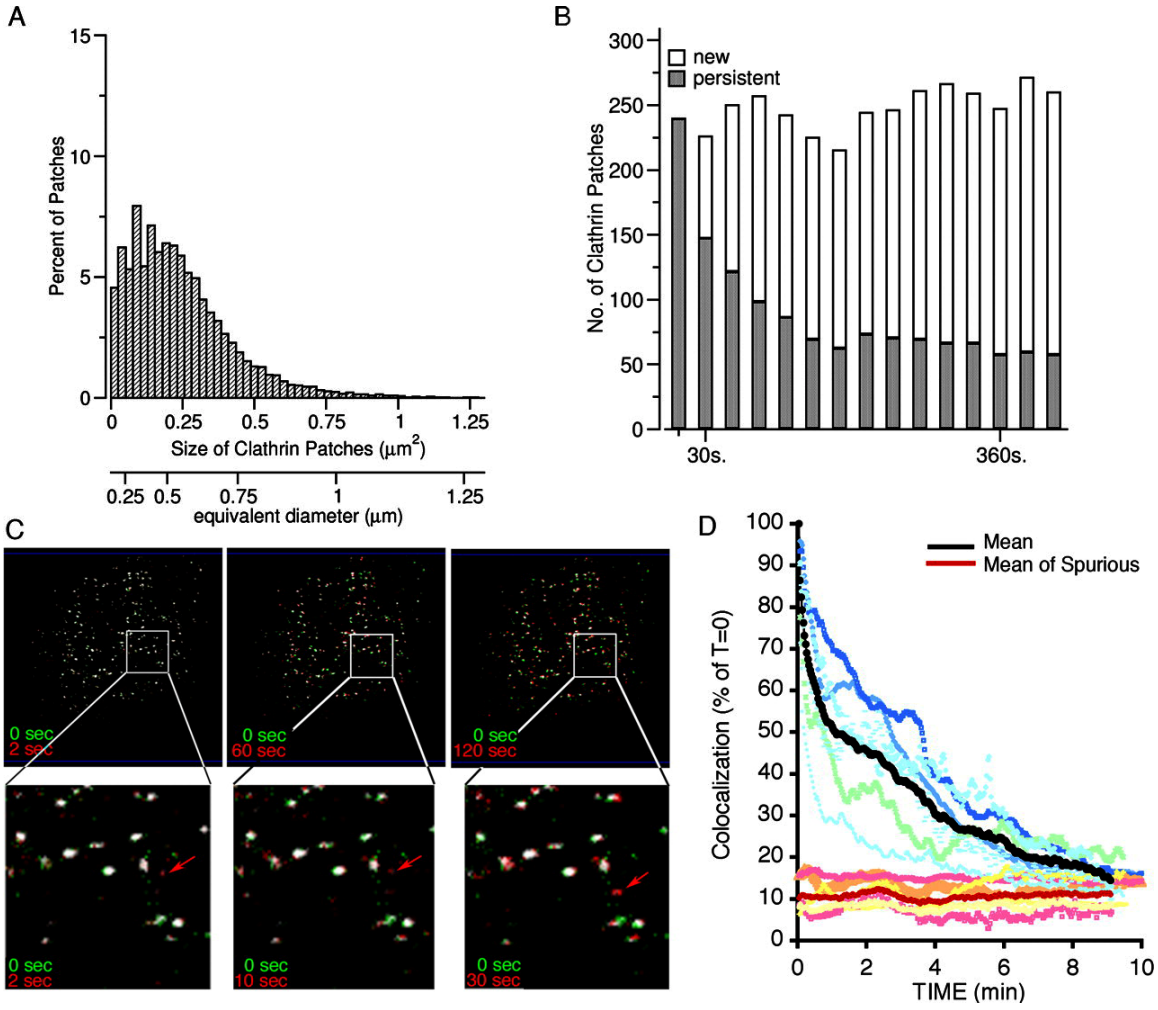

Figure 8. **Clathrin distribution and dynamics in COS cells.**
COS cells expressing GFP-clathrin were imaged by TIRF-M. *A*, histogram of size distribution of clathrin regions on the surface of a COS cell. Shown is the average histogram from 18 images/cell from three independent cells, which is similar to individual histograms before averaging. *B*, analysis of persistence of clathrin objects over a 7-min time period. Analysis was done as described for Fig. 3. *C*, an image obtained at $t = 0$(*green*) is overlaid with images of subsequent time points (*red*) as indicated in the *lower left corner of each panel*. The *lower panels* are magnifications of the areas depicted by the rectangles in the *upper panels*. *Arrows* point to regions that appear and disappear rapidly. Voxels co-localized between the two time points are displayed in *white*. *D*, co-localization of clathrin over the entire adherent surface over a 10-min period. Images were acquired every 2 s, and the co-localization between $t = 0$ and $t = 2$sis arbitrarily assigned the maximal value of 100%. Plotted are the results from six measurements from three independent cells, with the mean value depicted in *black*. Spurious co-localization for each cell was calculated using the $t = 0$ image flipped along the *x* axis; the mean value is depicted in *red*.

To determine whether these regions are static or actively exchange clathrin with the cytoplasm, we analyzed the pattern of recovery of fluorescence following photobleaching. After imaging by TIRF-M, the top left quadrant of the cell was bleached in epifluorescence mode for 2 min. Images were then acquired in TIRF mode for 20 additional minutes (Fig. 9*A*, *panels A*–C). Much of the signal appeared in regions that overlapped exactly with those visible prior to photo bleaching (Fig. 9*A*, *panels D–F*), revealing that these apparently static regions actively exchange clathrin with the cytoplasm. Measurements of the rate of recovery of fluorescence revealed a mean half-time of 479 ± 145s ($n = 3$) (Fig. 9*B*). This slow rate of recovery may be due to the bleaching of a substantial proportion of the cytoplasmic pool of clathrin. However, the kinetics may be an accurate reflection of the rate of clathrin exchange in long-lived clathrin regions (Figs. 6,7,8).

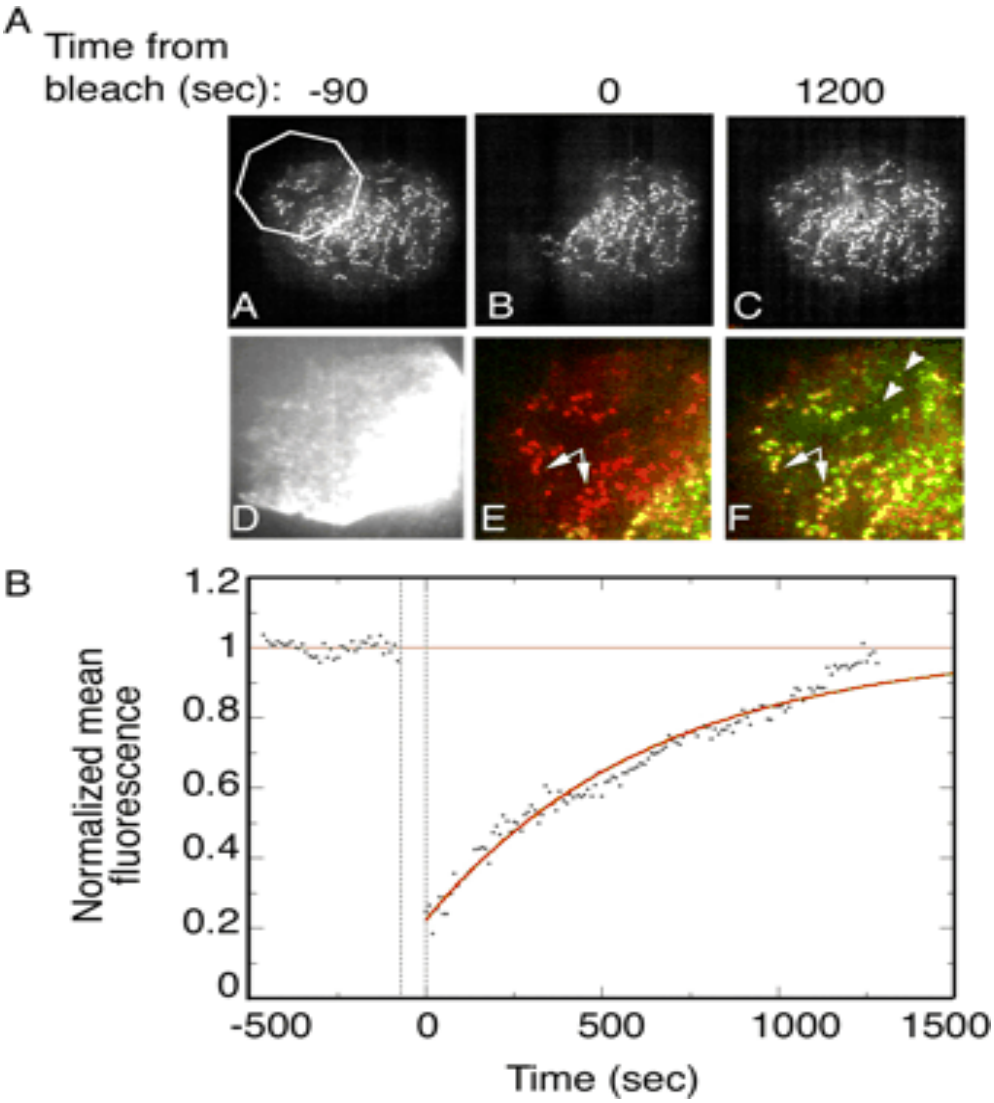

Figure 9. **Turnover of clathrin on regions of assembly.**
Cells expressing GFP-clathrin were imaged by TIRF-M for ~10 min to establish a base-line fluorescence intensity value. *A*, a region of the cell delineated by the polygon (shown in *panel A*, magnified in *panel D*) was bleached for 1.2 min. Images were then taken every 2 s for 25 min. Shown are images taken immediately before bleaching *(panel A*), during bleaching (*panel D*), immediately after bleaching (*panel B*), and 20 min after bleaching (*panel C*). The image in *panel A* was pseudo-colored *red*, and those in *panels B* and *C* were pseudo-colored *green*. *Panel E* is the overlap of the photobleached area of *panels A* and *B*, and *panel F* is the overlap of the photobleached area of *panels A* and *C*. Co localized voxels are in *yellow* and reveal extensive co-localization of newly assembled clathrin patches with those visible before bleaching. *B*, mean fluorescence intensity in the photobleached area over the course of the experiment. The half-time of recovery for this experiment was 638 s.

To determine whether large, persistent clathrin assemblies are competent for endocytosis, we simultaneously imaged GFP-clathrin and Alexa568-transferrin. Because only the fluorophore present within 100 nm of the coverslip surface is excited in TIRF mode, the fluorescence from transferrin bound to receptors at the plasma membrane is high enough relative to the fluorescence from transferrin in the buffer to provide an adequate signal to noise ratio. Soon after its addition to the medium, transferrin binding was observed both diffusely distributed and concentrated in regions of ~500 nm diameter over the entire surface (Fig. 10*A*, *top left panel*). Fluorescence in both areas increased steadily in the continuous presence of transferrin in the medium (Fig. 10*A*, *bottom left panel*). To determine the correspondence between regions of transferrin binding and of assembled clathrin, we superimposed masks of the clathrin images on corresponding transferrin images. Intense transferrin binding is seen in regions inside the mask, which correspond to large areas of persistent clathrin assembly (Fig. 10*B*, *upper panels, arrowheads*). The transferrin signal outside these regions is less intense and very diffuse at early time points (Fig. 10*C*, *upper panels*). After 10 min the transferrin signal within the clathrin mask remains intense (Fig. 10*B, lower panels, arrowheads*) but is now also seen in vesicular structures close to but outside the clathrin mask (Fig. 10*C*, *lower panels, arrows*).

To quantify these observations, we recorded total transferrin fluorescence (the product of total voxels and their mean intensity), as well as the concentration of transferrin (total intensity/number of voxels) inside and outside the clathrin mask over time (Fig. 10, *D* and *E*, respectively). Although the total amount of bound transferrin is

higher in the larger area outside the mask, the concentration of transferrin is higher inside than outside the mask throughout the time series (Fig. 10*E*). The greatest difference in concentration (~6-fold) is seen within the first few seconds (Fig. 10*F*), indicating that initial transferrin binding is on regions where clathrin is assembled (Fig. 10*F*). This is consistent with a higher concentration of transferrin receptors in clathrin-coated regions of the membrane at steady state.

After a few minutes, vesicular structures containing transferrin are seen outside the clathrin mask (Fig. 10*C*, *lower panels*) and appear to be emanating from regions of persistent clathrin assembly.

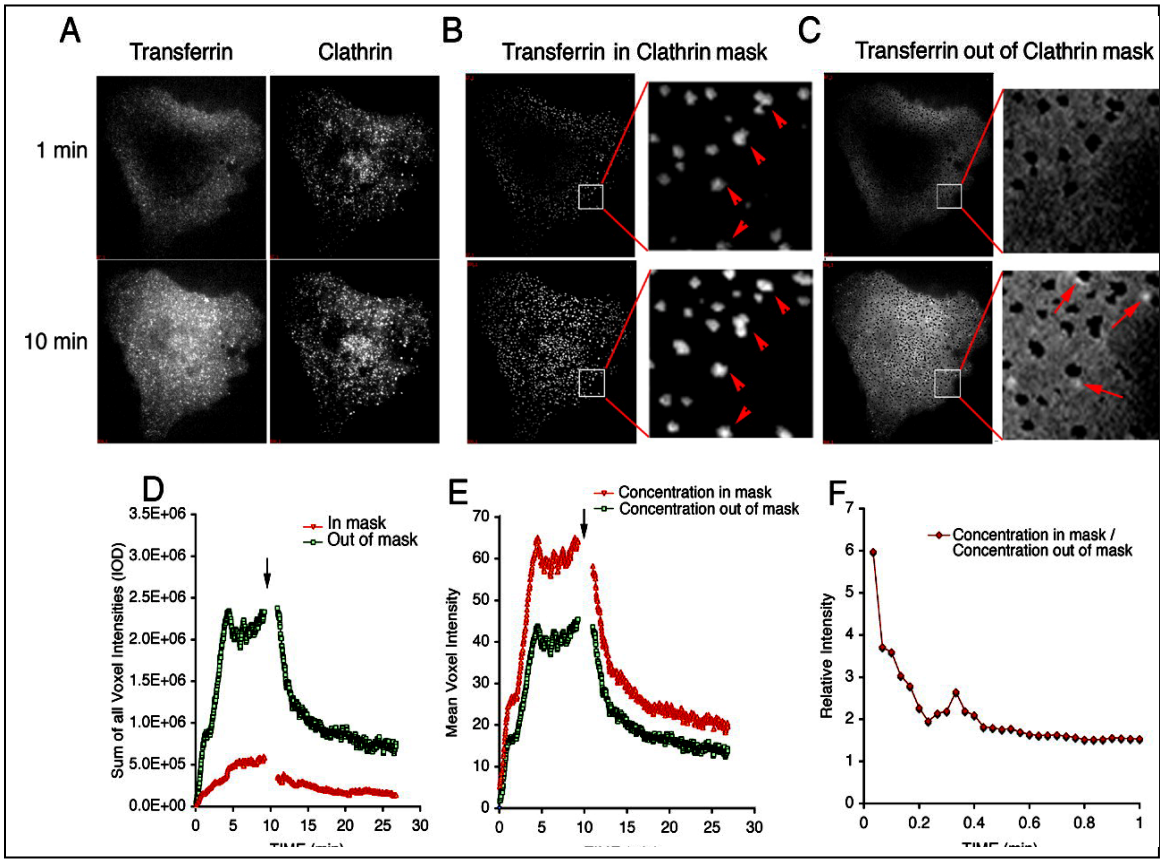

Figure 10. **Transferrin binding and uptake imaged by TIRF-M.**
A, COS cells expressing GFP-clathrin were incubated in the continuous presence of Alexa568-transferrin for the times indicated on the *left*. Shown are nonmasked images of clathrin (*right panels*) or transferrin (*left panels*). Masks of the clathrin images were superimposed on the transferrin images, and the signal inside the mask (*B*) or outside the mask (*C*) is shown. Magnifications of the areas demarcated by the rectangles are shown to the *right* of *each panel*. *Arrowheads* point to assemblies of clathrin persistent over the 10-min period of transferrin uptake, and *arrows* point to vesicular structures seen outside clathrin assemblies at 10 min after addition of transferrin. *D–F*, the transferrin signal inside the clathrin mask (*red trace*) or outside the clathrin mask (*green trace*) was expressed as the product of all voxels times their mean intensity (*D*), as the average voxel intensity (*E*), or as the ratio of voxel intensity inside and outside the masked areas (*F*). *Arrows* indicate the removal of fluorescent transferrin from the media.

Superimposition of clathrin and transferrin images illustrates this process (Fig. 11). Stable patches of clathrin (Fig. 11, *arrows*) become labeled rapidly upon addition of transferrin to the medium (notice the whiter appearance of the clathrin patches after time = 0, reflecting co-localization of GFP-clathrin and Alexa568-transferrin). Transferrin then appears in vesicular structures that emanate from the clathrin patches (Fig. 11, *arrowheads*). Transferrin accumulation within the cell distal from the plasma membrane was seen in epifluorescence images of the cells during this time (data not shown). When transferrin was removed from the medium, it gradually disappeared from clathrin patches, but the patches themselves remained present (Fig. 11, *arrows*; compare t = 0 with t = 18 min). These results demonstrate directly that transferrin endocytosis occurs through regions of persistent clathrin assembly.

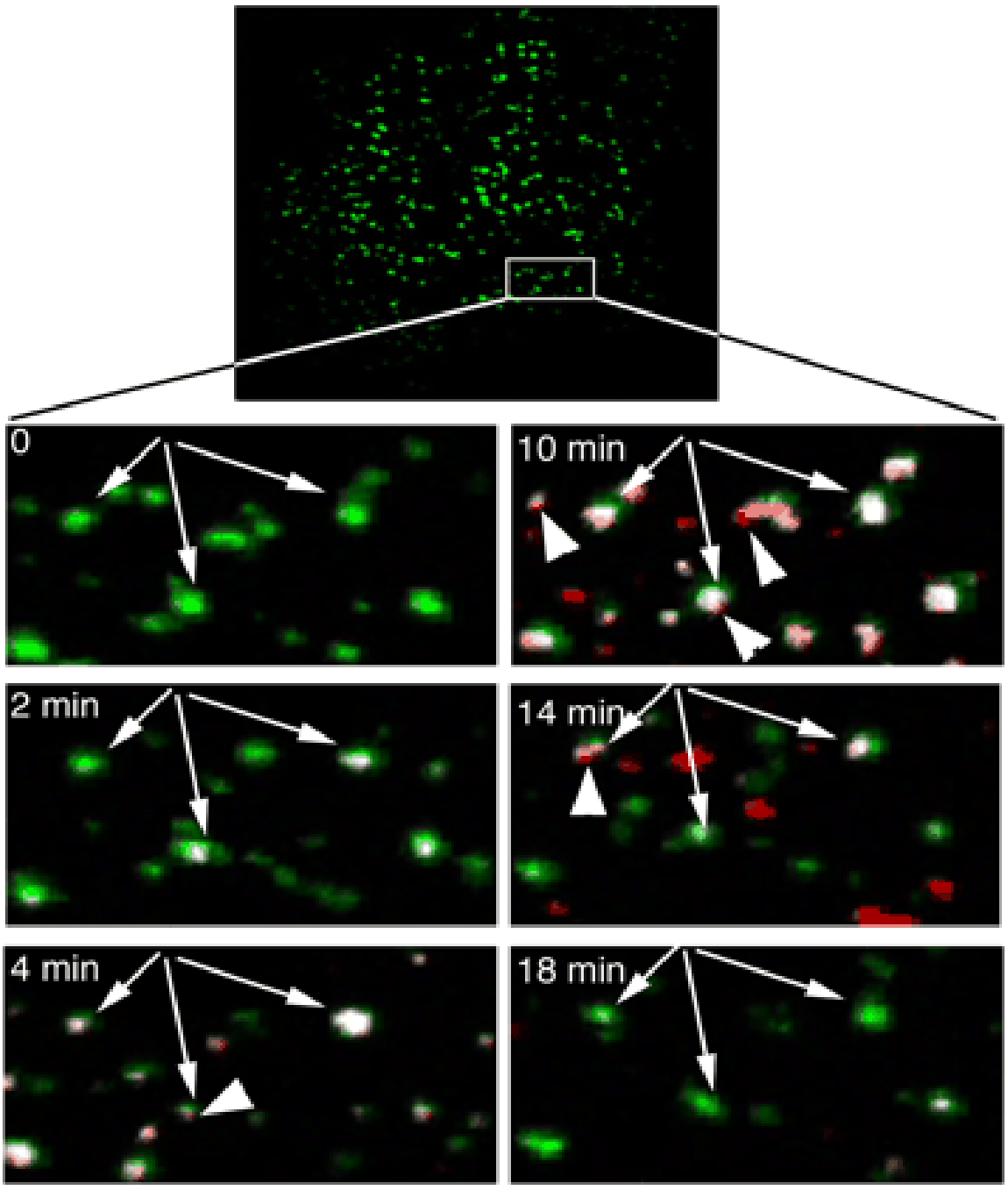

Figure 11. Uptake of transferrin through stable clathrin assemblies.
Cells expressing GFP-clathrin (*green pixels*) were continuously exposed to Alexa568-transferrin (*red pixels*) for 10 min and then washed to remove transferrin from the media. Shown are images from the time points indicated in the *upper left corner*. *Arrows* point to stable patches of clathrin that remained throughout the imaging period. *Arrowheads* point to examples of transferrin vesicles that formed from within the clathrin patches.

These results suggest that cargo-laden clathrin-coated vesicles are generated from within these larger clathrin assemblies. If so, fluorescence intensity fluctuations consistent with vesicle formation and detachment within these assemblies should be detectable at higher spatial and temporal resolution. To test this possibility we imaged clathrin patches at an optical resolution of 60 nm/pixel and at a rate of 50 Hz (50 images/s) for 60 continuous seconds. To rule out the possibility that observed intensity fluctuations might be due to nonbiological fluctuations in signal intensity (camera or laser noise) we re-imaged the same cells after fixation with 4% formaldehyde for 10 min followed by washes to remove the formaldehyde. Clear upward and downward fluctuations in intensity within clathrin patches were observed in live cells that were qualitatively different from the noise detected in the same patch after fixation (Fig. 12, *A* and *B*). The fluctuations seen in live cell patches resembled those seen when the process of coated pit formation from within a large patch was modeled mathematically (Fig. 12, *C–F*). These results are most consistent with the hypothesis that individual coated vesicles can bud off large clathrin arrays that form at specific sites on the plasma membrane. However, we cannot rule out the possibility that sites at the plasma membrane that support the assembly of compact clusters of many individual coated pits could also account for the data observed. Nevertheless, the results unambiguously demonstrate the existence of sites within the plasma membrane that preferentially support the formation of large clathrin assemblies competent for endocytosis.

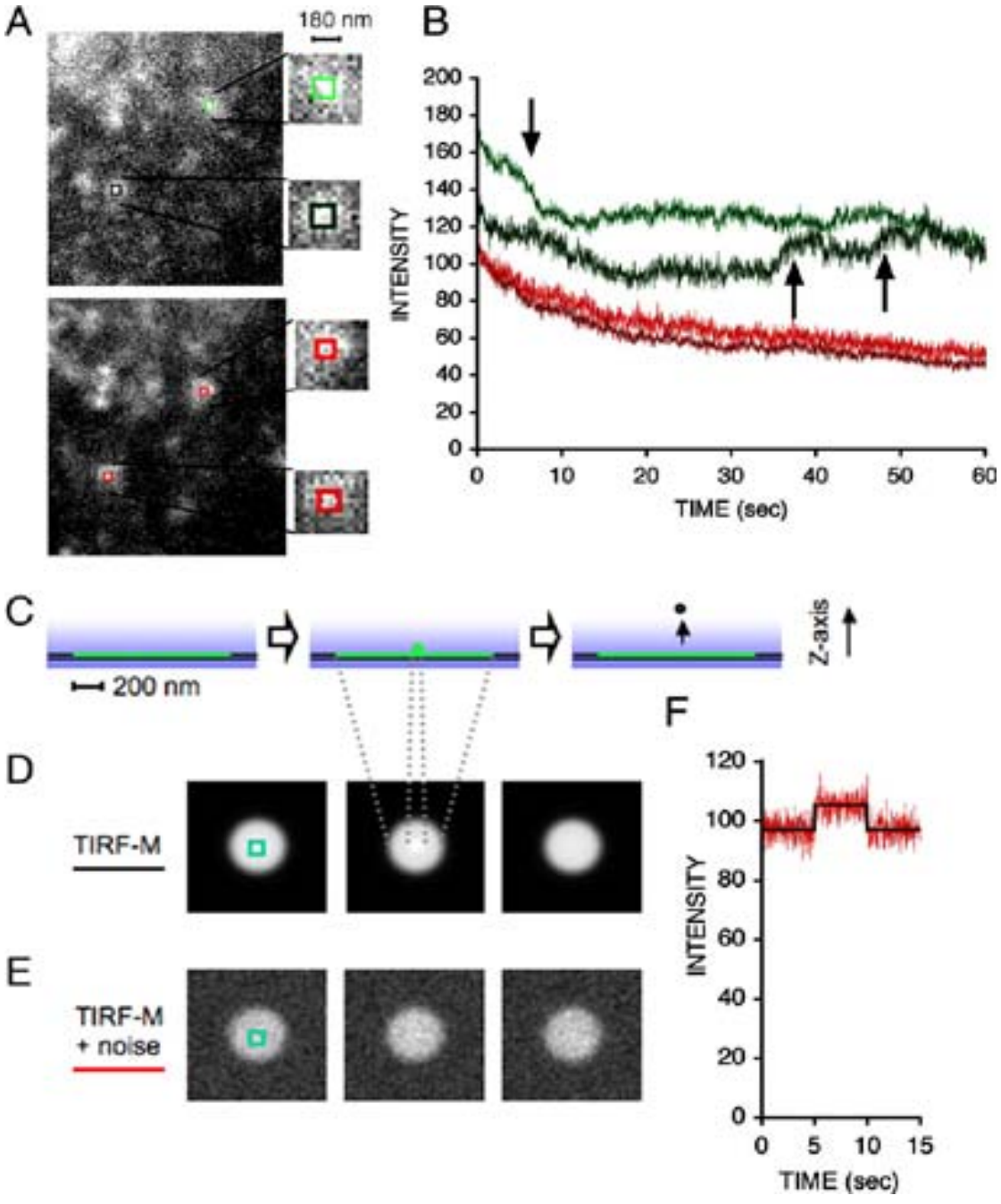
A
160 nm
B
INTENSITY
TIME (sec)
C
200 nm
Z-axis
D
TIRF-M
E
TIRF-M
+ noise
F
INTENSITY
TIME (sec)

Figure 12. High temporal resolution imaging of clathrin patches and simulation of TIRF imaging of a single clathrin-coated pit within a patch.

A, cells expressing GFP-clathrin were imaged by TIRF-M at a rate of 50 Hz (50 images/s). The mean fluorescence intensity within an 180 x 180-nm box centered on two separate patches on the cell surface was recorded before (*top panel*, *green rectangles*) or after (*bottom panel*, *red rectangles*) fixation with 4% formaldehyde and plotted in *B.* Clear upward and downward intensity fluctuations of several milliseconds duration are seen within patches before fixation (*arrows*), where only a steady decrease in intensity over time is seen after fixation, likely because of photobleaching. *C*, model used for the simulation, where a single, 50-nm diameter, clathrin-coated pit forms within a 1-μm diameter patch of clathrin (*green*) in the plasma membrane (*black line*). The vesicle remains attached to the patch for 5 s and then moves out of the TIRF field. *D*, simulation of the model in *C* imaged in TIRF with an exponential half-depth penetration of 90 nm at a rate of 50 Hz and scaled to match the intensities as shown in the data in *A*. The pit is faintly visible in the *middle panels*. *E*, same images as in *D* but with photon and charge-coupled device readout noise added as appropriate for the imaging conditions. The noise is great enough that the pit is no longer clearly visible in this single image. *F*, fluorescence intensity over time of the 3 x 3-pixel (180 nm) region centered over the pit (*green box*) for both the noiseless (*black*) and noisy (*red*) image sequences. The appearance of the pit causes a localized 8.7% increase in intensity in the patch that is approximately twice the noise levels in the measurement and is similar to the fluctuations seen in the actual cellular data shown in *A*.

Discussion

Diverse classes of clathrin assemblies have been seen by several groups[2, 11, 18, 81-83] when imaging fluorescent clathrin by TIRF-M, but the functional relevance of these assemblies remains unclear. Importantly, whether these types of assemblies occur physiologically in cells or are an aberrant response due to cell attachment to glass or plastic is not known. To address this question, we used primary adipocytes in which the buoyancy conferred by the fat globule renders the cells incapable of touching solid substrate. We find that the organization of clathrin on the membrane of isolated primary adipocytes is similar to that reported by others in cultured cells [2, 15, 17, 18, 80, 82] and is remarkable in that a large proportion of clathrin is found within large, apparently static assemblies.

These results raise two important questions: first, whether these large apparently static structures are competent for endocytosis and second, the molecular basis by which this organization is initiated and maintained. Experiments shown here indicate that large assemblies of clathrin support endocytosis. Our results are consistent with those of Merrifield *et al.* [15], who used a pH-sensitive transferrin receptor construct to determine the endocytic competence of cell surface clathrin assemblies and the timing of endocytosis relative to actin polymerization. Our results indicate that 60% of all clathrin assemblies persist for 60 s or more. Furthermore, by visualizing transferrin we have been able to follow the fate of the ligand as it transfers from these large assemblies into the endocytic pathway. Our results demonstrate that vesicles containing transferrin emanate from clathrin patches that are not consumed as transferrin is internalized. These regions

are not consumed, because clathrin is being continuously replaced into the patch from a pool of cytoplasmic clathrin, as evidenced by the recovery of fluorescence after photobleaching.

High temporal resolution imaging of clathrin patches also reveals fluorescence intensity fluctuations of several milliseconds within these assemblies; these fluctuations are qualitatively and quantitatively consistent with vesicle formation and detachment. Because both upward and downward regional fluctuations were observed, the results suggest that clathrin patches give rise to individual coated pits that form (upward intensity fluctuations) and detach (downward fluctuations), perhaps leaving small regions of uncoated membrane that can rapidly reassemble clathrin (Fig. 12). Whether clathrin patches contain a combination of flat arrays of clathrin as well as regions of coated pit clusters that rapidly assemble and disassemble cannot be distinguished at this point (Fig. 13). Regardless of this distinction, our results indicate unambiguously that clathrin organizes at the plasma membrane in specific persistent regions that are dynamic and support endocytosis.

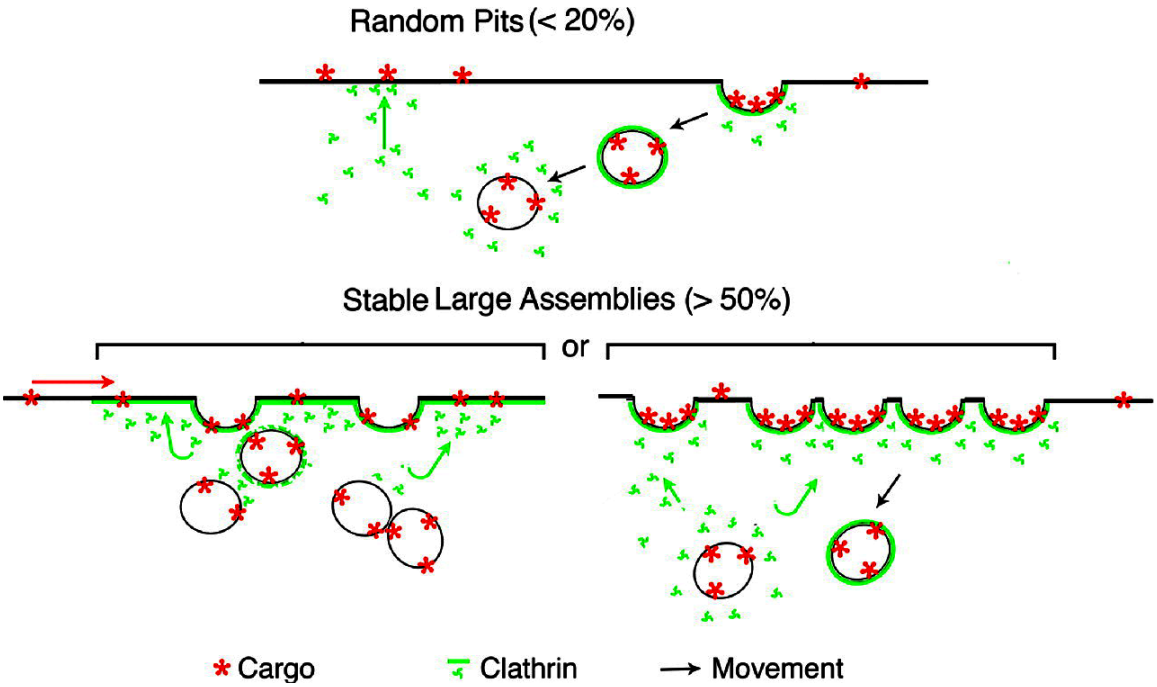

Figure 13. Model for clathrin organization.
Based on the quantification of all events on the adherent surface of primary and cultured cells presented here, the following model is proposed, where a subset of transient events (<20%) may be "randomly" initiated, and a larger subset (50–80%) occurs on defined, large regions on the plasma membrane. These regions may consist of flat lattices that give rise to individual coated vesicles (*left*) or clusters of l pits that form repeatedly on a defined region of the membrane (*right*).

Not all clathrin-mediated endocytic events take place from large assemblies [16]. In recent studies using spinning-disk confocal microscopy in which analysis was deliberately restricted to clathrin structures smaller than 3 pixels (600 nm) that appear and disappear within the imaging period of 7 min, the presence of cargo appeared to stabilize the transient assemblies of clathrin. These results suggested a model in which clathrin assembly at the plasma membrane occurs on random regions, which are then stabilized by the presence of cargo molecules. When restricted to the nonpersistent population of clathrin structures, and accounting for the fact that TIRF-M does not detect vesicles beyond 90–100 nm from plasma membrane assembly sites, the analysis of our data is not inconsistent with that reported by Ehrlich *et al.* [16] with regard to the kinetics of appearance and disappearance of this small subset of clathrin assemblies. However, our results demonstrating that large clathrin assemblies, which constitute the majority of the clathrin signal, are endocytically active underscore the importance of further investigation of the mechanism for initiation and maintenance of such assemblies.

The physiological significance of the organization of clathrin into large assemblies is not known. One possibility may be that the interaction of both clathrin and actin assembly factors with phosphoinositides such as phosphatidylinositol(4,5)P_2 may require organization around specific membrane regions enriched for these phospholipids. Further analysis of the spatial relationship between phospholipid metabolism and the different modalities of clathrin assembly may shed light on this important aspect of cellular architecture.

CHAPTER III

DYNAMIC REMODELING OF THE EARLY ENDOCYTIC PATHWAY FOR CARGO-SPECIFIC TRAFFICKING

This chapter is in the format submitted to Cell, as written by the authors, Deborah Leonard, Akira Hayakawa, Deirdre Lawe, Nachida Sitouah, Sylvie Boiteau, Edith Pfister, Anna Delprato, David Lambright, Karl Bellve, Clive Standley, Larry Lifshitz, Kevin Fogarty and Silvia Corvera

Imaging hardware and software was developed by Karl Bellve, Clive Standly, Larry Lifshitz and Kevin Fogarty. I performed all TIRF-M studies. GFP-Rab5 studies were performed by Anna Delprato and myself (Anna trasfected COS cells for imaging in the original experiment and I did the imaging and data analysis; all subsequent experiments were done in total by me.) The GFP-EEA1 experiments were done me. The EEA1 siRNA oligos were designed and characterized by Nachida Sitouah and Deirdre Lawe. All COS cell EEA1 siRNA knockdowns described were done by me. Akira Hayakawa prepared and validated the stable EEA1 knockdown Hela cells. The Tf and EGF binding studies with HeLa cells were done by Akira. EGFR degradation studies using EEA1 knockdown cells were done by me and repeated by two summer students working in our lab, Sylvie Boiteau and Edith Pfister.

Summary

EGF is a potent epithelial cell mitogen and EGFR internalization and degradation are required for appropriate cell growth control. We found within seconds of EGF binding to its receptor that EGF signals to key components of the endocytic pathway. We used TIRF-M to examine the early events of EGF endocytosis and found that EGFR liganded stimulation rapidly moves Rab5 to the plasma membrane, followed by an increase of the EGF-Rab5 vesicles with the EEA1 associated endosomes at the plasma membrane. In contrast, Tf binding to the TfR does not cause a redistribution of Rab5 at the plasma membrane; and there is no association of Tf vesicles with the EEA1 associated endosomes. Depletion of EEA1 by siRNA profoundly impaired EGF trafficking and EGFR degradation, but had no effect on Tf uptake nor Tf recycling. These data suggest that the early endocytic pathway rapidly remodels in response to cargo-specific trafficking signals and EEA1 plays an important and specific role in EGFR degradation.

Introduction

The EGF receptor (EGFR) plays an important role in epithelial cell proliferation [88-90], and enhanced signaling through this receptor is implicated in the genesis of cancers of the lung, breast and brain. The major mechanism by which EGF-stimulated signaling is limited is the process of endocytosis and degradation of the activated EGFR. Moreover, the regulation of the endocytic rate also determines qualitative aspects of signaling through the EGF and ErbB receptors, by defining the duration and intensity of diverse signaling [91]. Thus, a detailed understanding of the molecular mechanism of EGF binding and EGFR internalization is directly relevant to ongoing efforts to design cancer therapeutic agents based on EGF signaling.

The biochemical mechanism of EGFR downregulation involves the ubiquitination of its cytoplasmic domain, catalyzed by the ubiquitin-ligase Cbl [92-95]. When ubiquitination is prevented, EGFR recycle to the plasma membrane and display persistent activation [47]. In addition to the ubiquitination, EGFR degradation involves the actions of the ESCRT complex [36, 96] which is localized to endosomes that contain PtdIns(3)P, and is involved in recognizing ubiquitinated cargo. It remains unclear how the activated EGFR reaches ESCRT-containing endosomes following its clearance from the plasma membrane, and at what point it sorts away from other, non-lysosomally directed internalizing receptors, such as the transferrin receptor.

To address this question, we have used total internal reflection fluorescence (TIRF) microscopy, an imaging technique where only fluorophores residing within approximately 100 nm from the plasma membrane are illuminated [71, 97]. To study the

binding and internalization of EGF, we have visualized fluorescent EGF simultaneously with key components of the early endocytic pathway, including the small GTPase Rab5 and the PtdIns(3)P binding protein EEA1. Rab5 activity is required in the early steps of internalization from the plasma membrane [98], and EEA1 is a large coiled-coil dimer containing a FYVE domain at its extreme C-terminus that also interacts with the GTP-bound form of Rab5 [99-104]. EEA1 partially co-localizes with Hrs, one of the components of the ESCRT complex [105]. We have compared the early endocytic steps of EGF with that of transferrin, a non-lysosomally directed ligand believed to internalize by mechanisms similar to those of EGF.

We find that rapidly upon EGF binding Rab5 and EEA1 are recruited to the vicinity of the plasma membrane. Rab5 then concentrates in regions containing bound EGF, and the EGF/EGFR complex subsequently concentrates in endosomes containing EEA1. In contrast, no changes in the distribution of Rab5 or EEA1 are seen upon transferrin binding to its receptor, Rab5 is not actively concentrated in regions of transferrin binding, and transferrin does not concentrate in EEA1-enriched endosomes. Moreover, depletion of EEA1 by siRNA impairs EGF trafficking and EGFR degradation, but does not affect transferrin trafficking. These results indicate that the endocytic pathway rapidly remodels in response to the requirements of incoming cargo. A major role of EEA1 in this context may be to stabilize the interactions of incoming vesicles containing high concentrations of activated Rab5 with endosomes enriched in PtdIns(3)P, thus facilitating the transfer of specific incoming cargo into the ESCRT-dependent degradative pathway.

Results

EGF induces Rab5 recruitment to the TIRF zone.

Total internal reflection fluorescence (TIRF) microscopy is an imaging technique where only fluorophores residing within approximately 100 nm from the glass coverslip are illuminated [71, 97]. In previous studies of transferrin binding, we have found that the concentrated fluorescence from receptor-bound ligands on the plasma membrane is high enough relative to the diffuse fluorescence from un-bound ligand to provide an adequate signal to noise ratio and allow the direct visualization of ligand binding by TIRF-M [106]. When fluorescent EGF (50 ng/ml) is added to the media of Cos-7 cells at 35^{o}C, EGF binding to discrete punctate regions of the plasma membrane can be seen within 30 seconds (Figure 14*A, top panels*). The intensity of the EGF signal in the TIRF zone increases progressively, reaching a plateau after 8-10 minutes of continuous incubation (Figure 14*B*). Before addition of EGF, GFP-Rab5 can be seen distributed diffusely as well as in rapidly moving punctate, morphologically pleiotropic structures that appear and disappear from the TIRF zone (Figure 14*A, bottom panels*). Upon addition of EGF, the signal from GFP-Rab5 increases by 20% (42.7 +/- 1.0 vs 48.2 +/- 0.75, mean +/- standard deviation for 3 independent cells; values are the mean pixel intensity for images taken from -3 to 0 and 3-6 minutes before or after addition of EGF, respectively), both in the intensity of the diffuse component and in the number of punctate structures (Figure 14*A, bottom panels*), some of which co-localize with bound EGF (*arrows*). The increase in Rab5 intensity occurred within the first minutes after EGF binding (Figure 14*B*), suggesting that the stimulation of Rab5 redistribution occurs

very rapidly after activation of the EGFR by ligand binding.

The redistribution of Rab5 to the cell periphery can also be seen by epifluorescence (Figure 14*C*). In the absence of EGF, a substantial amount of GFP-Rab5 is concentrated in the perinuclear region, possibly representing Rab5 in its GDP-bound state [107]. GFP-Rab5 is redistributed from the perinuclear region to the cell periphery in response to EGF, where it extensively co-localizes with the ligand after 10 minutes of exposure. Thus, the redistribution of Rab5 to peripheral endocytic structures occurs rapidly and is sustained while EGF is present.

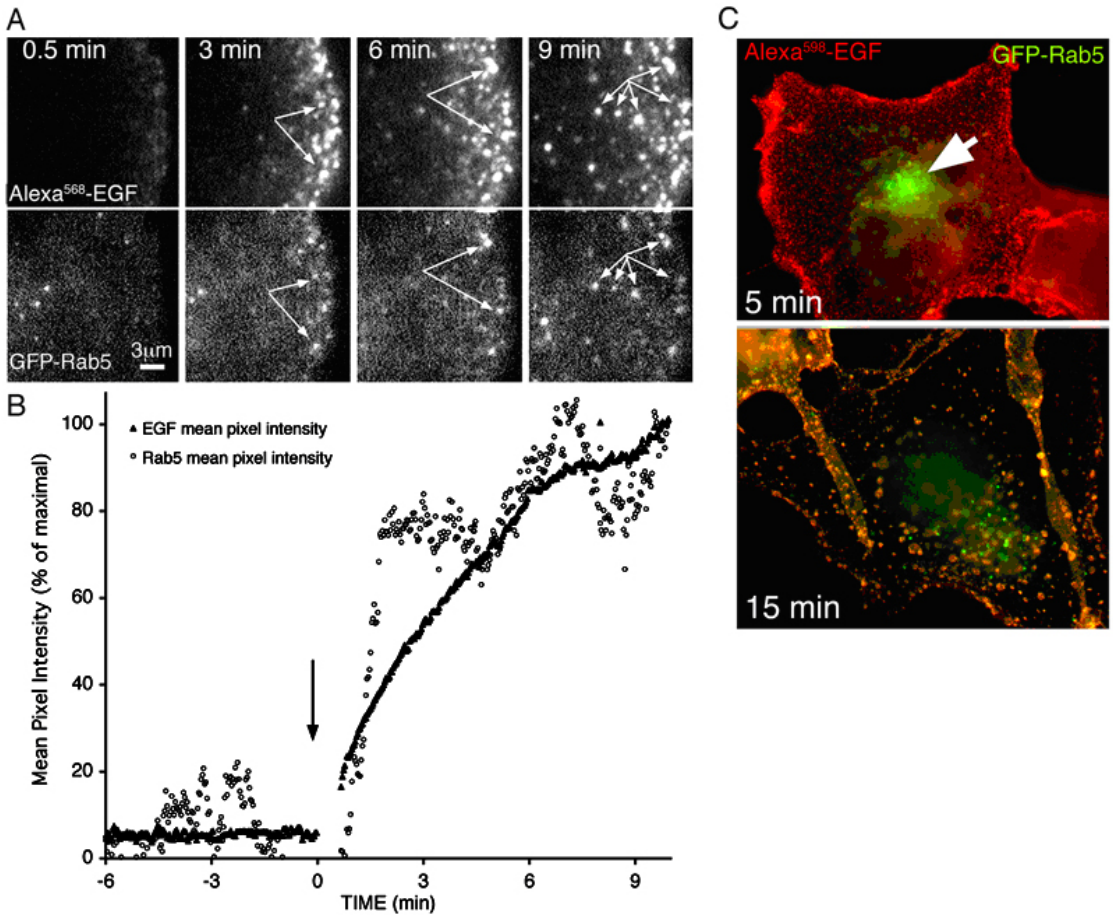

Figure 14. **EGF binding and co-localization with Rab5.**
A. Cos-7 cells expressing GFP Rab5 (bottom panels) were imaged by TIRF-M during continuous incubation with 50 ng/ml Alexa^{568}-EGF (top panels). Shown are unprocessed images from the time points after addition of Alexa^{568}-EGF indicated in the upper panels. Arrows point to regions of co-localization between the two signals. *B.* The intensity of each fluorophore within the whole adherent surface of the cell was calculated from masked images derived as described in the Methods. The trace shown is the average of four cells. The arrow represents the point at which Alexa^{568}-EGF was added to the media. *C.* Cells were fixed at the time points indicated and visualized by epifluorescence. The overlap between the signals is depicted in yellow. The arrow points to perinuclear GFP-Rab5 seen before EGF treatment.

EGF associates with Rab5-enriched structures

Inspection of TIRF-M and epifluorescence images suggests that EGF rapidly co-localizes with Rab5-enriched structures. To define the order of the steps that lead to this co-localization, we analyzed images acquired at a high temporal frequency (1 image/second) and compared the kinetics of EGF binding with the kinetics of EGF co-localization with Rab5 (Figure 15). A representative sequence of the images analyzed shows sub-domains containing bound EGF signal acquiring Rab5 signal, suggesting that co-localization occurs as a result of Rab5 being recruited into regions of activated EGFR (Figure 15*A*). Quantitative analysis of the images indicates that a statistically significant degree of co-localization between EGF and Rab5 (statistically different from spurious co-localization due to the high density of both signals in the same vicinity) is only seen after 2 minutes of EGF binding, which is subsequent to the observed recruitment of Rab5 to the TIRF zone (Figure 15*B*), which occurs within the first minute of EGF binding. The amount of co-localization of EGF with Rab5 increases with time, with almost 50% of the EGF signal co-localizing with Rab5 within 10 minutes of exposure of cells to the ligand. These results suggest that the sequence of events following EGFR activation is 1) the recruitment of Rab5 to the plasma membrane/TIRF zone and 2) concentration of Rab5 in domains containing activated EGFR.

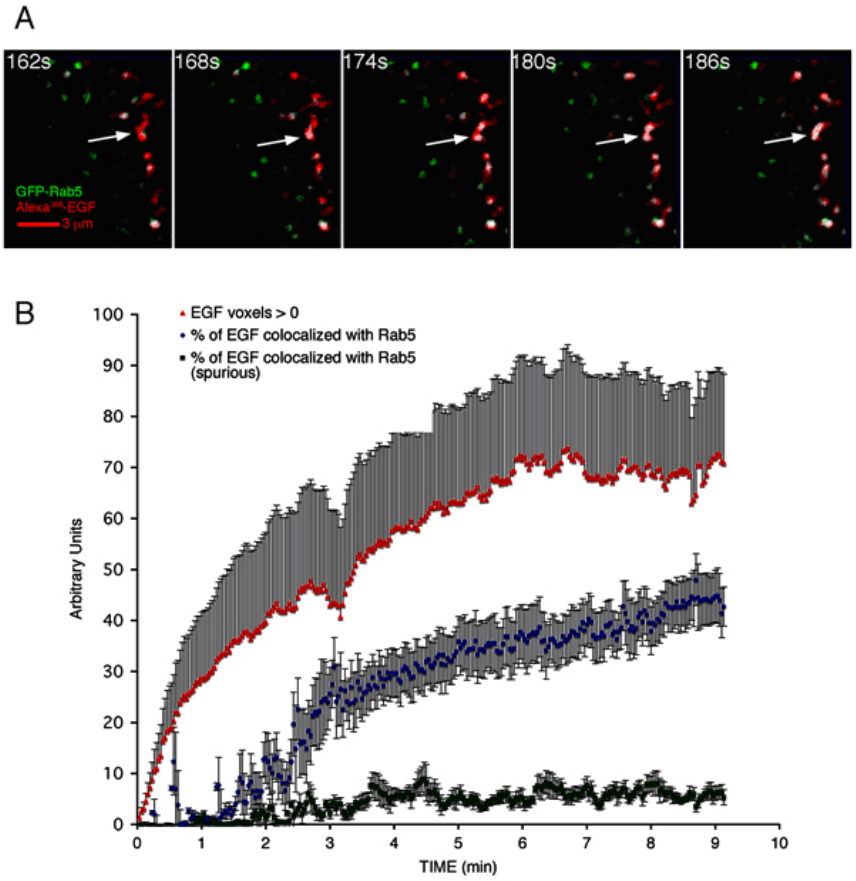

Figure 15. **Dynamics of EGF and Rab5 co-localization.**
A. Cos-7 cells expressing GFP-Rab5 were imaged by TIRF-M during continuous incubation with 50 ng/ml Alexa^{568}-EGF. The arrow points to a region containing bound Alexa^{568}-EGF, which becomes enriched in GFP-Rab5. Co-localized voxels are depicted in white. *B.* The mean intensity of Alexa^{568}-EGF over the adherent surface *(red trace)*. Co-localization with Rab5 *(blue trace)* expressed as percent of the total Alexa^{568}-EGF signal co-localized with GFP-Rab5 voxels in regions of the cell enriched in both signals. Spurious co-localization *(green trace)* was calculated by flipping one of the images along the X or Y axis. Plotted are the means and vertical lines are standard error of the mean of 2-3 regions from each of three independent cells.

EGF recruits EEA1-enriched endosomes to the TIRF zone, and is retained in or close to these endosomes.

To determine the fate of Rab5- and EGF-enriched peripheral structures, we analyzed the dynamics of EGF internalization relative to EEA1 (Figure 16). EEA1 resides on endosomes containing PtdIns(3)P, and can interact with Rab5-GTP through domains at its N- and C- terminus [99-101, 103]. EEA1 has been hypothesized to function as a tether mediating early endosome fusion. While the majority of endosomes containing EEA1 were found distributed throughout the cytoplasmic volume, a significant number could be seen within the 100 nm TIRF zone. Fluorescent EGF bound to the periphery of the cell onto discreet structures lacking EEA1 (Figure 16*A*). Three minutes after addition to the media, EGF co-localization with EEA1 was seen in some endosomes (Figure 16*A*, *arrows*), and significant co-localization (statistically significantly different from spurious) was consistently measurable after 4 minutes (Figure 16*B*). Co-localization of EGF with EEA1 continued to increase over time even while the total amount of EGF signal in the TIRF zone reached a plateau, indicating that EGF is retained and concentrated in these endosomes (Figure 16*B*).

In many cells, large endosomes enriched in EEA1 could be seen appearing at the periphery of the cell within the TIRF zone, and associating with the small vesicular structures carrying EGF (Figure 16*C*), which seemed to tether outside and inside the EEA1-coated surface. The appearance of these endosomes was not observed in the absence of EGF, and could be quantified as a small but statistically significant increase in the mean pixel intensity of EEA1 in the TIRF zone, measured over the entire area of the

cell (748 +/- 14 vs 914 +/- 5, mean +/- standard deviation of intensity values in the 0.5 minute interval before EGF addition and between 7 and 7.5 minutes after EGF addition. Results are derived from 3 independent experiments). Thus, EGF enhances the appearance or formation of EEA1-enriched endosomes in the TIRF zone, and vesicles containing EGF progressively co-localize with these endosomes. Together, the analyses of the relationship between EGF and Rab5, and of EGF and EEA1 suggest that Rab5 is recruited to the vicinity of EGF/EGFR complexes, and EGF/EGFR/Rab5-enriched structures then associate with EEA1-enriched endosomes, some of which are newly recruited to the TIRF zone. The direct comparison of the kinetics of co-localization between EGF and Rab5, and between EGF and EEA1 (Figure 16*D*) suggests that EGF populates Rab5-enriched structures approximately 2 minutes prior to populating EEA1-enriched endosomes. Because a high degree of EGF co-localization with Rab5 is seen for at least 10 minutes after initial binding, we infer that EGF, Rab5 and EEA1 co-reside in endosomes after approximately 4 minutes of EGF binding to the cell surface. By stimulating the recruitment of both Rab5 and EEA1-enriched endosomes into the TIRF zone, EGF causes a remodeling of the endocytic pathway as it traffics from the plasma membrane into the endosomal system.

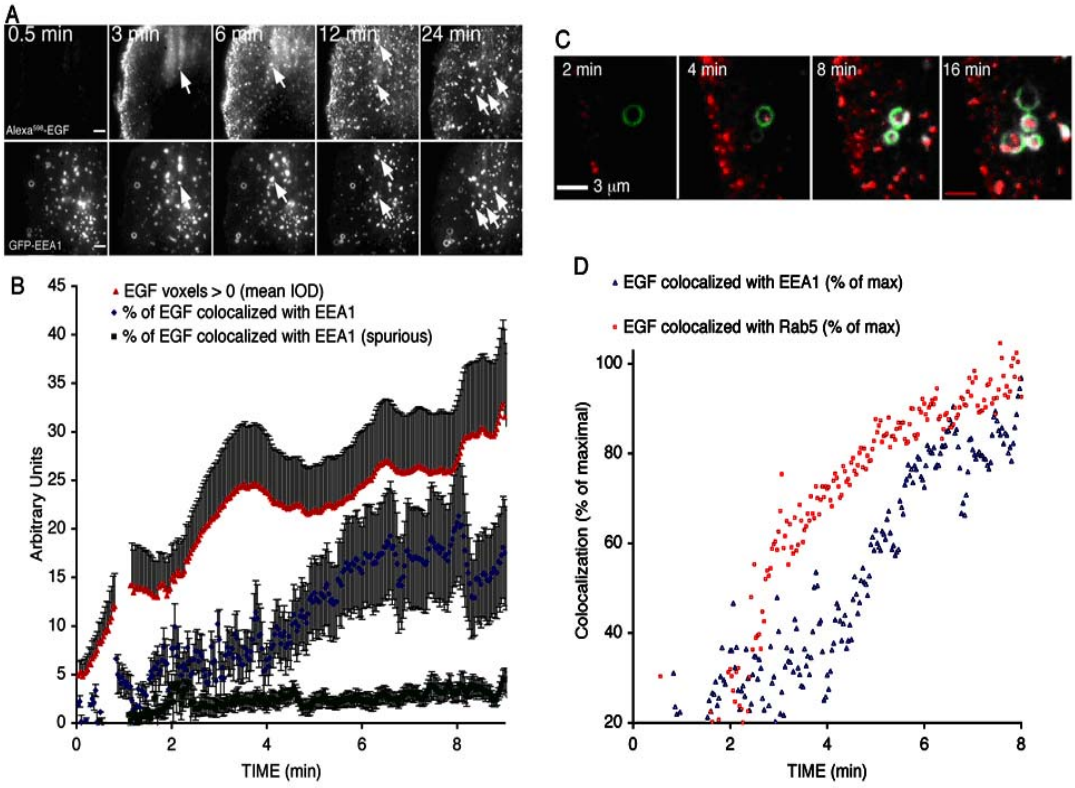

Figure 16. **Dynamics of EGF and EEA1 co-localization.**
A. Cos-7 cells expressing GFP-EEA1 *(bottom panels)* were imaged by TIRF-M during continuous incubation with 50 ng/ml Alexa^{568}-EGF *(top panels)*. Shown are unprocessed images from the time points after addition of Alexa^{568}-EGF indicated in the upper panels. Arrows point to regions of co-localization *(white voxels)* between the two signals. *B*. The mean intensity of Alexa^{568}-EGF over the adherent surface *(red trace)*. Co-localization with GFP-EEA1 *(blue trace)* expressed as percent of the total Alexa^{568}-EGF signal co-localized with GFP-EEA1 voxels, calculated using regions of the cell enriched in both signals. Spurious co-localization *(green trace)* was calculated by flipping one of the images along the X or Y axis. Plotted are the means and vertical lines are standard error of the mean of 2-3 regions from each of three independent cells. *C*. Higher magnification of a region containing ring-like endosomes enriched in EEA1 *(green)*, over time of incubation with Alexa^{568}-EGF *(red)*. Voxel overlap is depicted in white. *D*. Kinetics of co-localization of Alexa^{568}-EGF with either GFP-Rab5 *(red symbols)* or GFP-EEA1 *(blue symbols)*, expressed as the maximum degree of co-localization observed in the first 8 minutes after addition of Alexa^{568}-EGF. Points represent the mean values from 2-3 regions of 3-4 independent cells. Error bars are omitted for clarity.

Differences between EGF and Transferrin endocytic trafficking.

The EGFR is thought to internalize via a pathway similar to that of the transferrin receptor (TfR). However, while a large proportion of internalized EGFR is degraded, the TfR recycles to the plasma membrane. We therefore analyzed the trafficking of transferrin relative to Rab5 and EEA1, to determine the degree to which it resembles that of EGF. In contrast to EGF, addition of transferrin did not elicit a redistribution of Rab5 into the cell periphery (138 +/- 5 and 132 +/- 4, Mean +/- SEM values for minutes -1 to 0, and 4 to 5 from the addition of transferrin. P=0.43, from 5 independent experiments). When visualized by TIRF-M (Figure 17*A*), fluorescent transferrin bound to the entire adherent surface of the cell diffusely, as well as in punctate regions corresponding to clathrin-coated membrane domains [106]. With time, transferrin accumulated in Rab5-enriched structures, which were mobile and rapidly disappeared from the TIRF zone. Significant co-localization between transferrin and Rab5 was seen within a minute of transferrin binding, and plateaued after 4-5 minutes, when approximately 40% of the transferrin signal co-localized with Rab5 (Figure 17*B*). This behavior contrasts with that of EGF, where significant co-localization with Rab5 was not seen before 2 minutes, but continued to increase after 5 minutes of EGF binding (Figure 15*B*). Furthermore, the amount of Rab5 co-localized with EGF or transferrin also differed significantly, being 30.6 +/- 1.5 and 18.9 +/- 0.8 percent of the total Rab5 signal in the TIRF zone after 5 minutes of exposure to EGF or transferrin, respectively ($p<0.001$). Thus, while EGF and transferrin receptors both associate with Rab5-enriched endocytic regions early after binding, these associations are kinetically and quantitatively very different.

With time, transferrin accumulated in more vesicular structures, but only a few of these appeared to correspond to EEA1-enriched endosomes within the TIRF zone (Figure 17*C, arrows*). Nevertheless, statistical analysis indicates a small but significant degree of co-localization of transferrin with EEA1-enriched endosomes after approximately 2 minutes of transferrin binding (Figure 17*D*). The co-localization of transferrin with EEA1 remained at a constant low level (~15%), despite a progressive increase in transferrin signal within the TIRF zone. This behavior contrasts with that of EGF which increases its co-localization with EEA1 even after EGF accumulation in the TIRF zone begins to saturate (Figure 16*B*). These results suggest that transferrin/TfR complexes may traffic near or through EEA1–enriched endosomes near the plasma membrane, but are not retained near or within these structures. Furthermore, while the mean intensity of EEA1 signal in the TIRF zone increased in response to EGF, it remained unchanged upon addition of transferrin.

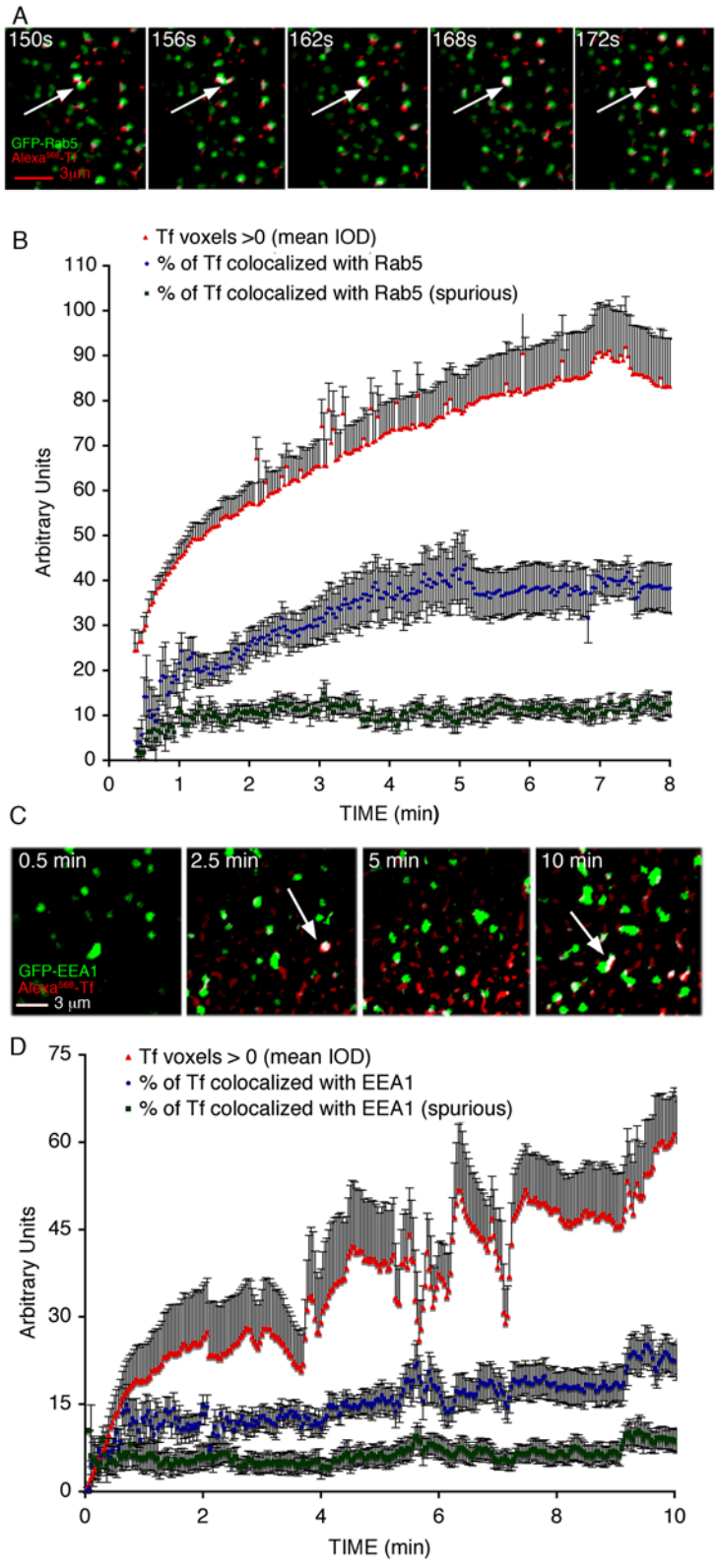
A
150s
156s
162s
168s
172s
GFP-Rab5
Alexa568-Tf
3μm
B
Tf voxels >0 (mean IOD)
% of Tf colocalized with Rab5
% of Tf colocalized with Rab5 (spurious)
Arbitrary Units
TIME (min)
C
0.5 min
2.5 min
5 min
10 min
GFP-EEA1
Alexa568-Tf
3 μm
D
Tf voxels > 0 (mean IOD)
% of Tf colocalized with EEA1
% of Tf colocalized with EEA1 (spurious)
Arbitrary Units
TIME (min)

Figure 17. **Dynamics of Transferrin co-localization with Rab5 and EEA1.** *A*. Cos-7 cells expressing GFP-Rab5 *(green)* were imaged by TIRF-M during continuous incubation with 20 ug/ml Alexa^{568}-Transferrin *(red)*. The arrow points to a enriched in GFP-Rab5 acquiring Alexa^{568}-Transferrin (Tf). Co-localized voxels are depicted in white. *B*. The mean intensity of Alexa^{568}-Tf over the adherent surface over time of continuous incubation *(red symbols)*. Co-localization with Rab5 *(blue trace)* expressed as percent of the total Alexa^{568}-Tf signal co-localized with GFP-Rab5 voxels, calculated using regions of the cell enriched in both signals. Spurious co-localization *(green trace)* was calculated by flipping one of the images along the X or Y axis. Plotted are the means and vertical lines are standard error of the mean of 2-3 regions from each of four independent cells. *C*. Cos-7 cells expressing GFP-EEA1 *(green)* were imaged by TIRF-M during continuous incubation with 20 ug/ml Alexa^{568}-Tf *(red)*. Arrows point to regions of co-localization *(white voxels)* between the two signals. *D*. The mean intensity of Alexa^{568}-transferrin over the adherent surface *(red trace)*. Co-localization with GFP-EEA1 *(blue trace)* expressed as percent of the total Alexa^{568}-Tf signal co-localized with GFP-EEA1. Spurious co-localization *(green trace)* was calculated by flipping one of the images along the X or Y axis. Plotted are the means and vertical lines are standard error of the mean of 2-3 regions from each of three independent cells.

EEA1 is necessary for EGF but not for transferrin endocytic trafficking.

The differences in trafficking between EGF and transferrin relative to EEA1-enriched endosomes suggested the possibility that EEA1 may have a specific role in trafficking of EGF receptors. To test this hypothesis we studied the effects of EEA1 depletion using RNA interference. EEA1 was depleted from Cos-7 cells using siRNA oligonucleotides, and the trafficking of transferrin was visualized. There was no noticeable difference in the amount or distribution of transferrin in cells with high or low amounts of EEA1, assessed by immunofluorescence (Figure 18*A*).

To quantitatively analyze the trafficking of transferrin, we generated a stable HeLa cell line harboring a shRNA directed to EEA1 (Figure 18*B*). The levels of EEA1 mRNA in these cells (KO cells) were approximately 30% of those in control HeLa cells stably expressing a non-specific shRNA (NC cells). The levels of EEA1 protein were decreased by 80-90% as assessed by western blotting and immunofluorescence (Figure 18*C* and *D*). The levels of transferrin receptors (Figure 18*C*) and the kinetics of transferrin uptake (Figure 18*E*) and recycling (Figure 18*F*) in these cells were indistinguishable between KO and NC cells.

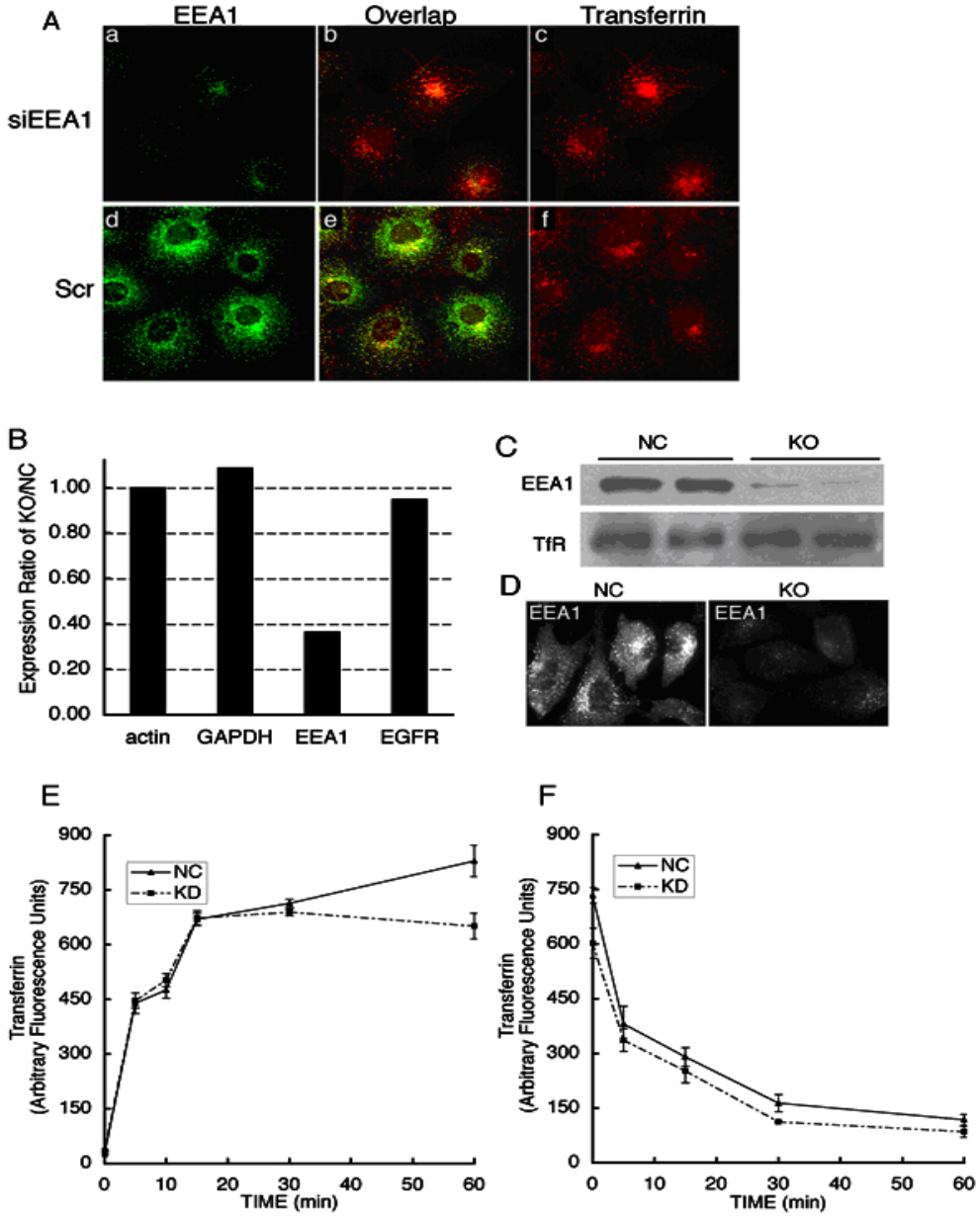

Figure 18. **Effect of EEA1 knockout on transferrin trafficking.**
A. Cos-7 cells were treated with siRNA oligos to EEA1 or scrambled, and then incubated with 20 ug/ml Alexa^{568}-Transferrin *(red)*. Cells were fixed, permeabilized and stained for endogenous EEA1 *(green)*. *B.* Real time quantitative PCR in Hela cells stably expressing a control shRNA (NC) or an EEA1-directed shRNA (KO). The mRNAs examined are indicated along the X-axis. *C.* Western blotting of EEA1 and transferrin receptor (TfR) in two independent stable clones. *D.* NC or KO cells stained for endogenous EEA1. Kinetics of transferrin uptake *(E)* or recycling *(F)* in NC and KO cells. Plotted are means and lines are SEM of three experiments performed in duplicate.

Interestingly, western bloting consistently revealed an increased level of EGFR in KO cells compared to NC cells (Figure 19*A*). Because the levels of EGFR mRNA were indistinguishable between NC and KO cells (Figure 18*C*) these results suggest that the rate of EGFR degradation at steady state may be decreased in the KO cells. To directly test this hypothesis, the rate of EGF-stimulated EGFR degradation was measured (Figure 19*B* and *C*). In NC cells the EGFR was almost completely degraded 60-180 minutes after exposure of serum-starved cells to EGF. In contrast, at least 50% of the EGFR remained present in KO cells after a similar exposure. These results reveal a specific defect in trafficking of the EGFR in response to depletion of EEA1.

We further explored the mechanism by which EEA1 depletion results in impaired EGFR degradation. We first tested the possibility that EEA1 depletion might result in defective formation of PtdIns(3)P enriched endosomes. To detect PtdIns(3)P-containing structures we expressed the monomeric FYVE domain of Hrs fused to GFP-Fv, the binding protein for the membrane permeable dimerizer AP20187, which we have previously characterized [108]. In the absence of dimerizer, GFP-HrsFYVE-Fv was localized to the cytosol (not illustrated), but translocated to endocytic structures in response to dimerizer (Figure 19*D, top panels*). Endosomal structures were present in both NC and KO cells. To determine whether EEA1 knockdown rendered endosomes incapable of fusion, we expressed persistently activated Rab5. GFP-Rab5Q79L was localized to greatly enlarged endosomes in both NC and KO cells (Figure 19*D, bottom panels*). These results suggest that the machinery for PtdIns(3)P-enriched, Rab5-enriched endosome formation and fusion is unimpaired in the near absence of EEA1, yet EGFR

degradation is significantly impaired. These results suggest that the role of EEA1 in EGFR trafficking may be to promote the sorting of EGFR into the PtdIns(3)P-enriched, ESCRT-containing degradative pathway.

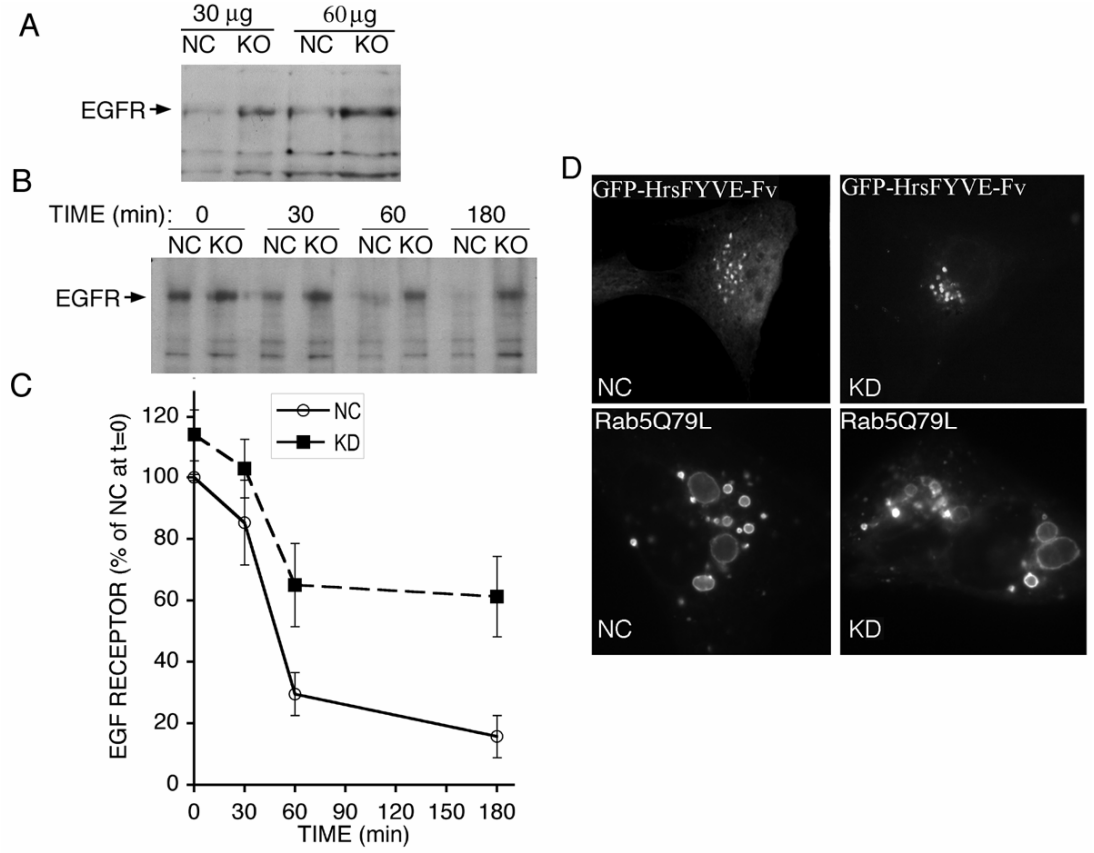

Figure 19. **Effect of EEA1 knockout on EGFR trafficking.**
A. Extracts (30 and 60 ug of total protein) from Hela cells stably expressing a control shRNA (NC) or an EEA1-directed shRNA (KO) were analyzed by western blotting with anti-EGFR antibodies. A major band at the expected molecular weight of the EGFR is indicated by the arrow. *B.* Cells were serum starved, and incubated in the presence of cycloheximide and EGF for the times indicated. Extracts were analyzed by western blotting with anti-EGFR antibodies. *C.* Densitometric analysis of EGFR bands. Plotted are the means and lines represent SEM of four independent experiments. *D.* NC *(left panels)* and KO cells *(right panels)* were transfected with GFP-Hrs-FYVE *(top panels)* or GFP-Rab5Q79L *(bottom panels)*. Cells expressing GFP-Hrs-FYVE were treated with dimerizer for 45 min.

Discussion

The use of TIRF-M coupled with quantitative fluorescent image analysis has allowed us to define the sequence of events involved in the earliest phases of EGF internalization, and compare them with those of another cargo molecule, transferrin. Our results reveal that EGF internalization occurs by a sequence of events that include a) the translocation of Rab5 to the plasma membrane region, b) the concentration of Rab5 around activated EGFR, and c) the subsequent retention of Rab5 enriched, EGFR-containing vesicles by EEA1-enriched endosomes. In contrast, Rab5 is not actively concentrated in vesicles containing incoming transferrin, and these fail to be retained in EEA1-enriched endosomes. This visual information is consistent with prior biochemical studies showing an activation of Rab5 in response to EGF [107], and leads to novel, testable hypotheses on the significance of this activation in the context of EGFR trafficking. The qualitative and quantitative comparison between the trafficking of EGF and transferrin relative to Rab5 and EEA1 also suggest specific hypotheses on the general principles that govern sorting in the endocytic pathway.

The process of internalization of cargo molecules is classically thought to require their interaction with one of several endocytic pathways that continuously operate at the plasma membrane, which include clathrin-dependent and clathrin-independent mechanisms. These pathways deliver cargo to the endosomal system, where sorting decisions are made. For the most, it is assumed that the internalization and sorting machineries operate at a continuous pace, and endocytosis and sorting occur as a function of the affinity between a specific cargo molecule and one endocytic/sorting pathway. In

this view, endocytosis and sorting of cargos to different cellular destinations involve qualitatively distinct internalization and sorting machineries. However, an alternative view, supported by the results shown here, is that cargo sorting may be determined by quantitative mechanisms involving qualitatively similar elements of a single sorting machinery. Specifically, our results suggest that the effect of EGF to rapidly recruit activated Rab5 to the activated EGFR, and to enter the cell in vesicles containing a large amount of active Rab5 may result in the enhanced retention of EGFR-enriched vesicles by EEA1-enriched endosomes, and thereby perhaps facilitate fusion of such vesicles with these endosomes. In contrast, vesicles containing lower amounts of Rab5, carrying for example the transferrin receptor, may interact weakly with EEA1, fail to be retained by EEA1- enriched endosomes, and progress to a different stage in the endocytic pathway. Thus, the remodeling of the endocytic pathway, where similar elements (e.g Rab5 GTPase) operate with greater or lower efficiencies, leads to cargo-specific sorting mechanisms.

This hypothesis is consistent with much of the biochemical and morphological data reported by other investigators working on either EGF or transferrin trafficking. They are consistent with the reported stimulatory effects of EGF on Rab5 activation and EEA1 recruitment to endosomes [107] , with the presence of EGF and EGFR in EEA1-enriched endosomes following internalization[109], and the interaction between activated Rab5 and EEA1 [101, 103, 110]. The model is also consistent with the finding that several receptors, including the TfR [56], the m4 muscarinic acetylcholine receptor [111], and the EGFR in the absence of EGF [112]are downregulated from the cell surface and

accumulate in EEA1-enriched Rab5-enriched endosomes only when persistently active forms of Rab5 are expressed, suggesting that the level of activated Rab5 determines retention in EEA1-enriched endosomes, and prevents progression of cargo into the recycling pathway. It also raises the question of the mechanism by which EGFR activation can so rapidly lead to Rab5 activation and recruitment to the vicinity of the plasma membrane. Further experiments in which the ability of known Rab5 exchange factors [113, 114]to enhance Rab5 recruitment to the TIRF zone, and its further concentration around EGFR will be necessary to answer these questions.

The results shown here also reveal the specific role of EEA1 in the endocytosis pathway. EEA1 interacts with PtdIns(3)P and with activated Rab5 through two distinct C-terminal and N-terminal binding sites, and has been proposed to facilitate early endosome fusion by functioning as a tether between endosomes [99-101, 104, 115]. However, the presence of EEA1 in subsets of early endosomes suggested a more specific function for this protein [116]. Moreover, EEA1 is not particularly well conserved among species, being absent in D. melanogaster and in S. cereviseae, again suggesting a more specialized role for this protein in the context of specific trafficking pathways or regulatory mechanisms. The finding that EEA1 is enriched in endosomes in which EGFR is retained, and is important for EGFR down regulation but not for transferrin uptake or recycling suggests that this protein may function to target specific incoming cargo into the subset of endosomes destined to form multivesicular bodies and eventually direct cargo toward lysosomal degradation. This function could be realized by the interaction of Rab5 present in incoming vesicular cargo with the N-terminal Rab5

binding domain of EEA1 [101, 103]. The images obtained in these studies also reveal that EEA1 enriched endosomes are recruited to the cell periphery in response to EGF signaling. The appearance of these endosomes is likely to result from enhanced recruitment of EEA1 to their surface. Because EEA1 binds to endosomes through interactions between its FYVE domain and PtdIns(3)P, it is possible that changes in the levels of this lipid in response to EGF may underlie this effect. Alternatively, Rab5 activation in response to EGF may also lead to enhanced EEA1 binding to endosomes through the C-terminal Rab5 interacting domain [110]. Further experiments will be required to test these possibilities.

Experimental Procedures

Optical system: Epi-fluorescence imaging was done using a Zeiss Axiovert 200 inverted microscope (Thornwood, NY); with a Zeiss 100 X 1.40 NA oil-immersion objection and equipped with a Zeiss AxioCam HR CCD camera with 1,300 X 1,030 pixel resolution. For TIRF imaging, two Coherent Innova 70C lasers are used. An Argon ion and an Argon-Krypton ion lasers are used to produce the 488 and 568 nm light respectively. The combined beams are coupled into a single mode fiber using a KineFLEX fiber coupler manufactured by Point Source. A modified Olympus IX81 inverted microscope, a modified Olympus TIRF fiber illuminator, and an Olympus Plan APO 60x objective with an NA of 1.45 are used. TIRF illumination is introduced through the edge of the objective at an angle set between 65 and 68 degrees giving a penetration depth of 90-121 nm at 488 nm and 105-141 nm at 568 nm. Light is collimated through the objective and a layer of immersion oil onto the cover-slip. The quality of the collimation is set half way between the best for 488 nm and 568 nm. Light from the fluorophores is collected and relayed onto a 640 x 448 pixel CCD camera developed with Lincoln Labs (MIT). A Physik Instruments pifoc is used for fine focus control. The entire microscope is contained in a heated chamber held at 35^{o}C. Imaging hardware and software were previously described [106].

For quantitative image analysis, the following strategy was used: First, raw images were corrected by subtracting the background fluorescence outside the cell. Second, a running average of three time points comprising a 4 second interval was generated, which removed slight speckling due to camera noise but had a negligible

effect on the data. Third, images were smoothed by convolving with a small, 2-dimensional Gaussian spot (s =160 nm) that preserved the mean intensity. The local background around punctate structures was estimated by convolving with a larger, 2-dimensional Gaussian (s =320 nm) and subtracting this from the smoothed images. From this we generated a binary masking image by setting the intensity of all positive-valued pixels to one and all other pixels to zero, and multiplied the mask by the original image to display areas in the image with intensity exceeding the average local background. The masked images were then used to measure the pixel intensities and co-localization over the entire adherent surface of the cell.

Fluorescent probes, antibodies and cells: Alexa^{568or594}transferrin, Alexa$^{568or\ 594}$-EGF obtained from Molecular Probes, (Eugene, OR) were applied to the cells at 20 µg/ml and 50 ng/ml respectively. Rab5c and EEA1 constructs were as previously described [110, 115]. In the experiments described here, Cos-7 cells were transfected using 1-4 µg of plasmid DNA using calcium phosphate transfection, and imaged 48 hr later. Cells were transferred from complete media to KRH (NaCl (125 mM), KCl (5 mM), $CaCl_2$ (1.3 mM), $MgSO_4$ (1.2 mM), HEPES pH 7.4 (25 mM), sodium pyruvate (2 mM), and bovine serum albumin (2.5% BSA) just prior to imaging. All imaging procedures were performed at 35^{o}C. Chicken anti-EEA1 was previously described (Hayakawa, et al., 2006), and mouse anti-human transferrin receptor was purchased from Zymed laboratories, Inc (San Francisco, CA), and rabbit anti-EGFR from Santa Cruz Biotechology (Santa Cruz, CA). Secondary anti-chicken conjugated with HRP was

purchased from Sigma (Atlanta, GA) and HRP conjugated anti-mouse and anti-rabbit antibodies were purchased from Promega (Madison, WI).

Binding studies: Cells were seeded at 1 x 10^5 cells/well in 6-well plates in DMEM containing antibiotics and 10% FBS. Cells were serum-starved for 2 h and incubated with Alexa^{594}transferrin (20 ug/ml) at 37^{o}C for the times indicated in each experiment. Cells were then placed on ice, washed twice with ice-cold PBS and incubated for 5 minutes in acidic buffer (0.2 M Acetic Acid, 0.5 M NaCl in ddH_2O) to remove non-internalized ligand. Cells were washed twice in ice-cold PBS , harvested, centrifuged for 20 min at 1200 g at 4^{0}C, resuspended in 100 ul ice-cold PBS and added to wells on a 96-well plate. For transferrin recycling studies, cells were incubated with Alexa^{594}transferrin (20 ug/ml) 37^{o}C for two hours, washed twice with ice-cold PBS, and then placed at 37^{o}C for the times indicated before harvesting. The fluorescence intensity of each well was measured using a plate reader at an excitation/emission wavelength of 594/ 625. Non-specific binding was calculated using a 100 fold excess of non fluorescent ligand. The protein concentration in each well was then measured using the BCA protein assay kit (PIERCE), and the fluorescence value normalized to the amount of protein per well. Statistical analyses were done using 2-tailed equal variance Student t-tests.

EEA1 knockdown. Cos-7 cells were plated at 6 X 10^4 cells per well of a 6-well tissue culture dish and grown overnight in DMEM supplemented with antibiotics and 10% fetal calf serum (Invitrogen, Carlsbad, CA). Si oligonucleotides to EEA1 (sense 5'-

AACUUGCUACUGAAAUUGCAG) were purchased from Dharmacon (Lafayette, CO) and transfected by using HiPerFect (Qiagen, Valencia, CA). Cells were transfected with 100 pmol per well of siRNA oligo for 24 hours; transfection media was replaced with supplemented DMEM and cells were allow to recover for an additional 24 hours before use.

For stable EEA1 knockdown, a siRNA directed to EEA1 was cloned into a p*Silencer* 3.1-H1 puro (Ambion) as a 54-nucleotide hairpin loop, between restriction sites *Bam*HI and *Hin*dIII using the oligos: *sense:* 5'-GATCCGAAGCCTGTTCGTGTCTGTT-TCAAGAGAACAGACACGAACAGGCTTCTTTTTTGGAAA-3', and *antisense:* 5'-AGCTTTTCCAAAAAAGAAGCCTGTTCGTGTCTGTTCTCTTGAAACAGACACGA ACAGGCTTCG-3'. Insert sequence was confirmed by DNA sequencing analysis. The construct (pSilencer-EEA1) was then used for stable transfection in HeLa cells using Fu-gene6 transfection reagent. HeLa cells were also transfected with a negative control vector (pSilencer-negative) provided by Ambion. The negative control vector has a hairpin siRNA insert whose sequence is not found in the human or mouse database. Two days after the transfection,1 ug/ml puromycin (Sigma-Aldrich) was used for clone selection.

EGFR Degradation Studies. Cells were plated at 10 X 10^4 cells per well of a 6-well tissue culture dish, and allowed to grow overnight in supplemented DMEM. The next day cells were serum-starved for 30 minutes before treatment with 50 μM cycloheximide (Calbiochem, EMD Biocsciences, LaJolla, CA) for 60 minutes. Serum-free conditions

and treatment with cycloheximide were continued through the duration of the experiment. Cells were then incubated with EGF (Molecular Probes, Invitrogen,Eugene, OR) at 1 μg/ml for the time indicated. Cells were then placed on ice, washed twice with ice-cold PBS and lysed in 100 μl of PBS/TDS buffer (10 mM Dibsic sodium phosphate, 150 mM Sodium chloride, 1% Triton X-100, 0.5% Sodium deoxycholate, 0.1% Sodium dodecyl sulfate, 0.2% Sodium azide, 0.004% Sodium fluoride, pH 7.25) with protease inhibitors. Nuclei were removed and samples were analyzed by western blotting using the Western Lighting system by Perkin Elmer LAS, Inc (Boston, MA).

CHAPTER IV

THE WD40 AND FYVE DOMAIN CONTAINING PROTEIN 2 DEFINES A CLASS OF EARLY ENDOSOMES NECESSARY FOR ENDOCYTOSIS

This chapter is in the format that it was published in the the PNAS (2006), 103: 11928-11933, as written by the authors, Hayakawa A, **Leonard D**, Murphy S, Hayes S, Soto M, Fogarty K, Standley C, Bellve K, Lambright D, Mello C, and Corvera S.

I was also responsible for all the TIRF experiments, including GFP-WDFY2 and RFP-EEA1; GFP-WDFY2 and Tf; and GFP-WDFY2 and RFP-clathrin. I was also responsible for the co-localization experiment of endogenous WDFY2 with Rab4, 5, or 11, and Akira looked for co-localization of endogenous WDFY2 and a constitutively active Rab5 mutant. I was responsible for the 3-D imaging and restoration of the co-localization of endogenous WDFY2 and EEA1. Imaging hardware and software was developed by Karl Bellve, Clive Standly, Larry Lifshitz and Kevin Fogarty. Susan Hayes in collaboration with Martha Soto from Craig Mello's lab screened *C. elegans* with siRNA knockdowns of FYVE domain proteins and identified only WDFY2 to have a phenotypic effect on endocytosis. Akira Hyakawa and Stephanie Murphy made the various constructs of WDFY2 used for co-localization studies. They preformed the preliminary epifluorescent studies with flag tagged-WDFY2 and RFP-EEA1 and Wortmannin. Akira was also responsible for the preparation and characterization of of the rabbit anti-WDFY2 antibody under the guidance of David Lambright. In addition, Akira prepared a siRNA knockdown of WDFY2 in Hela cells, and characterized the effect of the knockdown on tranferrin internalization.

Summary

PI(3)P is an important signaling molecule that regulates vesicular transport. Proteins with the conserved FYVE domain bind to vesicles by its highly specific binding to PI(3)P. In addition to endosome fusion, the SARA-FYVE domain protein has also been implicated to participate in signal transduction through the TGF-β receptor. There are some 30 identified FYVE domain proteins in the human; however, our understanding of their function is still incomplete. We used *Caenorhabditis elegans* to further our understanding of FYVE domain protein function.

We screened using RNA interference, 12 known *C. elagan* FYVE domain proteins that have known human homologs. Only one protein, WDFY2, produced a strong inhibition of endocytosis when silenced. In addition to a FYVE domain, WDFY2 contains seven WD40 motifs and is highly conserved between species. Localization studies showed that this protein coats small endosomes that are located within 100 nm of the plasma membrane, but does not co-localize with two classical early endosome markers, Rab5 and EEA1. These WDFY2 decorated endosomes are involved in Tf uptake and Tf uptake is disrupted as a result of the WDFY2 knockdown due to RNA interference.

This work demonstrates the existence of a subset of WDFY2 coated endosomes at the early steps of endocytosis that are distinct from Rab5/EEA1 coated endosomes and may represent the first step of endocytic processing of internalized cargo.

Introduction

Phosphorylated phosphoinositides play critical roles in the process of endocytosis. Phosphatidylinositol 3-phosphate [PtdIns(3)P], a major product of PtdIns 3-kinase, is found almost exclusively on the surface of endosomes, where it can recruit proteins containing FYVE or PX domains [117, 118]. The first protein found to be recruited onto endosomes in a PtdIns 3-kinase-dependent manner was EEA1 [100, 119, 120]. EEA1 also interacts with the GTPase Rab5 [101, 121], and calmodulin [122-124] and has been proposed to function as a tether to facilitate early endosome fusion [101, 104, 125-127].

Many other proteins containing FYVE domains are recruited to early endosomes. Examples include the proteins Rabenosyn5 [128] and Rabip4 [129], which appear to coordinate the functions of the small GTPases Rab4 and Rab5, and Hrs, which is involved in ubiquitin-mediated lysosomal degradation [48, 130]. In addition, Fab1p/PIKfyve, which catalyzes the phosphorylation of PtdIns(3)P to PtdIns(3,5)P2 appears to have an important role in multivesicular body formation [131-133]. FYVE domain-containing proteins also function in pathways not primarily related to endosomal trafficking. These include SARA [134-136], which mediates signal transduction through the TGF-β receptor. The human UniGene collection lists 30 different FYVE-domain-containing proteins, indicating that many more functions involving PtdIns(3)P and FYVE-domain interaction remain to be discovered. Of these, it is not known how many or which are involved in the control of trafficking in the endocytic pathway, or which are involved in other functions, such as specific signal transduction events.

The *Caenorhabditis elegans* genome contains only 12 proteins that contain FYVE domains predicted to bind PtdIns(3)P on the basis of their primary amino acid sequence. The function of each of these proteins can be analyzed in transgenic strains of worms engineered to report the activity of specific cellular processes. For example, endocytosis can be monitored indirectly or directly by looking for an Unc (uncoordinated) phenotype, which can indicate deficient synaptic vesicle recycling [137, 138], by accumulation of yolk in the pseudocoelom [139], or by the lack of rhodamine-dextran endocytosis by intestinal cells of the gut [140]. Resistance of aldicarb treatment in hypersensitive strains can identify genes involved in endocytosis or exocytosis at the neuromuscular synapse [141]. We have used a system developed by Fares and Greenwald [140] in which endocytosis is monitored by looking at the uptake of secretory GFP into coelomocytes. Coelomocytes are six cells that actively internalize fluid and degrade the GFP secreted from the muscle cells into the pseudocoelom. When Vps34, dynamin, RME-1, and other proteins involved in endocytosis are targeted by injection of dsRNA, GFP fails to internalize into coelomocytes and accumulates in the pseudocoelom. With this screen we have uncovered an important role for the WD40 and FYVE domain-containing protein 2 in the endocytic pathway and the existence of a subset of early endosomes that lack canonical markers EEA1 and Rab5.

Experimental Procedures

RNAi Experiments in C. elegans. The cDNAs encoding for the various FYVE-domain-containing genes were a gift from Yugi Kohara (University of Tokyo, Tokyo, Japan). Some were received as plasmids, and some were received in phage. The cDNAs were excised from the phage. The dsRNA was generated by using the *in vitro* RNAi transcription kit from Ambion (Austin, TX). L4 to young adult worms were injected, and the progeny of the injected worms were analyzed by phase and fluorescence microscopy.

Constructs. The cDNA clone MGC:20275 (IMAGE Id 3842598) for the human WDFY2 was obtained from the American Tissue Culture Collection (Manassas, VA) and sequenced fully for verification. The cDNA was then cloned in-frame with a Flag tag or EGFP at the N terminus of the protein by using standard techniques. Clathrin and EEA1 constructs have been described [106, 110, 122].

*Immunofluorescence***.** Rabbit antibodies to the full-length WDFY2 protein made in bacteria and affinity-purified against full-length WDFY2 were used. Chicken or mouse antibodies to the N terminus of EEA1 were used. Secondary detection was with Alexa-coupled species-specific antibodies obtained from Molecular Probes (Eugene, OR).

Optical Systems. High-resolution images were generated by using a Zeiss (Thornwood, NY) Axiovert 200 inverted microscope equipped with a Zeiss AxioCam HR CCD camera with 1,300 x 1,030 pixels basic resolution and a Zeiss 100 x 1.40 NA oil-immersion objective. For image restoration, 3D stacks of images spaced by 250 nm were obtained and deconvolved with the super resolution algorithm developed by Carrington *et*

al. [142], resulting in a resolution of 66 nm/pixel. The TIRF microscope has been described in detail [106] and includes a modified Olympus (Center Valley, PA) IX81 inverted microscope, a modified Olympus TIRF fiber illuminator, IX2-RFAEVA, and a high-speed CCD camera developed in collaboration with the Lincoln Laboratory at the Massachusetts Institute of Technology. The objective used is an Olympus Plan APO x60 objective with an NA of 1.45. Imaging analysis procedures have been described in detail [106].

*Cell Culture and Transfection of HeLa or Cos7 Cells***.** HeLa or Cos-7 cells were maintained in DMEM supplemented with antibiotics and 10% FCS (Invitrogen, Carlsbad, CA). Expression vectors were transfected into HeLa cells by using FuGENE 6 transfection reagent (Roche Applied Science, Indianapolis, IN).

*siRNA Experiments***.** siRNA oligonucleotides to the human homolog of the proteins studied were purchased as Smart*pool*s from Dharmacon (Lafayette, CO) and transfected by using HiPerFect (Qiagen, Valencia, CA). Cells were transfected twice according to HiPerFect transfection reagent manual protocol with 100 pmol per well of siRNA oligos at 24-h intervals. Forty-eight hours after the second transfection, cells were serum-starved for 2 h and incubated with Alexa^{568}-Tf (Molecular Probes) at 20 μg/ml for the times indicated. Cells were then placed on ice, washed twice with ice-cold PBS, and incubated for 5 min in acidic buffer (0.2 M acetic acid/0.5 M NaCl in double-distilled H_2O) to remove noninternalized Tf. Cells were either fixed for fluorescence microscopy or harvested, centrifuged for 20 min at 1,200 x *g* at 4°C, resuspended in 100 μl of ice-cold

PBS, and added to wells on a 96-well plate. The fluorescence intensity of each well was measured with a plate reader at an excitation/emission wavelength of 594/625. Statistical analyses were done by using two-tailed equal variance Student's *t* tests.

Results and Discussion

Proteins were classified as FYVE-domain-containing proteins if the sequence contained the following: a WXXD motif, four CXXC motifs, a R(R/K)HHCR motif, and a RVC motif. The cDNAs of 12 different genes in *C. elegans* that conformed to this criteria (Table 1) were transcribed *in vitro* into dsRNAs and individually injected. Although no single protein was found to be essential for viability, the absence of lethality could be caused by redundancy in pathways involving FYVE-domain-containing proteins or inefficient RNA knockdown, necessitating further studies in which genes are deleted, silenced in combination, or both to reveal potential functions and interactions. Thus, our results up to now can only rule in, not out, a function for a particular FYVE-domain-containing protein.

Table 1. Genes screened for coelomocyte uptake deficiency.

Clone	Gene	Protein	Homolog
Yk15a2	*Aka-1*	WP:CE02581	*SARA/AKAP*
Yk1334h08	*ZK632.12*	WP:CE01110	*Phafin2*
Yk877d04	*Pqn-9*	WP:CE32574	*Hrs*
Yk1281a05	*R160.7*	WP:CE33815	*KIAA1643*
Yk523h7	*Y42H9AR.3*	WP:CE29111	*Rabenosyn5*
Yk1121h09	*VT23B5.2*	WP:CE20122	
Yk1334f06	*Ppk-3*	WP:CE18979	*PIP5K*
Yk1189b03	*D2013.2*	WP:CE00928	*WDFY2*
Yk5g8	*T10G3.5*	WP:CE31066	*EEA1*
Yk212f9	*F22G12.4*	WP:CE27740	
Yk394e11	*C28C12.10*	WP:CE28920	*ANKHZN*
Yk553e11	*Mtm-3*	WP:CE03708	*Myotubularin-related protein 2*

To reveal defects specifically in the endocytic pathway we used a transgenic strain (arIs37[pmyo::ssGFP] I; dpy-20(e1282) IV) in which GFP is under control of the myosin promoter. The progeny of the injected worms was scored for coelomocyte endocytosis by analyzing the relative amounts of GFP in the pseudocoelom versus the coelomocytes (Fig.20). Two dsRNAs yielded a phenotype different from the uninjected worm. These transcripts were t10g3.5 (yk5g8), which corresponds to the homolog of EEA1 and displayed a slight increase in GFP fluorescence in the pseudocoelom, and d2013.2 (yk1189b03), which displayed a much greater accumulation of pseudocoelomic GFP (Fig. 20). A BLAST search for homology revealed extensive similarity between yk1189b03 and the mammalian protein WDFY2.

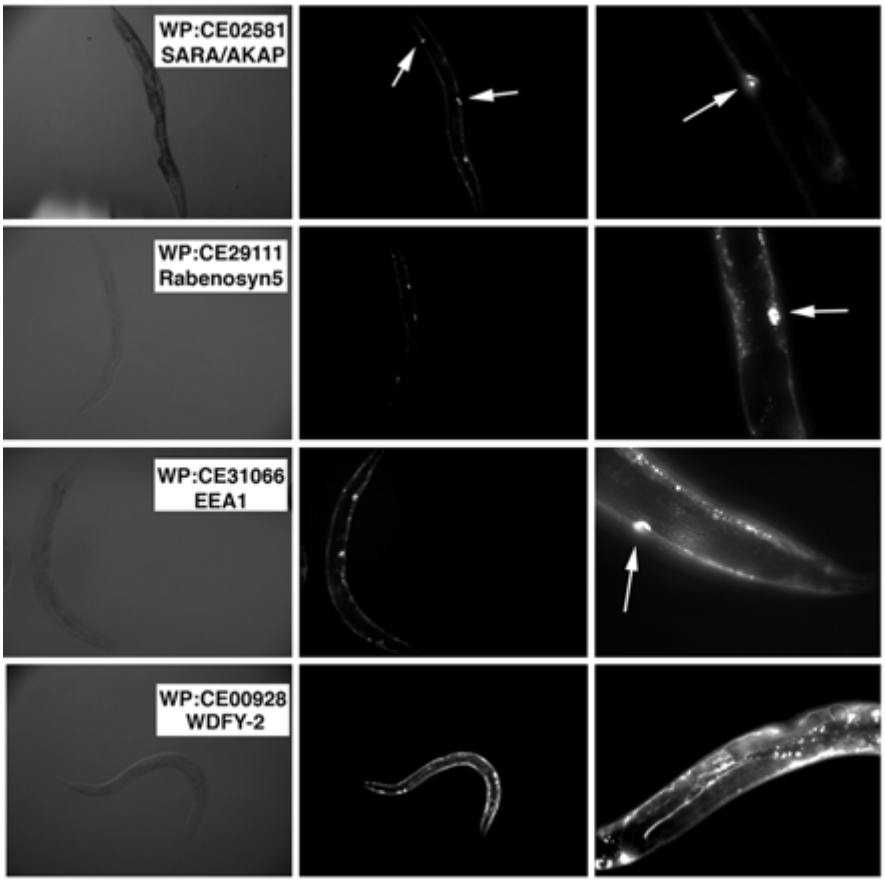

Figure 20. **Disruption of coelomocyte endocytosis by WDFY2 silencing.** Worms were injected with the dsRNAs for the proteins indicated (*Left*), and the progeny were visualized by phase microscopy (*Left*) or fluorescence microscopy (*Right*) at low (x15) (*Center*) and higher (x45) magnifications (*Right*). All images were taken with the same exposure time and are representative of at least 10 worms from each of three different experiments. The phenotypes of the worms injected with dsRNAs to SARA or Rabenosyn5 (top two panels) were indistinguishable from noninjected control worms and are included as examples of the WT phenotype. Coelomocytes are clearly visible over the background in these worms (arrows) but are less apparent in worms injected with dsRNA to WDFY2, which have much brighter GFP levels.

WDFY2 contains a FYVE domain and seven WD40 motifs, and its amino acid sequence is highly conserved among species. The FYVE domains of both *C. elegans* and human WDFY2 display the structural properties known to be critical for PtdIns(3)P binding (Fig 21). Both WDFY2 and the closely related mammalian protein WDFY1 (also called FENS-1) [143], contain a large insertion N terminal to the predicted membrane insertion or "turret" loop of the FYVE domain. The role of this insertion is not known. To determine whether indeed WDFY2 is targeted to endosomes in mammalian cells, a full-length construct of human WDFY2 was cloned in-frame with a Flag tag.

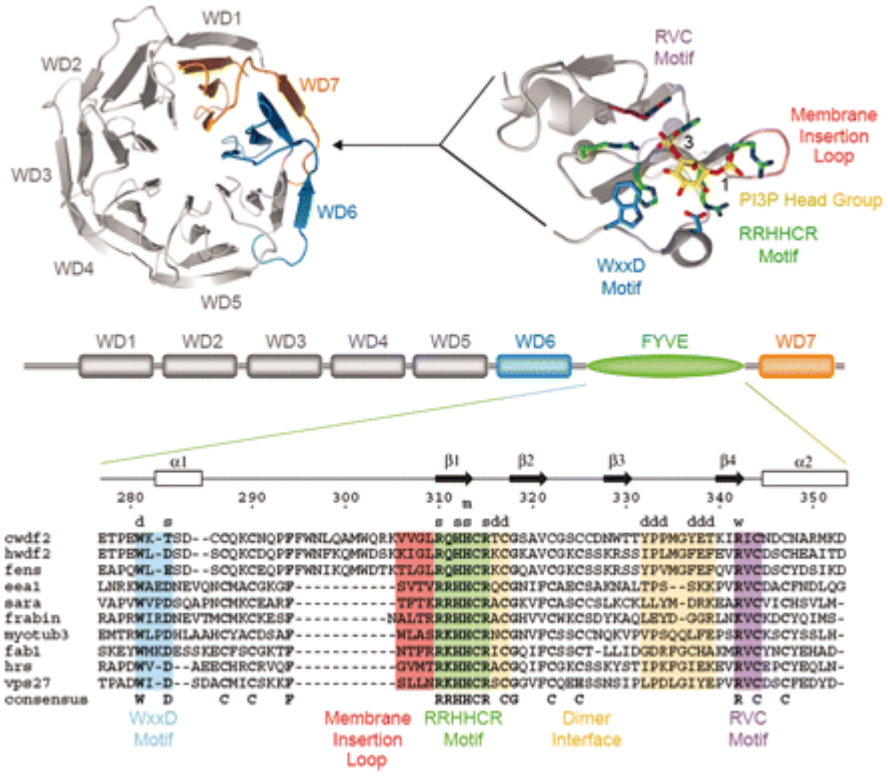

Figure 21. **Structural organization of WDFY2 and conservation of functional motifs.**
C. elegans WDFY2 (cWDFY2) and the human homolog (hWDFY2) consist of seven WD40 repeats with a FYVE domain inserted between repeats WD6 and WD7. The WD40 repeats are predicted to form a b propeller structure with seven blades. The predicted site of insertion in the loop connecting repeats WD6 and WD7 of human WDFY2 is indicated with respect to the structure of UNC-78 (Protein Data Bank ID code 1PEV), which represents the closest structural homolog identified by threading by using the Phyre fold recognition server. The FYVE domain of EEA1 (Protein Data Bank ID code 1JOC) is depicted on the right. Note that the FYVE domains of WDFY2 and FENS-1 contain a large insertion at the N terminus of the membrane insertion loop. Structural images were rendered with PyMol (www.pymol.org).

When transiently transfected into Cos cells, WDFY2-Flag was visualized on vesicular structures of varying sizes, consistent with its endosomal localization, and treatment of cells with wortmannin caused its rapid redistribution into the cytoplasm (Fig 22*A*), indicating that WDFY2 is targeted to endosomes in a PtdIns 3-kinase-dependent manner. We noticed that the distribution of WDFY2-Flag did not completely match that of endogenous EEA1 (Fig. 22*B*), being more prominent in smaller and more peripherally distributed endosomes.

To determine whether endogenous WDFY2 displayed this distribution or whether it was an artifact of overexpression, we generated affinity-purified rabbit anti-WDFY2 antibodies by using recombinant full-length protein. The distribution of WDFY2 relative to that of EEA1 was analyzed by using deconvolution microscopy as described in *Experiment Procedures*. Antibody to WDFY2 stained vesicular structures of various sizes distributed over the entire cytoplasmic volume. Some co-localization with endogenous EEA1 was seen in non-nonrestored images (Fig. 22*C*), but it was mostly in the perinuclear region where the cytoplasmic volume is largest and was not apparent in restored images where structures that reside in close proximity can be resolved from each other (Fig. 22*D* and *E*). Analysis of the 3D images revealed a more peripheral localization of endosomes containing WDFY2 compared to those enriched in EEA1 (Fig. 22*E, arrows*), suggesting that vesicles containing WDFY2 are closer to the plasma membrane that those containing EEA1.

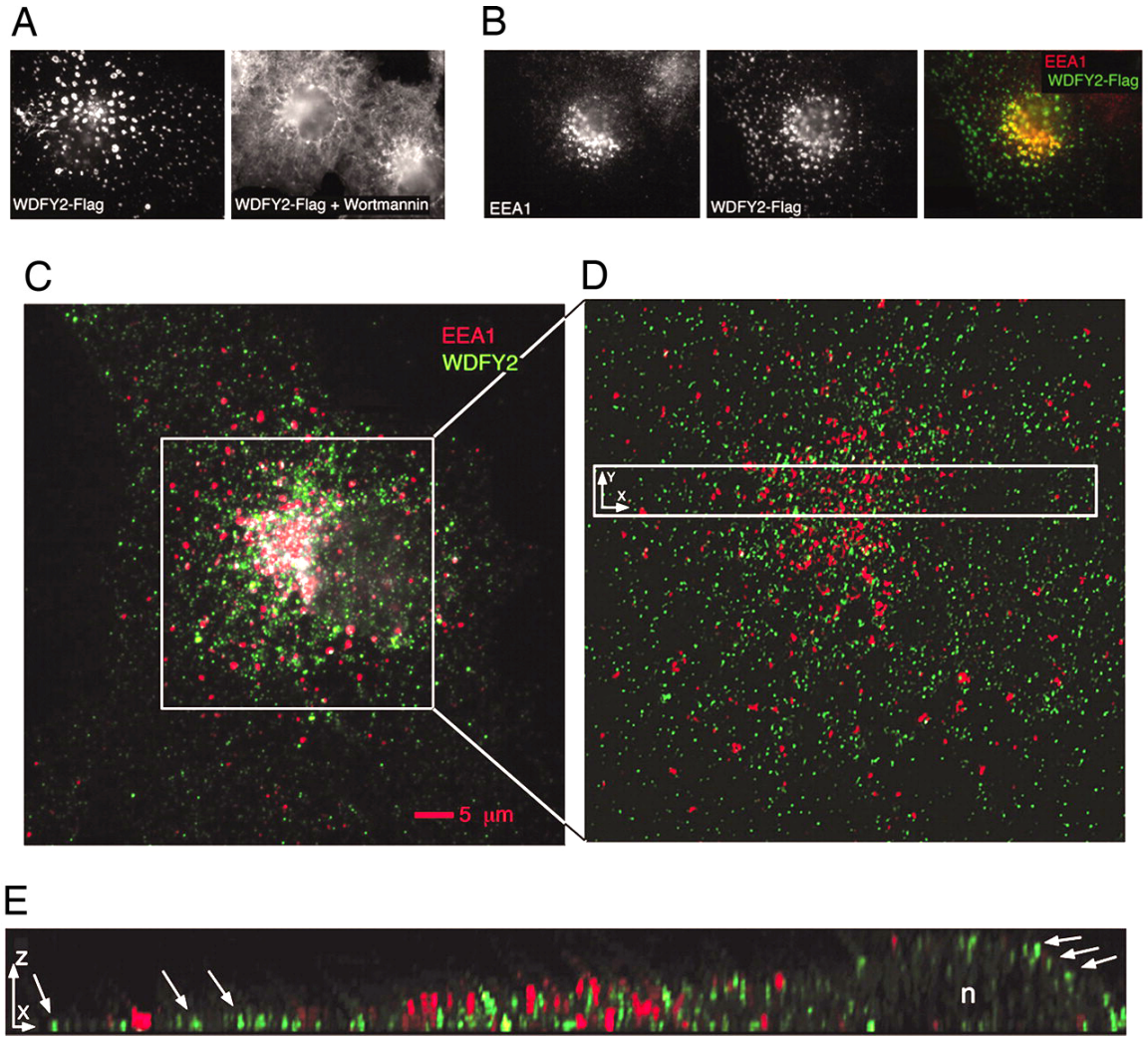

Figure 22. **Localization of expressed Flag-tagged and endogenous WDFY2.** (*A*) Flag-tagged WDFY2 was expressed in Cos-7 cells, which were incubated in the presence or absence of wortmannin as indicated, fixed, and stained with anti-Flag antibodies. (*B*) Cos cells expressing Flag-WDFY2 were fixed and stained with antibodies to EEA1 and Flag. The overlap between the two signals is depicted in yellow (*Right*) and is likely to result from overexpression of Flag-WDFY2. (*C*) Nontransfected Cos-7 cells were stained with antibodies to EEA1 *(red)* and endogenous WDFY2 *(green)*. Shown is the 2D projection of a 3D image stack before restoration. (*D*) Area in square in *C*, after restoration. (*E*) Area in rectangle in *D*, projected after 90° rotation along the *y* axis; *n* = nucleus. Arrows point to few of the many peripherally localized structures that contain WDFY2 but no detectable endogenous EEA1. (Magnifications: *A* and *B*, x1,000.)

To determine whether indeed WDFY2 targets to a population of endosomes closer to the plasma membrane, live cells expressing GFP-WDFY2 and RFP-EEA1 were analyzed by using total internal reflection fluorescence (TIRF) microscopy (TIRF-M), which reveals exclusively those fluorophores present within 100 nm from the plasma membrane [97]. In preliminary experiments, we verified the co-localization of expressed protein with the endogenous protein detected with anti-WDFY2 antibodies. When imaged by TIRF-M, many vesicles containing GFP-WDFY2 could be observed near the surface, but very few structures containing RFP-EEA1 were detected (Fig 23, *Left*). This difference was not caused by lack of RFP-EEA1 expression, for when the same cells were visualized by epifluorescence a very bright signal of RFP-EEA1 could be detected (Fig. 23, *Center* and *Right*). Interestingly, in these images endosomes containing EEA1 appear to be surrounded by smaller endosomes containing WDFY2, suggesting the possibility that WDFY2 may mark a subset of endosomes that serves as a first stage of endocytic transport, operating between the plasma membrane and EEA1-enriched endosomes.

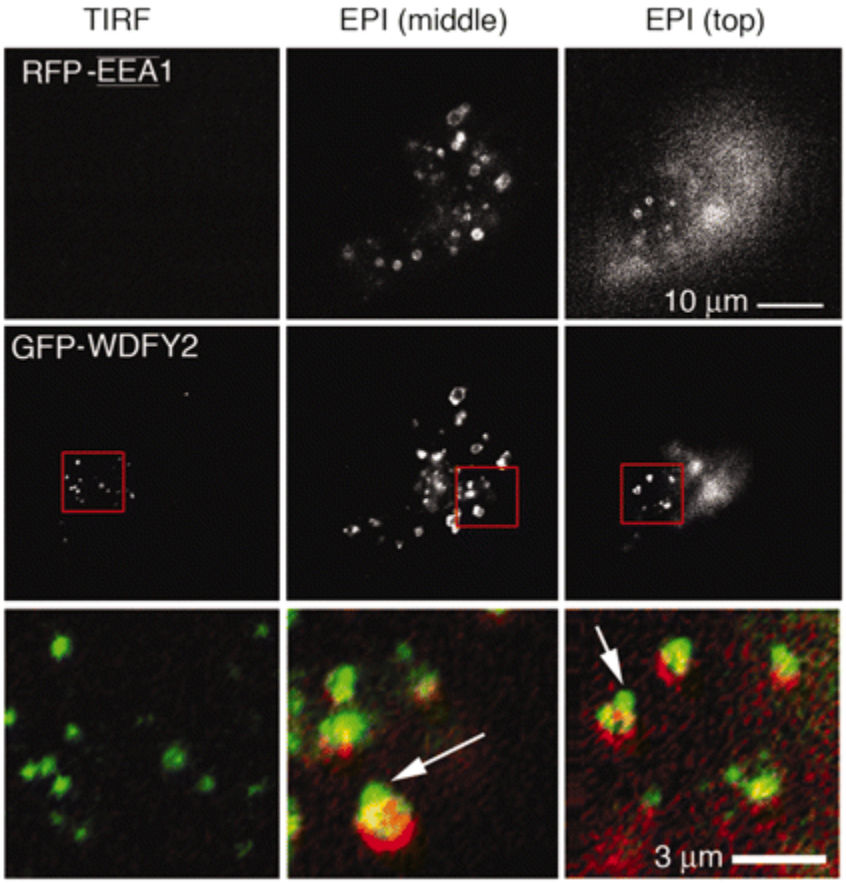

Figure 23. **WDFY2 marks an endosomal population adjacent to the plasma membrane.**
Cos-7 cells were cotransfected with RFP-EEA1 (*Top*) and GFP-WDFY2 (*Middle*). Cells were imaged by using TIRF-M (*Left*) and then by epifluorescence (EPI) focusing on planes through the middle of the cell (*Center*) or at the top of the cell (*Right*). The regions marked by the red squares are expanded to display the overlap between the red and green signals (*Bottom*). Note the virtual absence of RFP-EEA1 in the TIRF images, which represent the region within 100 nm of the plasma membrane, and the apparent binding of GFP-WDFY2 containing vesicles onto RFP-EEA1-enriched endosomes seen by epifluorescence *(arrow)*. A similar distribution was seen in cells expressing divergent ratios of WDFY2-GFP and RFP-EEA1 (>1, =1, or <1).

To further test the hypothesis that WDFY2 defines a novel subset of endosomes we compared the effect of Rab5Q79L expression on the localization of endogenous EEA1 and WDFY2. Expression of persistently active mutants of Rab5 (Rab5Q79L) results in enlargement of endosomes containing EEA1 and an almost quantitative recruitment of cellular EEA1 to these endosomes [101, 110]. RFP-Rab5Q79L displayed the characteristic distribution into enlarged endosomes and co-localized extensively with endogenous EEA1 (Fig. 24*A, Left*), but not with endogenous WDFY2 (Fig. 24*A, Right*), which remained associated with smaller vesicular structures. To determine whether WDFY2 preferentially associates with another member of the endocytic Rab GTPase family, we measured its co-localization with endogenous Rabs 4, 5, and 11. Some co-localization with all three Rabs was seen in restored images, but it was small (<6%) and not significantly selective for any of these three GTPases (Fig. 24*B* and *C*). In contrast, significant clocalization (>30%) was seen between EEA1 and endogenous Rab5 and to a lower extent between EEA1 and Rab11.

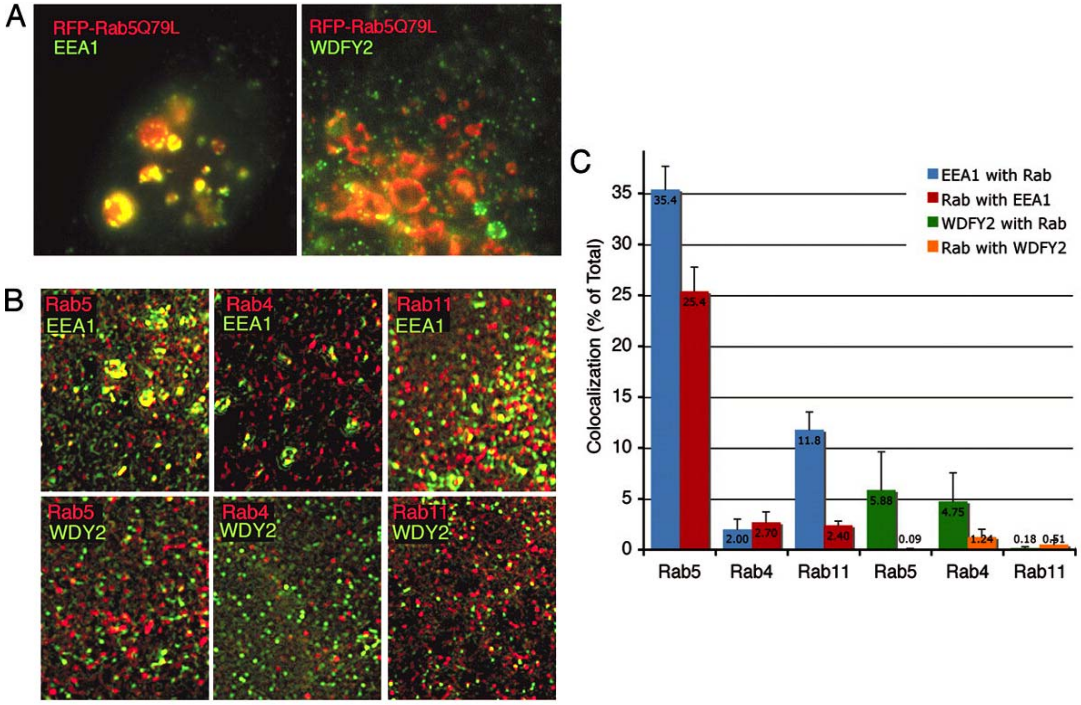

Figure 24. **Co-localization of WDFY2 with endocytic Rab GTPases.**
(*A*) HeLa cells were transiently transfected with RFP-Rab5Q79L *(red)*, and after 24 h they were fixed and stained with antibodies (green) to EEA1 (*Left*) or WDFY2 (*Right*). Co-localization is depicted in yellow. (*B*) Cos-7 cells were fixed and stained with antibodies to WDFY2 or EEA1 *(green)* and antibodies *(red)* to Rab5 (*Left*), Rab4 (*Center*), and Rab11 (*Right*). Image stacks were obtained and restored; shown are single 250-nm-thick regions enriched in both signals. Co-localized regions are rendered in yellow. (*C*) The degree of co-localization of WDFY2 with each Rab, and of each Rab with WDFY2, was determined by using areas of the cell enriched in both signals, such as those shown in *B*. Co-localization is expressed as the percent of the total fluorescence from WDFY2 or EEA1 colocalizing with each Rab and vice versa. Spurious co-localization was obtained by flipping one of the images along the *x* axis. The value for spurious co-localization was subtracted from the properly aligned co-localization values. Bars represent the mean, and vertical lines indicate the SEM, from 12 regions (3 regions per cell) obtained from four independent cells. (Magnifications: *A*, x2,000; *B*, x3,000.)

The lack of co-localization with endogenous or transfected, activated Rab5 suggests that WDFY2 marks a set of endosomes that differ functionally from those enriched in EEA1. To determine whether WDFY2-enriched endosomes function in the endocytic pathway of the transferrin (Tf) receptor, we analyzed the binding and early steps of internalization of fluorescent Tf in live HeLa cells stably expressing GFP-WDFY2 by using TIRF-M [106]. Within 5 min of addition of Tf to the media, significant co-localization with endosomes enriched with GFP-WDFY2 was seen in the TIRF zone (Fig. 25*A–E*), which increased over time of continuous incubation with ligand. After 10 min of continuous incubation with Tf, ~40% of GFP-WDFY2 co-localized with the ligand (Fig. 25*F*). Co-localization was also seen when the cells were visualized in epifluorescence (Fig. 25*F–J*). This degree of co-localization exceeded that seen with GFP-EEA1 (data not shown) and demonstrates that WDFY2 is present in endosomes involved in the early steps of Tf receptor internalization.

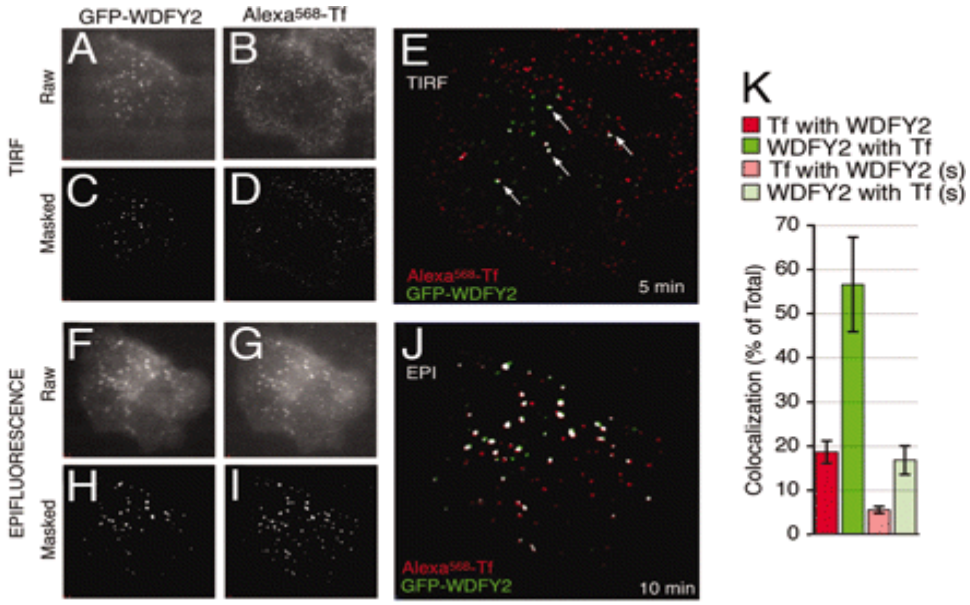

Figure 25. **Trafficking of Tf through WDFY2-containing endosomes.**
(*A–J*) HeLa cells stably expressing GFP-WDFY2 were incubated with fluorescent transferrin (Alexa^{568}-Tf) and imaged by TIRF (*A–E*) and epifluorescence (*F–J*). TIRF images were obtained after 5 min, and epifluorescence images of the same cell were obtained after 10 min of continuous exposure to Alexa^{568}-Tf. Raw (*A*, *B*, *F*, and *G*) and masked (*C*, *D*, *H*, and *I*) images of GFP-WDFY2 (*A*, *C*, *F*, and *H*) and Alexa^{568}-Tf (*B*, *D*, *G*, and *I*) are shown. Co-localization between GFP-WDFY2 *(green)* and Alexa^{568}-Tf *(red)* is rendered in white in overlaps of the masked images (*E* and *J*). Arrows point to co-localized voxels in the TIRF images. (*K*) The co-localization between Tf and WDFY2 in TIRF images from cells incubated for 10 min in the continuous presence of Tf was quantified. Rectangular areas enriched in both signals were analyzed, and co-localization was expressed as the percent of the total fluorescence from Tf colocalizing with WDFY2 and vice versa. Spurious co-localization was obtained by flipping one of the images along the *x* axis. Bars and vertical lines represent the mean and standard error of the real (red and green) or spurious (light red and light green) co-localization measured in 10 regions from 10 independent cells. (Magnifications: *A–D*, x1,000; *F–G*, x2,000.)

To determine whether WDFY2 is required for Tf uptake we analyzed the effects of disruption of WDFY2 expression by using siRNA. Silencing oligonucleotides to WDFY2 reduced the levels of endogenous WDFY2 mRNA (data not illustrated) and protein (Fig. 26*C*) by >80%. Cells treated with scrambled siRNA or oligos directed to clathrin or WDFY2 for 48 h were exposed to fluorescent Tf. Tf was detected in >90% of cells treated with scrambled siRNA after 5 min of uptake (Fig. 26*A*, *Top*). In contrast, the Tf signal was faint or undetectable in >80% of cells treated with siRNA oligos directed to clathrin and strongly diminished in the majority of cells treated with siRNA directed to WDFY2. The total amount of fluorescence associated with lysates of cells incubated for different periods with Alexa^{594}-Tf was determined (Fig. 26*B*). Although the results of this assay seemed in general less pronounced than those collected from microscopy images, they fully confirm the observation of a comparable inhibition of Tf uptake in response to clathrin or WDFY2 silencing.

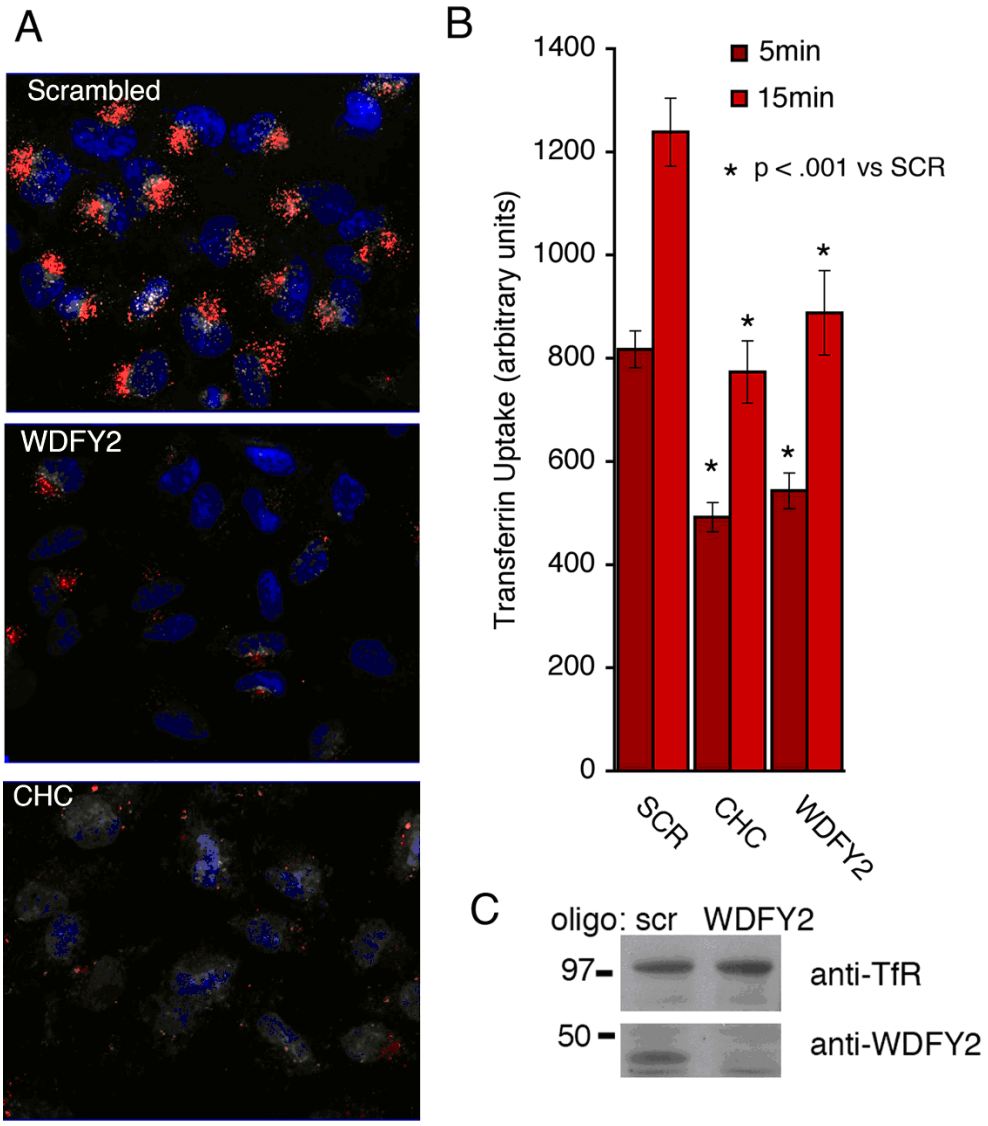

Figure 26. Inhibition of Tf uptake by silencing of WDFY2.
HeLa cells were treated with silencing oligonucleotides to the proteins indicated. (*A*) Cells were incubated for 5 min with fluorescent Tf, acid-washed to remove noninternalized Tf, fixed, counterstained with DAPI, and visualized. (Magnification : X200.) (*B*) Cells were incubated for 5 or 15 min with Tf, acid-washed, and lysed, and total fluorescence in the lysate was quantified. Plotted are the means and SEM of three independent experiments performed in triplicate. (*C*) Western blots of cell lystaes stained with antibodies to the Tf receptor (anti-TfR) or WDFY2.

The rapid entry of Tf into WDFY2-enriched structures and its requirement for Tf internalization raised the possibility that WDFY2 may directly localize to clathrin-coated structures. To determine whether WDFY2 might be localized to clathrin-coated pits or clathrin-coated vesicles, we analyzed cells expressing RFP-clathrin and GFP-WDFY2 by TIRF-M (Fig.27, *A*). As previously shown, clathrin localized to pleomorphic regions at the plasma membrane, many of which displayed little lateral mobility over a 1-min time frame [2, 15, 82, 106]. Endosomes containing GFP-WDFY2 displayed very different dynamics, undergoing rapid changes in localization caused by both lateral movements and appearance and disappearance from the TIRF zone. Some overlap could be seen between WDFY2 and clathrin-coated membrane regions, indicating that endosomes can localize to regions within 100 nm of clathrin-coated membrane domains. However, the amount of specific co-localization of WDFY2 and clathrin at any given time point was low (~4%), being almost the same as the co-localization caused by spurious coincidence of the two fluorophores (~13%), assessed by flipping one of the channels along the *x* axis (Fig. 27*B*). Thus, we believe it unlikely that WDFY2-enriched structures close to the plasma membrane represent clathrin-coated pits or budding vesicles, but we do not rule out that a functional relationship may exist in which WDFY2-enriched endosomes may transiently interact with clathrin-coated membrane regions. Further studies simultaneously visualizing clathrin, WDFY2, and endocytic ligands will be necessary to better define the pathway of endocytic cargo from clathrin-coated membrane domains into endosomal populations enriched in specific FYVE-domain-containing proteins.

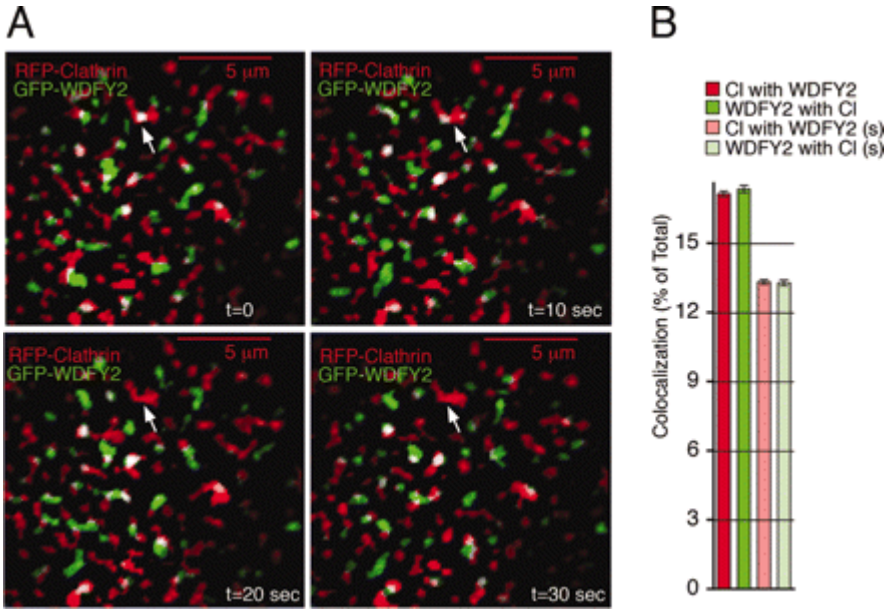

Figure 27. **Simultaneous imaging of GFP-WDFY2 and RFP-clathrin.**
(*A*) Cos-7 cells cotransfected with GFP-WDFY2 *(green)* and RFP-clathrin *(red)* were imaged by TIRF-M. Shown are four time points taken 10 s apart. The arrow indicates a clathrin-coated membrane region colocalizing with WDFY2 in the first time point. Clathrin persists in the region in the four time points shown, but WDFY2 does not. (*B*) Co-localization is expressed as the percent of total WDFY2 colocalizing with clathrin and clathrin colocalizing with WDFY2. Spurious co-localization was calculated by flipping one image along the *x* axis and calculating the co-localization as above. Bars and vertical lines represent the mean and standard error values for real *(red and green)* or spurious *(light red and light green)* co-localization measured in 1,500 frames from five cells imaged at 0.5 frames per s (300 frames per cell, 10 min total imaging time). Although small, the difference between real and spurious co-localization was statistically significant ($P < 0.001$, paired two-tailed Student's *t* test).

In summary, the results shown here reveal the existence of a set of endosomes in mammalian cells defined by the presence of WDFY2 that participate in the uptake of Tf. Future experiments will determine the mechanisms involved in the biogenesis of these endosomes, their relationship to those containing EEA1, and their possible involvement in stage or cargo-specific endocytic uptake. Ligands such as Tf and EGF are taken up by receptors that differentially interact with diverse microdomains at the plasma membrane, which include clathrin-coated membrane regions and raft-like microdomains [65]. The possibility that cargo proteins enriched in these different regions may preferentially be targeted to diverse sets of endosomes is an interesting possibility, supported by the recent identification of heterogeneity of early endosomes based on their motility on microtubules [22]. The precise function of WDFY2 in the endocytic pathway is not known, but the simplicity of its structure, consisting only of WD40 motifs and a FYVE domain, suggests it serves to coordinate the interaction between compartments containing PtdIns(3)P and other WD40 motif-binding proteins at one or several stages of the early endocytic pathway. The identification of such proteins will be required to better understand these mechanistic details.

CHAPTER V

DISCUSSION

Endocytosis is a fundamental process in all eukaryotic cells that involves a series of highly complex sorting events leading to the delivery of cargo to specific intracellular destinations (for reviews see [1, 4, 14]). In recent years, the discovery of an ever increasing number of new players and mechanisms of endocytosis has led to modifications of the working model(s) of this process, although the specific role of each new player is often not fully characterized. In my studies of the early events in endocytosis, I found that the sorting of ligands begins at the very earliest stages of endocytosis, at the plasma membrane. For the Tf and EGF receptors, their mutually exclusive distribution on the cell's surface predetermined how the liganded receptor was internalized and subsequentently processed. Once internalized, the cargo laden vesicle recruited endosomes coated with unique member(s) of the family of FYVE domain proteins. Importantly, the recruitment of the EEA1-decorated early endosome to the EGF loaded vesicle is mediated by interactions of Rab5 and its binding domain at the N-terminus of EEA1.

Because of the dynamic nature of the early steps of endocytosis, I employed tools that allowed me to collect data in real time. Using the recently developed optical techniques of TIRF-M, which allows the visualization of cellular events within 100 nm of the plasma membrane, I was able to collect high resolution images in real-time with less distortion and noise than those obtained by conventional wide-field epifluorescence microscopy. Together with standard biochemical and molecular biological tools, I was

able to define the early events in the endocytosis for two classical ligands, Tf and EGF. Preliminary work using real-time TIRF-M revealed that early events in the endocytosis of Tf and EGF were very different and that these two ligands did not co-mingle in early vesicles, suggesting that classical models of endocytosis, which predicted that endocytosis was a random event over the cell surface, required reevaluation.

Since the Tf loaded vesicle failed to recruit EEA1, and the TfR was not randomly distributed on the cell surface, contrary to conventional wisdom, I began by re-examining the early steps in Tf endocytosis. The earliest event in Tf endocytosis is the binding of Tf to the TfR and the accumulation of the liganded TfR in CCP, followed by the dynamin mediated release of the CCV from the plasma membrane [144]. Both the TfR and clathrin are the key players in these initial steps. Just as I observed in COS cells [106], Rappoport and co-workers found both static and dynamic populations of clathrin in HeLa cells and showed that the adaptor protein, AP-2, was associated with the static patches, presumably at sites of CCV formation [11]. By contrast, Ehrlich et al showed that Tf and LDL endocytosis proceeded through dynamic clathrin patches suggesting that short-lived nucleation sites, which were composed of clathrin, AP-2 and liganded receptors, were the primary means by which cargo was internalized in the kidney epithelial cell line, BSC-1 and in COS cells [16]. More recently, Merrifield and co-workers suggested that both the dynamic and static clathrin patches were sites of the endocytosis of a pH sensitive, Tf-fusion protein in Swiss 3T3 cells [13].

In COS cells, I found that most, if not all, of the TfR and its cargo was associated with the larger, less mobile patches of clathrin and that these static patches were active

sites of Tf endocytosis [106]. These findings are in agreement with Rappoport and co-workers, who used TIRF-M for their imaging of clathrin and AP-2; however, they did not evaluate ligand endocytosis or receptor distribution [11]. Ehrlich and co-workers used spinning disc confocal microscopy to examine a stably transfected kidney cell line that constitutively expressed exogenous clathrin, AP-2 and dynamin and measured changes in fluorescent clathrin intensity relative to changes in fluorescent AP2 and dynamin [16]. However, the use of the relatively large changes in reporter fluorescence intensity and the limitations of speed and resolution of confocal microscropy will completely miss any activity occurring in pre-existing, stable clathrin patches with a time span of only 5 sec, as determined in my study [106]. To eliminate this problem, I used high speed (160-fold faster), high resolution (2-3 fold greater) TIRF-M to capture the slight fluctuations in the clathrin fluorescent intensity of the large clathrin patches in COS cells. In fact, examination of the images of Tf endocytosis acquired by Ehrlich revealed that Tf was associated with large clathrin structures, even though this group focused their attention on the smaller clathrin spots.

Finally, work by Merrifield and co-workers suggested that Tf used both large and small clathrin structures for endocytosis [13], but once again, there was no direct, real-time analysis of ligand internalization, rather indirect co-localization of dynamin with clathrin was used to determine which clathrin structures were responsible for endocytosis. Moreover, their use of the indirect, *in vitro*, measurement of Tf uptake by ELISA to evaluate cargo endocytosis, while a perfectly acceptable method to measure Tf uptake at a single point in time, does not provide any information about the temporal sequence of

events that occur in seconds not minutes. Perhaps more importantly, Merrifield and co-workers preloaded the TfR on the cell surface with saturating levels of reporter Tf at 4^{o}C, conditions that block endocytosis, and then initiated TfR internalization by warming the cell to 37^{o}C. Such large temperature changes are potent inducers of early response genes that are likely to influence basic cell functions such as endocytosis, and the cell chilling leads to a phase shift in the lipid bilayer that dramatically alters the physiology of receptor movement, so that the biological relevance of such approaches is compromised.

In contrast, in all my work, a constant physiological temperature was maintained throughtout the experiment and physiological levels of Tf were used to evaluate Tf internalization. On the other hand, it has been suggested that the use of culture cells with artifical focal attachments could be responsible for the large clathrin arrays. To address this possibility, I examined the distribution of clathrin in freshly isolated adipocytes that do not attach to coverslips or to culture dishes. Just as I found in COS cells, more than 60% of clathrin in adipocytes was organized in larger, persistent (remained 60 s or more) patches [106]. This finding clearly showed that the large clathrin patches were not an artifact of cell culture or the COS cell, and that these “fixed” structures function as sites for the accumulation of TfR, where they serve as regionally distributed platforms for Tf endocytosis. The mobile, dynamic clathrin structures did not appear to play a major role in Tf endocytosis in COS cells.

With the observation that the TfR was restricted to these large fixed clathrin structures, I then looked to see if this was true with other receptors. Using EGF, I immediately saw a difference in the pattern of distribution of the EGF liganded EGFR on

the cell surface; when I used both EGF and Tf together, it was clear that these two ligands were being sorted at the plasma membrane long before entering the cell. This is most likely due to differences in the distribution of their cognate receptors and in fact, I found that the EGFR was predominately concentrated in glycosphingolipid, GM_1 rich, lipid rafts (see Future Studies), while the TfR was concentrated in the larger, clathrin patches. These data support the observation that ligand sorting occurs at the earlies stages of endocytosis, at the plasma membrane.

The localization of the EGFR to lipid rafts/caveolae is still a subject of intense study [61, 62, 64, 65]. Couet and co-workers reported that the unliganded EGFR directly interacts with the caveolin scaffolding domain through it's cytoplasmic tail [62] and that the ligand activated receptor signaling is inhibited by this association with lipid rafts. The prevailing view of EGF endocytosis suggests that the binding of EGF to the EGFR in lipid rafts initiates the translocation of the ligand-receptor complex from the lipid raft to the CCP [65]. My data clearly does not agree with this supposition. Rather, my results are consistent with a popular alternative mechanism that suggests that the EGFR containing lipid rafts do not transit through the CCP, but upon EGF binding triggers their own clathrin independent endocytosis [145].

If sorting occurs at the plasma membrane, does the early endosome participate in cargo sorting? Mellman has suggested that early endosomes are responsible for the dissociation and sorting of receptor and ligands in an environment that minimizes the risk of damaging receptors intended for re-utilization. He also reported that early endosomes exist in two distinct populations each with a discrete function [4]. Using EEA1 as a

marker for the early endosome, I saw that the separation of Tf and EGF continued through its association with the EEA1 coated early endosome. This was very surprising since Tf has long been thought to use EEA1 coated endosomes during the recycling process. This is based on work done by Christoforidis and co-workers, who used *in vitro* fusion assays to show that EEA1 and Rab5 were necessary for the fusion of Tf loaded vesicles [125]. However, these findings highlight a major short coming of *in vitro* fusion assays, components are made from crude endosome preparations that contain not only early endosomes, but also include CCV, late endosomes, recyling endosomes, MVBs and components of the Golgi. Thus, it is likely that the reported relationship between Tf and EEA1 may only be artifact resulting from the loss of spatial separation of the individual elements of the endocytotic pathway and the complex mixture of vesicles at various stages of processing present in the crude preparations. In fact, the report that EEA1 decorated vesicles still underwent fusion even after Wortmannin treatment, suggests that the normal sequence of events has been compromised. My work specifically looks at the earliest step of Tf endocytosis in a living cell and using real-time TIRF-M imaging, 3-D epifluorescent imaging and Tf uptake studies I was unable to find any apparent relationship between Tf loaded vesicle and the EEA1 coated vesicle.

Unlike the Tf-loaded vesicle, the relationship between the EEA1-early endosome and EGF endocytosis was confirmed as was reported by others [109, 146, 147]. However, many of the original studies in this field used *in vitro* fusion assays with vesicles loaded in the cold with fluorescent EGF, rather than real-time analysis in living cells. I used biologically relevant EGF concentrations and a constant physiological

temperature to observe the endocytosis of EGF and its relationship with EEA1-coated vesicles in real-time by TIRF-M. EGF loaded vesicles were internalized without the aid of clathrin and within 2 min of internalization the EGF-loaded vesicle interacted with the EEA1-early endosome. Subsequent work showed that the 2 min delay between EGF internalization and its interaction with the EEA1-early endosome was due to the time it took to recruit Rab5 to the EGF vesicle. These data complement those of Barbieri, et al who showed that expression of a dominant negative Rab5 mutant aborted the signal transduction cascade that is coupled to the binding of EGF to the EGFR [66].

The key role of the EEA1-early endosome in the EGF endocytic pathway was established by additional studies (data not shown) that showed that internalized EGF vesicles were unable to move from the plasma membrane in COS cells lacking EEA1 by specific siRNA knockdown. Similarly, *in situ* EGF uptake studies showed the interruption of EGF internalization due to the loss of EEA1 did not alter the binding of EGF to its receptor on the cell surface. Western analysis of the EEA1 knockdown cells revealed that the loss of EEA1 not only aborted EGF vesicle trafficking, but also interrupted EGFR degradation. These data show the trafficking of the EGF-loaded vesicle along its endocytic pathway has an absolute requirement for the EEA1-early endosome.

Preliminary studies using an N-terminal truncation mutation of EEA1 that removed the N-terminal Rab5 binding domain (see Future Studies), showed that the loss of the effector domain aborted the further processing of EGF vesicles, suggesting that the N-terminal Rab5 binding domain of EEA1 plays an important role in interactions

between the EEA1-early endosome and newly internalized EGF vesicles. Using a more specific point mutation in the N-terminal Rab5 binding domain that completely inhibits Rab5 binding, also led to the failure of newly internalized EGF vesicles to leave the vicinity of the plasma membrane (personal communication, DML). These are the first data that indicate a functional role for the N-terminus of EEA1 in EGF endocytosis.

Since the Tf-loaded vesicle did not interact with Rab5 and thus EEA1 [148], we turned our attention to the role of other FYVE domain proteins in the early steps of endocytosis. All proteins with a FYVE domain have the ability to bind with high specificity to PI(3)P. PI(3)P is found almost exclusively on the surface of endosomes and is critical in the process of endocytosis and cell signaling [119, 149, 150]. Because of the affinity of the FYVE domain for this membrane signal, many of the FYVE domain proteins are recruited to vesicle populations throughout the endocytic pathway, where they presumably function to assist with vesicle trafficking. For example, the FYVE domain proteins like Rabip4 and Rabenosyn5 coordinate Rab4 and Rab5 binding, respectively, and along with Hrs are important for vesicle delivery for lysosomal degradation [128-130]. However, not all FYVE domain proteins have primary roles in endocytosis; SARA, for example, mediates signal transduction through the TGF-β receptor [136, 151].

Our lab, in collaboration with the laboratory of Dr. Craig Mello at UMASS Medical School identified a new FYVE domain protein, WDFY2, which was involved in endocytosis in C. elegans, and we wondered if it could have a role in endocytosis, in particular, Tf endocytosis in mammalian cells. My work verified that WDFY2 labeled a

subset of endosomes that differed from the EEA1-decorated endosome and studies using both Tf and EGF showed that WDFY2 colocalized with Tf vesicles, but did not interact with EGF-loaded vesicles[148]. The essential role of WDFY2 in Tf endocytic pathway was verified by studies done in cells lacking WDFY2 by specific siRNA knockdown cells [148]. Loss of WDFY2 specifically aborted Tf vesicle trafficking, without altering the dynamics of the EGF endocytosis. These data are some of the first to show that different FYVE domain proteins may participate is the early stages of the trafficking of specific cargo laden vesicles.

Functional studies done with Tf confirmed a lack of interaction between WDFY2 and clathrin or the CCP indicating that it is unlikely that WDFY2 interacts with CCPs or the emerging CCV. While it is also possible that the relationship between WDFY2 and clathrin may be too transient to be seen by TIRF-M—although such an interaction would have a dwell time of less that 2 seconds—it is more likely that WDFY2 is recruited to the Tf-loaded endosome after the clathrin coat is shed.

The identification of a new set of FYVE domain vesicles that participate in Tf endocytosis illustrates the potential for other such proteins to participate in the trafficking of specific cargoes; however, such functional relationships remain to be established. It is tempting to speculate that different FYVE domain proteins are recruited by their interaction with PI(3)P on vesicles loaded with unique cargoes, and serve to direct the target vesicle to different destinations in the endocytic pathway through the other functional domains of the individual FYVE domain protein. For example, the binding of the FYVE domain of WDFY2 to the vesicle wall tethers its WD40 propeller motif to a

specific subset of vesicles, where this domain can coordinate the interaction(s) with the other WD40 motif binding proteins at one or several stages of the endocytic pathway. The multifunctional nature of the FYVE domain proteins provides a vast repertoire of potential signaling domains that may serve to direct vesicle traffic.

Consistent with this hypothesis, WDFY2 participates in Tf endocytosis, but not in the EGF endocytotic pathway (data not shown), while EEA1 is required for EGF endocytosis, but not in Tf internalization. If this dichotomy represents a fundamental property of FYVE domain proteins, it is likely that individual cargo-receptor complexes recruit specific FYVE domain proteins, which in turn, are used to assemble the appropriate protein scaffolds required to escort the vesicle and its contents to its final destination. Thus, the cargo receptor assumes a pre-eminent role in directing its ligand to a specific intracellular destination, and the order of events that occur at the plasma membrane assume greater importance. In this scenario, cargo based signals originating at the plasma membrane may determine such fundamental events as whether the cargo will be internalized through CME or through an alternative endocytic pathway.

In conclusion, I have systematically re-examined some of the components of endocytosis of two of the most widely used ligands for endocytosis, using TIRF-M and biochemical analyses. The results of my studies allow me to revise the classical model of CME to include the larger clathrin platforms as a major component of this fundamental form of endocytosis. I also showed the cargo and its receptor play an important role in the control of their own internalization by selecting among several common endocytotic entry points. It is clear from my studies, that the earliest events in endocytosis play an

important role in directing the destination of endocytosed cargo, but there is still much to be learned regarding molecular events that mediate such selection processes.

FUTURE STUDIES

The goal of my future studies is to define and characterize the molecular events that mediate cargo sorting at early steps in endocytosis. Progress on the fundamental process has been limited because of the lack of tools capable of following dynamic events that occur at or near the plasma membrane. The observation that large clathrin arrays serve as platforms for endocytosis raised several important new questions regarding their molecular organization, how does clathrin recycle from the CCV back to the CCP and how are they held in specific domains on the cell membrane? It remains unclear whether these clathrin patches are organized in flat arrays or whether these patches are simply multilayered clusters of CCPs that rapidly assemble and disassemble. It is also interesting to wonder whether these clathrin platforms and the actin cytoskeleton cooperate through PIs signals to set up specific membrane regions that are organized for specific internalization and/or signaling functions.

I was unable to demonstrate that EGF was internalized through the large clathrin patches. As shown, preliminary studies, illustrated in Fig. 28*a*, co-localization of EGF: and clathrin was sporadic. While clathrin signal (Fig.28*b, green trace*) at the membrane remains constant over the 9 minutes studied, the EGF signal (Fig. 25*b, red trace*) steadily increased, and when I examined the percent of clathrin voxels that co-localized with EGF (Fig. 28*c, red trace*) and the percent of EGF voxels that co-localized with clathrin (Fig. 28*c*, *blue trace*), only 10% of the fluorescent EGF was associated with clathrin, the remaining EGF was internalized by some other mechanism of endocytosis other than CME. Importantly, the EGF vesicles did not co-localize with caveolin, a major

component for caveolae endocyctosis; however they could be labeled with cholera toxin, a marker of sphingolipid-rich microdomains (Fig. 28*d*), suggesting that the EGF vesicle is internalized on lipid rafts.

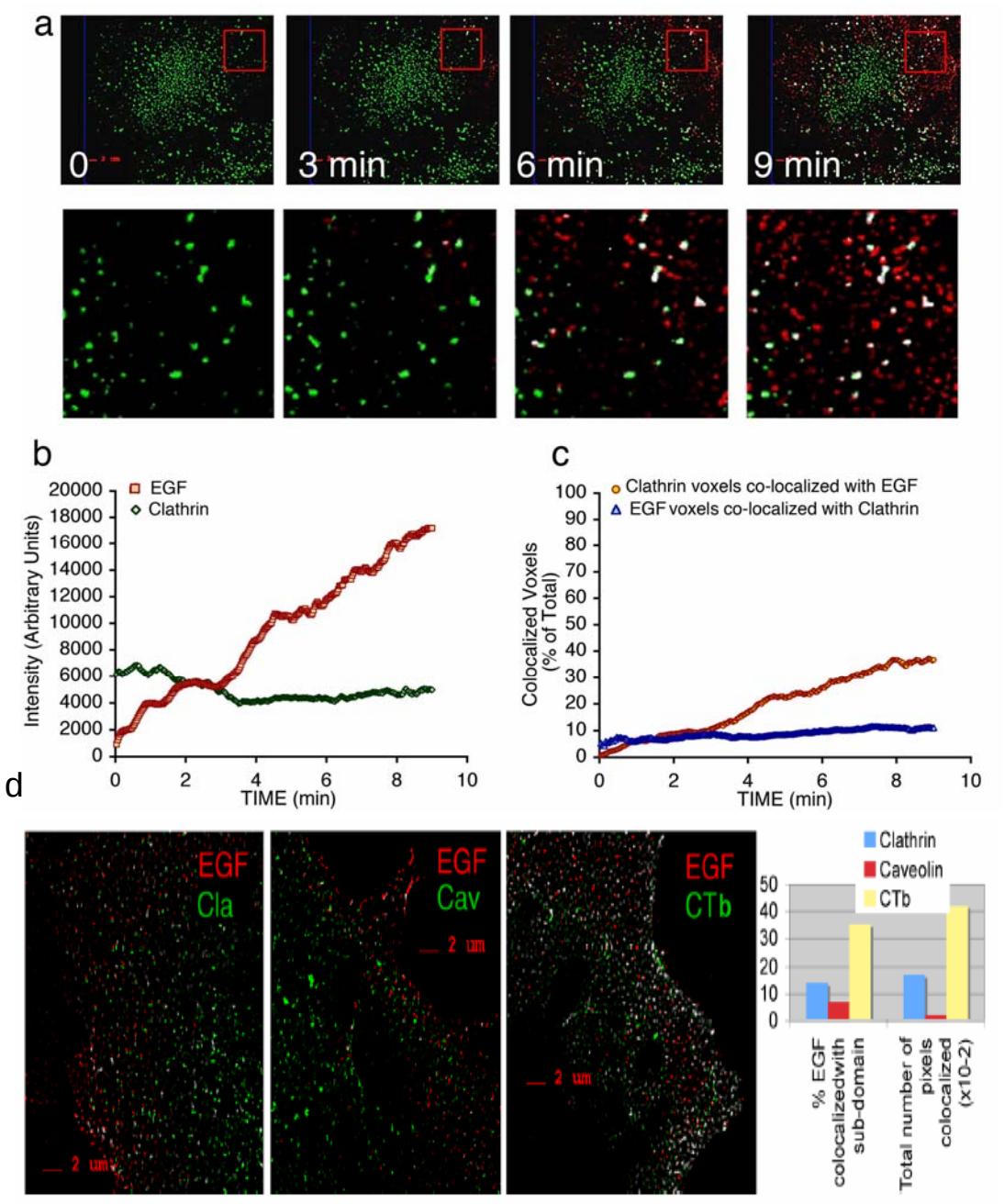
a
0
3 min
6 min
9 min
b
EGF
Clathrin
Intensity (Arbitrary Units)
TIME (min)
c
Clathrin voxels co-localized with EGF
EGF voxels co-localized with Clathrin
Colocalized Voxels (% of Total)
TIME (min)
d
EGF Cla
EGF Cav
EGF CTb
2 um
Clathrin
Caveolin
CTb
% EGF colocalizedwith sub-domain
Total number of pixels colocalized (x10-2)

Figure 28. EGF binding and uptake imaged by TIRF-M.
a), COS cells expressing GFP-clathrin were incubated in the continuous presence of Alexa^{568}-EGF for the times indicated. Magnifications of the areas demarcated by the rectangles are shown to the *below each panel*. *b),* the EGF signal (*red trace*) and the clathrin signal *(green trace*) over 9 minutes. *c),* the percent clathrin voxels co-localized with EGF *(orange trace)* and the percent EGF voxels co-localized with clathrin *(blue trace).* *d),* COS cells expressing GFP-clathrin, GRP-caveolin or stained with cholera toxin were treated with EGF for 10 minutes.

These preliminary studies suggest that lipid rafts may have a significant role in EGF internalization, at 35^{o}C—the temperature used in this study. Work by others has been done at very different temperatures and pilot studies indicated that this variable has a profound effect on EFG endocytosis. A systematic evaluation of the temperature dependence of EGF endocytosis will be necessary to reconcile our results with the disparate results in the literature. Others have suggested that the EGF concentration serves an important role in the selection of endocytic pathways and further studies are needed to determine if ligand concentration plays a role in the selection of endocytic mechanism used.

Further studies to determine the steps of endocytosis that are upstream of Rab5 recruitment by vesicles harboring the activated EGFR will not only fine tune this particular endocytic pathway, but should enhance our understanding of the role of the Rab-GTPases in endocytosis. It would be interesting to see if other receptor-ligand complexes, especially those ligands directed to degradative/lysosomal pathway, such as PDGF, also recruit Rab5 at the very early steps of endocytosis. Or do other ligands, Tf or LDL, use other Rabs to direct their final destination within the cell?

Finally, the possibility that individual members of the FYVE domain family determine the destination of endocytosed cargo is an appealing hypothesis. In CHAPTER IV, I found that WDFY2 played a role in Tf endocytosis, while EEA1 did not. Is it possible that different FYVE domain proteins act as monitors to direct the fate of individual ligands and that the known differences in the proximal and distal effector

domains may define this function? Preliminary studies using an N-terminal deletion of EEA1 found that the loss of this domain interrupts EGF internalization at the plasma membrane (Fig. 29), suggesting that N-terminus of EEA1 is important for EGF endocytosis.

Figure 29*A* shows a representative sequence of the images that follow the liganded EGFR in cells expressing the deletion mutant of EEA1, GFP-EEA1$^{632\text{-}1411}$. Cell associated EGF increases over time; while there is little, if any, recruitment of the mutated EEA1 in contrast to the robust co-localization normally seen with full-length EEA1. Quantitative analysis of the images shows a steady increase in EGF signal (Fig. 29*B, blue trace*); however there was little change in truncated EEA1$^{632\text{-}1411}$ intensity (Fig. 29*B, red trace*) over the 9 min time course. Quantitative analysis of the images confirms the lack of significant co-localization between EGF and EEA1$^{632\text{-}1411}$. The data in Figure 29*C*, shows the percent of maximum EGF co-localized with the truncated EEA1$^{632\text{-}1411}$ *(blue trace*) and the percent of maximum of truncated EEA1$^{632\text{-}1411}$ co-localized with EGF (*red trace*). Spurious co-localization—chance events when the two fluorescent signals occupy the same space—was calculated by flipping one of the images along the X or Y axis and the patterns were very similar to those shown in Fig. 29*C* (data not shown) suggesting that the marginal apparent co-localization of EGF with the truncated EEA1$^{632\text{-}1411}$ was coincidental. These results suggest that the N-terminus of EEA1 plays an active role in EGF internalization and further studies are required to determine if and how Rab5 coordinates the delivery of EGF vesicles to the EEA1 endosomes.

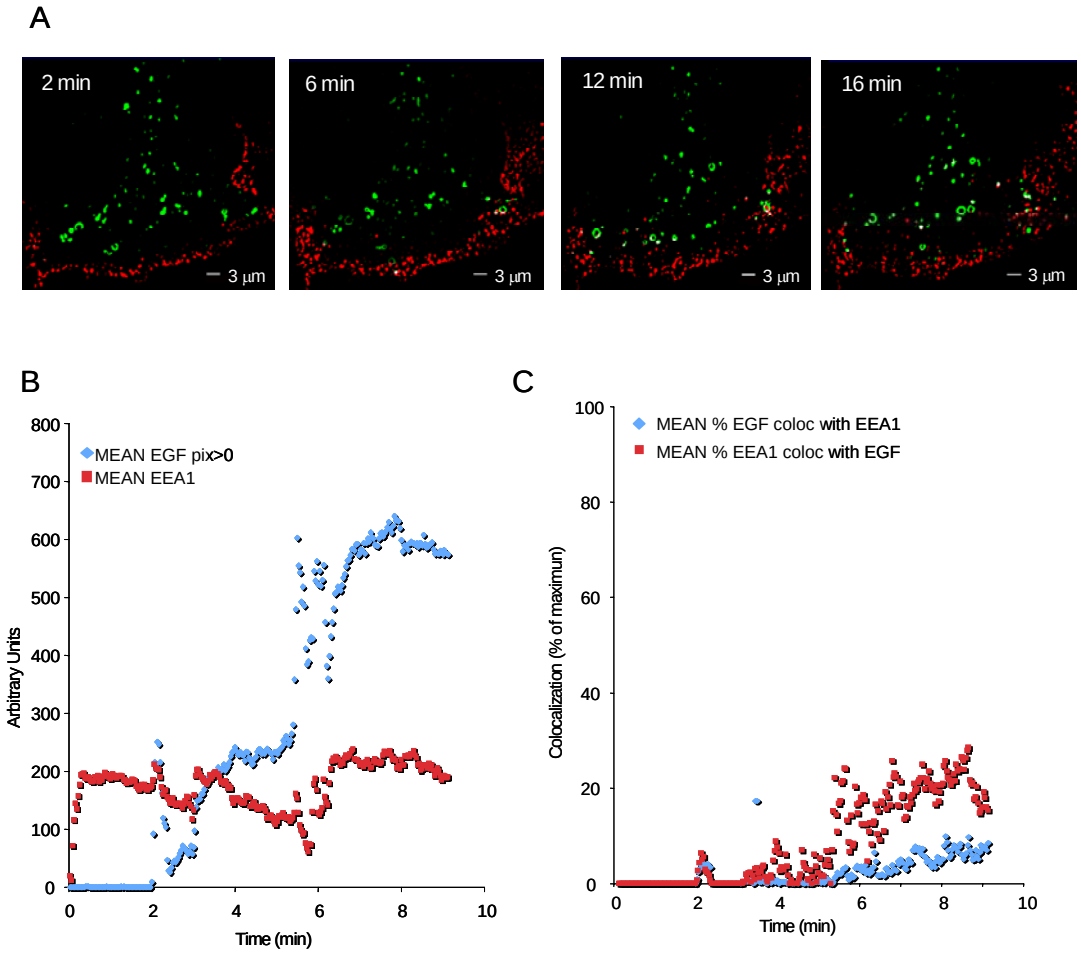

Figure 29. EGF binding and co-localization with GFP-EEA1$^{632\text{-}1411}$ mutant.
A. Cos-7 cells expressing GFP-EEA1$^{632\text{-}1411}$ were imaged by TIRF-M during continuous incubation with 50 ng/ml Alexa^{568}-EGF. *B.* The mean intensity of Alexa^{568}-EGF *(blue trace)* and GFP-EEA1$^{632\text{-}1411}$ *(red trace)*, over the cell surface. *C.* The percent of the total Alexa^{568}-EGF signal co-localized with GFP-EEA1$^{632\text{-}1411}$ voxels *(blue trace)* and the percent of the total GFP-EEA1$^{632\text{-}1411}$ signal co-localized with Alexa^{568}-EGF *(red trace)*.

These studies will further our understanding of the complex process of endocytosis. Our improved understanding of this process will assist with the development and delivery of drugs that can be specifically used to treat and/or prevent several forms of cancer.

REFERENCES

1. Conner, S.D. and S.L. Schmid, *Regulated portals of entry into the cell.* Nature, 2003. **422**(6927): p. 37-44.
2. Moskowitz, H.S., C.T. Yokoyama, and T.A. Ryan, *Highly cooperative control of endocytosis by clathrin.* Mol Biol Cell, 2005. **16**(4): p. 1769-76.
3. Warren, R.A., et al., *Distinct saturable pathways for the endocytosis of different tyrosine motifs.* J Biol Chem, 1998. **273**(27): p. 17056-63.
4. Mellman, I., *Endocytosis and molecular sorting.* Annu Rev Cell Dev Biol, 1996. **12**: p. 575-625.
5. Warren, R.A., F.A. Green, and C.A. Enns, *Saturation of the endocytic pathway for the transferrin receptor does not affect the endocytosis of the epidermal growth factor receptor.* J Biol Chem, 1997. **272**(4): p. 2116-21.
6. Sorkin, A., *Cargo recognition during clathrin-mediated endocytosis: a team effort.* Curr Opin Cell Biol, 2004. **16**(4): p. 392-9.
7. Brodin, L., P. Low, and O. Shupliakov, *Sequential steps in clathrin-mediated synaptic vesicle endocytosis.* Curr Opin Neurobiol, 2000. **10**(3): p. 312-20.
8. Motley, A., et al., *Clathrin-mediated endocytosis in AP-2-depleted cells.* J Cell Biol, 2003. **162**(5): p. 909-18.
9. Rapoport, I., et al., *Regulatory interactions in the recognition of endocytic sorting signals by AP-2 complexes.* Embo J, 1997. **16**(9): p. 2240-50.
10. Beattie, E.C., et al., *Regulation of AMPA receptor endocytosis by a signaling mechanism shared with LTD.* Nat Neurosci, 2000. **3**(12): p. 1291-300.
11. Rappoport, J.Z., et al., *The AP-2 complex is excluded from the dynamic population of plasma membrane-associated clathrin.* J Biol Chem, 2003. **278**(48): p. 47357-60.
12. Benmerah, A., et al., *AP-2/Eps15 interaction is required for receptor-mediated endocytosis.* J Cell Biol, 1998. **140**(5): p. 1055-62.
13. Merrifield, C.J., et al., *Imaging actin and dynamin recruitment during invagination of single clathrin-coated pits.* Nat Cell Biol, 2002. **4**(9): p. 691-8.
14. Maxfield, F.R. and T.E. McGraw, *Endocytic recycling.* Nat Rev Mol Cell Biol, 2004. **5**(2): p. 121-32.
15. Merrifield, C.J., D. Perrais, and D. Zenisek, *Coupling between clathrin-coated-pit invagination, cortactin recruitment, and membrane scission observed in live cells.* Cell, 2005. **121**(4): p. 593-606.
16. Ehrlich, M., et al., *Endocytosis by random initiation and stabilization of clathrin-coated pits.* Cell, 2004. **118**(5): p. 591-605.
17. Gaidarov, I., et al., *Spatial control of coated-pit dynamics in living cells.* Nat Cell Biol, 1999. **1**(1): p. 1-7.
18. Rappoport, J.Z. and S.M. Simon, *Real-time analysis of clathrin-mediated endocytosis during cell migration.* J Cell Sci, 2003. **116**(Pt 5): p. 847-55.
19. Trowbridge, I.S., J.F. Collawn, and C.R. Hopkins, *Signal-dependent membrane protein trafficking in the endocytic pathway.* Annu Rev Cell Biol, 1993. **9**: p. 129-61.

20. Sonnichsen, B., et al., *Distinct membrane domains on endosomes in the recycling pathway visualized by multicolor imaging of Rab4, Rab5, and Rab11.* J Cell Biol, 2000. **149**(4): p. 901-14.
21. Gaborik, Z. and L. Hunyady, *Intracellular trafficking of hormone receptors.* Trends Endocrinol Metab, 2004. **15**(6): p. 286-93.
22. Lakadamyali, M., M.J. Rust, and X. Zhuang, *Ligands for clathrin-mediated endocytosis are differentially sorted into distinct populations of early endosomes.* Cell, 2006. **124**(5): p. 997-1009.
23. Ward, E.S., et al., *From sorting endosomes to exocytosis: association of Rab4 and Rab11 GTPases with the Fc receptor, FcRn, during recycling.* Mol Biol Cell, 2005. **16**(4): p. 2028-38.
24. Vonderheit, A. and A. Helenius, *Rab7 associates with early endosomes to mediate sorting and transport of Semliki forest virus to late endosomes.* PLoS Biol, 2005. **3**(7): p. e233.
25. Gruenberg, J., *The endocytic pathway: a mosaic of domains.* Nat Rev Mol Cell Biol, 2001. **2**(10): p. 721-30.
26. Kuhn, L.C., A. McClelland, and F.H. Ruddle, *Gene transfer, expression, and molecular cloning of the human transferrin receptor gene.* Cell, 1984. **37**(1): p. 95-103.
27. Jing, S.Q. and I.S. Trowbridge, *Identification of the intermolecular disulfide bonds of the human transferrin receptor and its lipid-attachment site.* Embo J, 1987. **6**(2): p. 327-31.
28. Schneider, C., M. Kurkinen, and M. Greaves, *Isolation of cDNA clones for the human transferrin receptor.* Embo J, 1983. **2**(12): p. 2259-63.
29. Zerial, M., et al., *The transmembrane segment of the human transferrin receptor functions as a signal peptide.* Embo J, 1986. **5**(7): p. 1543-50.
30. Ward, J.H., J.P. Kushner, and J. Kaplan, *Transferrin receptors of human fibroblasts. Analysis of receptor properties and regulation.* Biochem J, 1982. **208**(1): p. 19-26.
31. Tosoni, D., et al., *TTP specifically regulates the internalization of the transferrin receptor.* Cell, 2005. **123**(5): p. 875-88.
32. Huebers, H.A. and C.A. Finch, *The physiology of transferrin and transferrin receptors.* Physiol Rev, 1987. **67**(2): p. 520-82.
33. Trischler, M., W. Stoorvogel, and O. Ullrich, *Biochemical analysis of distinct Rab5- and Rab11-positive endosomes along the transferrin pathway.* J Cell Sci, 1999. **112 (Pt 24)**: p. 4773-83.
34. Dautry-Varsat, A., A. Ciechanover, and H.F. Lodish, *pH and the recycling of transferrin during receptor-mediated endocytosis.* Proc Natl Acad Sci U S A, 1983. **80**(8): p. 2258-62.
35. Ghosh, R.N., D.L. Gelman, and F.R. Maxfield, *Quantification of low density lipoprotein and transferrin endocytic sorting HEp2 cells using confocal microscopy.* J Cell Sci, 1994. **107 (Pt 8)**: p. 2177-89.
36. Bache, K.G., et al., *Hrs regulates multivesicular body formation via ESCRT recruitment to endosomes.* J Cell Biol, 2003. **162**(3): p. 435-42.

37. Katzmann, D.J., M. Babst, and S.D. Emr, *Ubiquitin-dependent sorting into the multivesicular body pathway requires the function of a conserved endosomal protein sorting complex, ESCRT-I.* Cell, 2001. **106**(2): p. 145-55.
38. Futter, C.E., et al., *Multivesicular endosomes containing internalized EGF-EGF receptor complexes mature and then fuse directly with lysosomes.* J Cell Biol, 1996. **132**(6): p. 1011-23.
39. Kornfeld, S. and I. Mellman, *The biogenesis of lysosomes.* Annu Rev Cell Biol, 1989. **5**: p. 483-525.
40. Le Roy, C. and J.L. Wrana, *Clathrin- and non-clathrin-mediated endocytic regulation of cell signalling.* Nat Rev Mol Cell Biol, 2005. **6**(2): p. 112-26.
41. Ogiso, H., et al., *Crystal structure of the complex of human epidermal growth factor and receptor extracellular domains.* Cell, 2002. **110**(6): p. 775-87.
42. Pike, L.J., *Growth factor receptors, lipid rafts and caveolae: an evolving story.* Biochim Biophys Acta, 2005. **1746**(3): p. 260-73.
43. Schlessinger, J., *Ligand-induced, receptor-mediated dimerization and activation of EGF receptor.* Cell, 2002. **110**(6): p. 669-72.
44. Mineo, C., et al., *Localization of epidermal growth factor-stimulated Ras/Raf-1 interaction to caveolae membrane.* J Biol Chem, 1996. **271**(20): p. 11930-5.
45. Schlessinger, J., *Cell signaling by receptor tyrosine kinases.* Cell, 2000. **103**(2): p. 211-25.
46. de Melker, A.A., et al., *c-Cbl ubiquitinates the EGF receptor at the plasma membrane and remains receptor associated throughout the endocytic route.* J Cell Sci, 2001. **114**(Pt 11): p. 2167-78.
47. Levkowitz, G., et al., *c-Cbl/Sli-1 regulates endocytic sorting and ubiquitination of the epidermal growth factor receptor.* Genes Dev, 1998. **12**(23): p. 3663-74.
48. Katzmann, D.J., et al., *Vps27 recruits ESCRT machinery to endosomes during MVB sorting.* J Cell Biol, 2003. **162**(3): p. 413-23.
49. Kil, S.J. and C. Carlin, *EGF receptor residues leu(679), leu(680) mediate selective sorting of ligand-receptor complexes in early endosomal compartments.* J Cell Physiol, 2000. **185**(1): p. 47-60.
50. Waterman, H. and Y. Yarden, *Molecular mechanisms underlying endocytosis and sorting of ErbB receptor tyrosine kinases.* FEBS Lett, 2001. **490**(3): p. 142-52.
51. Ringerike, T., et al., *High-affinity binding of epidermal growth factor (EGF) to EGF receptor is disrupted by overexpression of mutant dynamin (K44A).* J Biol Chem, 1998. **273**(27): p. 16639-42.
52. Wilde, A., et al., *EGF receptor signaling stimulates SRC kinase phosphorylation of clathrin, influencing clathrin redistribution and EGF uptake.* Cell, 1999. **96**(5): p. 677-87.
53. Huang, F., et al., *Analysis of clathrin-mediated endocytosis of epidermal growth factor receptor by RNA interference.* J Biol Chem, 2004. **279**(16): p. 16657-61.
54. Larkin, J.M., et al., *Depletion of intracellular potassium arrests coated pit formation and receptor-mediated endocytosis in fibroblasts.* Cell, 1983. **33**(1): p. 273-85.

55. Stahlhut, M. and B. van Deurs, *Identification of filamin as a novel ligand for caveolin-1: evidence for the organization of caveolin-1-associated membrane domains by the actin cytoskeleton.* Mol Biol Cell, 2000. **11**(1): p. 325-37.
56. Thomsen, P., et al., *Caveolae are highly immobile plasma membrane microdomains, which are not involved in constitutive endocytic trafficking.* Mol Biol Cell, 2002. **13**(1): p. 238-50.
57. Le Lay, S., et al., *Cholesterol-induced caveolin targeting to lipid droplets in adipocytes: a role for caveolar endocytosis.* Traffic, 2006. **7**(5): p. 549-61.
58. Smart, E.J., et al., *Caveolins, liquid-ordered domains, and signal transduction.* Mol Cell Biol, 1999. **19**(11): p. 7289-304.
59. Simons, K. and D. Toomre, *Lipid rafts and signal transduction.* Nat Rev Mol Cell Biol, 2000. **1**(1): p. 31-9.
60. Glebov, O.O., N.A. Bright, and B.J. Nichols, *Flotillin-1 defines a clathrin-independent endocytic pathway in mammalian cells.* Nat Cell Biol, 2006. **8**(1): p. 46-54.
61. Lim, K.I. and J. Yin, *Localization of receptors in lipid rafts can inhibit signal transduction.* Biotechnol Bioeng, 2005. **90**(6): p. 694-702.
62. Couet, J., M. Sargiacomo, and M.P. Lisanti, *Interaction of a receptor tyrosine kinase, EGF-R, with caveolins. Caveolin binding negatively regulates tyrosine and serine/threonine kinase activities.* J Biol Chem, 1997. **272**(48): p. 30429-38.
63. Lambert, S., et al., *Ligand-independent activation of the EGFR by lipid raft disruption.* J Invest Dermatol, 2006. **126**(5): p. 954-62.
64. Pike, L.J. and L. Casey, *Cholesterol levels modulate EGF receptor-mediated signaling by altering receptor function and trafficking.* Biochemistry, 2002. **41**(32): p. 10315-22.
65. Puri, C., et al., *Relationships between EGFR signaling-competent and endocytosis-competent membrane microdomains.* Mol Biol Cell, 2005. **16**(6): p. 2704-18.
66. Barbieri, M.A., et al., *Role of rab5 in EGF receptor-mediated signal transduction.* Eur J Cell Biol, 2004. **83**(6): p. 305-14.
67. McPherson, P.S., B.K. Kay, and N.K. Hussain, *Signaling on the endocytic pathway.* Traffic, 2001. **2**(6): p. 375-84.
68. Penengo, L., et al., *Crystal structure of the ubiquitin binding domains of rabex-5 reveals two modes of interaction with ubiquitin.* Cell, 2006. **124**(6): p. 1183-95.
69. Lill, N.L., et al., *The evolutionarily conserved N-terminal region of Cbl is sufficient to enhance down-regulation of the epidermal growth factor receptor.* J Biol Chem, 2000. **275**(1): p. 367-77.
70. Mizuno, E., et al., *Regulation of epidermal growth factor receptor down-regulation by UBPY-mediated deubiquitination at endosomes.* Mol Biol Cell, 2005. **16**(11): p. 5163-74.
71. Axelrod, D., *Total internal reflection fluorescence microscopy in cell biology.* Traffic, 2001. **2**(11): p. 764-74.
72. Steyer, J.A. and W. Almers, *A real-time view of life within 100 nm of the plasma membrane.* Nat Rev Mol Cell Biol, 2001. **2**(4): p. 268-75.

73. Hinrichsen, L., et al., *Effect of clathrin heavy chain- and alpha-adaptin-specific small inhibitory RNAs on endocytic accessory proteins and receptor trafficking in HeLa cells.* J Biol Chem, 2003. **278**(46): p. 45160-70.
74. Brodsky, F.M., et al., *Biological basket weaving: formation and function of clathrin-coated vesicles.* Annu Rev Cell Dev Biol, 2001. **17**: p. 517-68.
75. Kirchhausen, T., *Clathrin.* Annu Rev Biochem, 2000. **69**: p. 699-727.
76. Marsh, M. and H.T. McMahon, *The structural era of endocytosis.* Science, 1999. **285**(5425): p. 215-20.
77. Robinson, M.S., *Adaptable adaptors for coated vesicles.* Trends Cell Biol, 2004. **14**(4): p. 167-74.
78. Schmid, S.L., M.A. McNiven, and P. De Camilli, *Dynamin and its partners: a progress report.* Curr Opin Cell Biol, 1998. **10**(4): p. 504-12.
79. Beaumont, V., *Visualizing membrane trafficking using total internal reflection fluorescence microscopy.* Biochem Soc Trans, 2003. **31**(Pt 4): p. 819-23.
80. Keyel, P.A., S.C. Watkins, and L.M. Traub, *Endocytic adaptor molecules reveal an endosomal population of clathrin by total internal reflection fluorescence microscopy.* J Biol Chem, 2004. **279**(13): p. 13190-204.
81. Rappoport, J.Z., A. Benmerah, and S.M. Simon, *Analysis of the AP-2 adaptor complex and cargo during clathrin-mediated endocytosis.* Traffic, 2005. **6**(7): p. 539-47.
82. Rappoport, J.Z., S.M. Simon, and A. Benmerah, *Understanding living clathrin-coated pits.* Traffic, 2004. **5**(5): p. 327-37.
83. Rappoport, J.Z., B.W. Taha, and S.M. Simon, *Movement of plasma-membrane-associated clathrin spots along the microtubule cytoskeleton.* Traffic, 2003. **4**(7): p. 460-7.
84. Lizunov, V.A., et al., *Insulin stimulates the halting, tethering, and fusion of mobile GLUT4 vesicles in rat adipose cells.* J Cell Biol, 2005. **169**(3): p. 481-9.
85. Robinson, L.J., et al., *Translocation of the glucose transporter (GLUT4) to the cell surface in permeabilized 3T3-L1 adipocytes: effects of ATP insulin, and GTP gamma S and localization of GLUT4 to clathrin lattices.* J Cell Biol, 1992. **117**(6): p. 1181-96.
86. Lifshitz, L., et al. in *IEEE Workshop on Biomedical Analysis*. 1994. Los Alamitos, CA: IEEE Computer Society Press.
87. Gaidarov, I. and J.H. Keen, *Phosphoinositide-AP-2 interactions required for targeting to plasma membrane clathrin-coated pits.* J Cell Biol, 1999. **146**(4): p. 755-64.
88. Schlessinger, J., et al., *Regulation of cell proliferation by epidermal growth factor.* CRC Crit Rev Biochem, 1983. **14**(2): p. 93-111.
89. Yarden, Y., *The EGFR family and its ligands in human cancer. signalling mechanisms and therapeutic opportunities.* Eur J Cancer, 2001. **37 Suppl 4**: p. S3-8.
90. Yarden, Y. and J. Schlessinger, *The EGF receptor kinase: evidence for allosteric activation and intramolecular self-phosphorylation.* Ciba Found Symp, 1985. **116**: p. 23-45.

91. Yarden, Y. and M.X. Sliwkowski, *Untangling the ErbB signalling network.* Nat Rev Mol Cell Biol, 2001. **2**(2): p. 127-37.
92. Bowtell, D.D. and W.Y. Langdon, *The protein product of the c-cbl oncogene rapidly complexes with the EGF receptor and is tyrosine phosphorylated following EGF stimulation.* Oncogene, 1995. **11**(8): p. 1561-7.
93. Langdon, W.Y., *The cbl oncogene: a novel substrate of protein tyrosine kinases.* Aust N Z J Med, 1995. **25**(6): p. 859-64.
94. Levkowitz, G., et al., *Coupling of the c-Cbl protooncogene product to ErbB-1/EGF-receptor but not to other ErbB proteins.* Oncogene, 1996. **12**(5): p. 1117-25.
95. Thien, C.B. and W.Y. Langdon, *EGF receptor binding and transformation by v-cbl is ablated by the introduction of a loss-of-function mutation from the Caenorhabditis elegans sli-1 gene.* Oncogene, 1997. **14**(18): p. 2239-49.
96. Bache, K.G., et al., *The ESCRT-III subunit hVps24 is required for degradation but not silencing of the epidermal growth factor receptor.* Mol Biol Cell, 2006. **17**(6): p. 2513-23.
97. Axelrod, D., *Total internal reflection fluorescence microscopy in cell biology.* Methods Enzymol, 2003. **361**: p. 1-33.
98. Bucci, C., et al., *The small GTPase rab5 functions as a regulatory factor in the early endocytic pathway.* Cell, 1992. **70**(5): p. 715-28.
99. Stenmark, H., et al., *Endosomal localization of the autoantigen EEA1 is mediated by a zinc-binding FYVE finger.* J Biol Chem, 1996. **271**(39): p. 24048-54.
100. Patki, V., et al., *Identification of an early endosomal protein regulated by phosphatidylinositol 3-kinase.* Proc Natl Acad Sci U S A, 1997. **94**(14): p. 7326-30.
101. Simonsen, A., et al., *EEA1 links PI(3)K function to Rab5 regulation of endosome fusion.* Nature, 1998. **394**(6692): p. 494-8.
102. Dumas, J.J., et al., *Multivalent endosome targeting by homodimeric EEA1.* Mol Cell, 2001. **8**(5): p. 947-58.
103. Merithew, E., et al., *Determinants of Rab5 interaction with the N terminus of early endosome antigen 1.* J Biol Chem, 2003. **278**(10): p. 8494-500.
104. Mills, I.G., A.T. Jones, and M.J. Clague, *Involvement of the endosomal autoantigen EEA1 in homotypic fusion of early endosomes.* Curr Biol, 1998. **8**(15): p. 881-4.
105. Raiborg, C., et al., *FYVE and coiled-coil domains determine the specific localisation of Hrs to early endosomes.* J Cell Sci, 2001. **114**(Pt 12): p. 2255-63.
106. Bellve, K.D., et al., *Plasma membrane domains specialized for clathrin-mediated endocytosis in primary cells.* J Biol Chem, 2006. **281**(23): p. 16139-46.
107. Hoffenberg, S., et al., *A novel membrane-anchored Rab5 interacting protein required for homotypic endosome fusion.* J Biol Chem, 2000. **275**(32): p. 24661-9.
108. Hayakawa, A., et al., *Structural basis for endosomal targeting by FYVE domains.* J Biol Chem, 2004. **279**(7): p. 5958-66.

109. Oksvold, M.P., et al., *Immunocytochemical localization of Shc and activated EGF receptor in early endosomes after EGF stimulation of HeLa cells.* J Histochem Cytochem, 2000. **48**(1): p. 21-33.
110. Lawe, D.C., et al., *The FYVE domain of early endosome antigen 1 is required for both phosphatidylinositol 3-phosphate and Rab5 binding. Critical role of this dual interaction for endosomal localization.* J Biol Chem, 2000. **275**(5): p. 3699-705.
111. Volpicelli, L.A., J.J. Lah, and A.I. Levey, *Rab5-dependent trafficking of the m4 muscarinic acetylcholine receptor to the plasma membrane, early endosomes, and multivesicular bodies.* J Biol Chem, 2001. **276**(50): p. 47590-8.
112. Dinneen, J.L. and B.P. Ceresa, *Continual expression of Rab5(Q79L) causes a ligand-independent EGFR internalization and diminishes EGFR activity.* Traffic, 2004. **5**(8): p. 606-15.
113. Tall, G.G., et al., *Ras-activated endocytosis is mediated by the Rab5 guanine nucleotide exchange activity of RIN1.* Dev Cell, 2001. **1**(1): p. 73-82.
114. Carney, D.S., B.A. Davies, and B.F. Horazdovsky, *Vps9 domain-containing proteins: activators of Rab5 GTPases from yeast to neurons.* Trends Cell Biol, 2006. **16**(1): p. 27-35.
115. Lawe, D.C., et al., *Sequential roles for phosphatidylinositol 3-phosphate and Rab5 in tethering and fusion of early endosomes via their interaction with EEA1.* J Biol Chem, 2002. **277**(10): p. 8611-7.
116. Wilson, J.M., et al., *EEA1, a tethering protein of the early sorting endosome, shows a polarized distribution in hippocampal neurons, epithelial cells, and fibroblasts.* Mol Biol Cell, 2000. **11**(8): p. 2657-71.
117. DiNitto, J.P., T.C. Cronin, and D.G. Lambright, *Membrane recognition and targeting by lipid-binding domains.* Sci STKE, 2003. **2003**(213): p. re16.
118. Misra, S., G.J. Miller, and J.H. Hurley, *Recognizing phosphatidylinositol 3-phosphate.* Cell, 2001. **107**(5): p. 559-62.
119. Burd, C.G. and S.D. Emr, *Phosphatidylinositol(3)-phosphate signaling mediated by specific binding to RING FYVE domains.* Mol Cell, 1998. **2**(1): p. 157-62.
120. Gaullier, J.M., et al., *FYVE fingers bind PtdIns(3)P.* Nature, 1998. **394**(6692): p. 432-3.
121. Callaghan, J., et al., *Direct interaction of EEA1 with Rab5b.* Eur J Biochem, 1999. **265**(1): p. 361-6.
122. Lawe, D.C., et al., *Essential role of Ca2+/calmodulin in Early Endosome Antigen-1 localization.* Mol Biol Cell, 2003. **14**(7): p. 2935-45.
123. Mills, I.G., S. Urbe, and M.J. Clague, *Relationships between EEA1 binding partners and their role in endosome fusion.* J Cell Sci, 2001. **114**(Pt 10): p. 1959-65.
124. Mu, F.T., et al., *EEA1, an early endosome-associated protein. EEA1 is a conserved alpha-helical peripheral membrane protein flanked by cysteine "fingers" and contains a calmodulin-binding IQ motif.* J Biol Chem, 1995. **270**(22): p. 13503-11.

125. Christoforidis, S., et al., *The Rab5 effector EEA1 is a core component of endosome docking.* Nature, 1999. **397**(6720): p. 621-5.
126. McBride, H.M., et al., *Oligomeric complexes link Rab5 effectors with NSF and drive membrane fusion via interactions between EEA1 and syntaxin 13.* Cell, 1999. **98**(3): p. 377-86.
127. Rubino, M., et al., *Selective membrane recruitment of EEA1 suggests a role in directional transport of clathrin-coated vesicles to early endosomes.* J Biol Chem, 2000. **275**(6): p. 3745-8.
128. Nielsen, E., et al., *Rabenosyn-5, a novel Rab5 effector, is complexed with hVPS45 and recruited to endosomes through a FYVE finger domain.* J Cell Biol, 2000. **151**(3): p. 601-12.
129. Cormont, M., et al., *A FYVE-finger-containing protein, Rabip4, is a Rab4 effector involved in early endosomal traffic.* Proc Natl Acad Sci U S A, 2001. **98**(4): p. 1637-42.
130. Komada, M. and P. Soriano, *Hrs, a FYVE finger protein localized to early endosomes, is implicated in vesicular traffic and required for ventral folding morphogenesis.* Genes Dev, 1999. **13**(11): p. 1475-85.
131. Cooke, F.T., et al., *The stress-activated phosphatidylinositol 3-phosphate 5-kinase Fab1p is essential for vacuole function in S. cerevisiae.* Curr Biol, 1998. **8**(22): p. 1219-22.
132. Dove, S.K., et al., *Svp1p defines a family of phosphatidylinositol 3,5-bisphosphate effectors.* Embo J, 2004. **23**(9): p. 1922-33.
133. Odorizzi, G., M. Babst, and S.D. Emr, *Fab1p PtdIns(3)P 5-kinase function essential for protein sorting in the multivesicular body.* Cell, 1998. **95**(6): p. 847-58.
134. Hu, Y., et al., *SARA, a FYVE domain protein, affects Rab5-mediated endocytosis.* J Cell Sci, 2002. **115**(Pt 24): p. 4755-63.
135. Runyan, C.E., H.W. Schnaper, and A.C. Poncelet, *The role of internalization in transforming growth factor beta1-induced Smad2 association with Smad anchor for receptor activation (SARA) and Smad2-dependent signaling in human mesangial cells.* J Biol Chem, 2005. **280**(9): p. 8300-8.
136. Tsukazaki, T., et al., *SARA, a FYVE domain protein that recruits Smad2 to the TGFbeta receptor.* Cell, 1998. **95**(6): p. 779-91.
137. Nonet, M.L., et al., *Synaptic function is impaired but not eliminated in C. elegans mutants lacking synaptotagmin.* Cell, 1993. **73**(7): p. 1291-305.
138. Nonet, M.L., et al., *UNC-11, a Caenorhabditis elegans AP180 homologue, regulates the size and protein composition of synaptic vesicles.* Mol Biol Cell, 1999. **10**(7): p. 2343-60.
139. Grant, B. and D. Hirsh, *Receptor-mediated endocytosis in the Caenorhabditis elegans oocyte.* Mol Biol Cell, 1999. **10**(12): p. 4311-26.
140. Fares, H. and I. Greenwald, *Genetic analysis of endocytosis in Caenorhabditis elegans: coelomocyte uptake defective mutants.* Genetics, 2001. **159**(1): p. 133-45.

141. Sieburth, D., et al., *Systematic analysis of genes required for synapse structure and function.* Nature, 2005. **436**(7050): p. 510-7.
142. Carrington, W.A., et al., *Superresolution three-dimensional images of fluorescence in cells with minimal light exposure.* Science, 1995. **268**(5216): p. 1483-7.
143. Ridley, S.H., et al., *FENS-1 and DFCP1 are FYVE domain-containing proteins with distinct functions in the endosomal and Golgi compartments.* J Cell Sci, 2001. **114**(Pt 22): p. 3991-4000.
144. Harding, C., J. Heuser, and P. Stahl, *Receptor-mediated endocytosis of transferrin and recycling of the transferrin receptor in rat reticulocytes.* J Cell Biol, 1983. **97**(2): p. 329-39.
145. Orth, J.D., et al., *A novel endocytic mechanism of epidermal growth factor receptor sequestration and internalization.* Cancer Res, 2006. **66**(7): p. 3603-10.
146. Barbieri, M.A., et al., *Epidermal growth factor and membrane trafficking. EGF receptor activation of endocytosis requires Rab5a.* J Cell Biol, 2000. **151**(3): p. 539-50.
147. Chen, X. and Z. Wang, *Regulation of intracellular trafficking of the EGF receptor by Rab5 in the absence of phosphatidylinositol 3-kinase activity.* EMBO Rep, 2001. **2**(1): p. 68-74.
148. Hayakawa, A., et al., *The WD40 and FYVE domain containing protein 2 defines a class of early endosomes necessary for endocytosis.* Proc Natl Acad Sci U S A, 2006. **103**(32): p. 11928-33.
149. Corvera, S., *Phosphatidylinositol 3-kinase and the control of endosome dynamics: new players defined by structural motifs.* Traffic, 2001. **2**(12): p. 859-66.
150. Leevers, S.J., B. Vanhaesebroeck, and M.D. Waterfield, *Signalling through phosphoinositide 3-kinases: the lipids take centre stage.* Curr Opin Cell Biol, 1999. **11**(2): p. 219-25.
151. Hayes, S., A. Chawla, and S. Corvera, *TGF beta receptor internalization into EEA1-enriched early endosomes: role in signaling to Smad2.* J Cell Biol, 2002. **158**(7): p. 1239-49.

APPENDIX I

IMAGE RESTORATION AND DATA ANALYSIS

Custom hardware and software has been developed by the Department of Physiology's Imaging Group at UMASS Medical School that allows extremely high speed capture of events, at 50 images/second. Images are collected in each color channel at a rate of 0.5 Hz (1 image/channel every 2 seconds) for 10-20 continuous minutes, with a time lapse between each channel of 200 msec. A darkfield sample is collected to determine noise within the camera before imaging is started. To illustrate the process of image reconstruction/analysis, I am using COS7 cells expressing GFP-clathrin treated with Alexa^{568}-Tf for 20 continuous minutes (Fig. 1). Raw images are collected simultaneously from both channels (GFP was excited with an argon laser at 488 nm and Alexa^{568} was excited with an argon-krypton laser at 568 nm) at a rate of 30 images/channel/min. While TIRF-M yields a raw image data set of sufficient clarity to evaluate experimental manipulation, further image processing improves the quality of such analysis. Each 20 min experimental data set of 1200 images is separated into individual channel data sets of 600 images. Each image in these sets are first corrected for camera noise by subtraction of the darkfield data set and then by subtraction of "non-specific" fluorescence. The photomicrographs in Figure 1*a*, show a selected time point in each channel, for set A, GFP-clathrin and set B, Alexa^{568}-Tf after this first restoration step. Next a running average at three successive time points is taken to eliminate the slight speckling due to random camera noise (compare Fig. 1*a*, images A to C and B to D). Each image is then simultaneously convolved with both a small 2-D Gaussian filter

to reduce the noise and with an inverted (negatively valued) larger 2-D Gaussian filter to estimate and subtract the average local (background) intensity. This allows for the distinction of regions of high intensity, patches or spots over diffuse backgrounds of variable intensity. The data from this step are then converted to binary values, so that all positive pixels are changed to one and all zero or negative pixels to zero to produce a binary mask image (Fig. 1*a*, compare A to E and B to F). The last step of image processing the original image is multiplied by the binary mask (Fig. 1*a*, panels G and H) to produce images in which diffuse background over the cell is eliminated, while allowing direct quantification of the intensity of structured fluorescence signal within each image set and co-localization between the independent channel image sets. Figure 1*b* shows the overlap of the clathrin and transferrin image sets (overlapping voxels are rendered white) at several time points. These processed images show that within 2-3 minutes of exposure to Tf, Tf co-localizes with clathrin regions of the plasma membrane; and with time Tf can be seen in areas outside the clathrin patches that presumably represent early endocytic structures just below the plasma membrane.

The advantage to this processing is that the image data can then be used to give an objective, quantitative description of the intensity and topology of individual fluorophores over the whole adherent surface of the cell and at each time point. For example, the total fluorescent intensity (the product of the total pixels and their mean intensity) of the fluorophores is plotted over the whole cell for each time point; and as expected, the intensity of the clathrin (Fig. 1*c, green trace*) was unchanged during the experiment while the intensity of Tf (Fig. 1*c, red trace*) increased progressively. These

data can also be used to show the degree of co-localization between clathrin and Tf voxels (Fig. 1*d*) for each time point and, by eliminating the subjectivity of the observer, the process of Tf internalization is easier to follow. There is an almost complete co-localization of Tf voxels with clathrin voxels (Fig. 1*d, blue trace*) at the earliest time points after the addition of Tf. As time progressed, the number of clathrin voxels co-localized with Tf (Fig. 1*d, gold trace)* increased to a plateau of 70% of total. Coincidentally, the number of Tf voxels that co-localized with the clathrin progressively decreased, presumably due to the processing of internalized Tf into the endosomes that are present within the 100 nm EF, but are not associated with the clathrin. This information, coupled with the image analysis that shows that much of the membrane bound Tf is associated with the larger patches of clathrin led us to examine the function of the larger, static clathrin arrays. Thus the power of this analysis allowed me to make unique observations of ligand behavior that would have been blurred by standard imaging techniques.

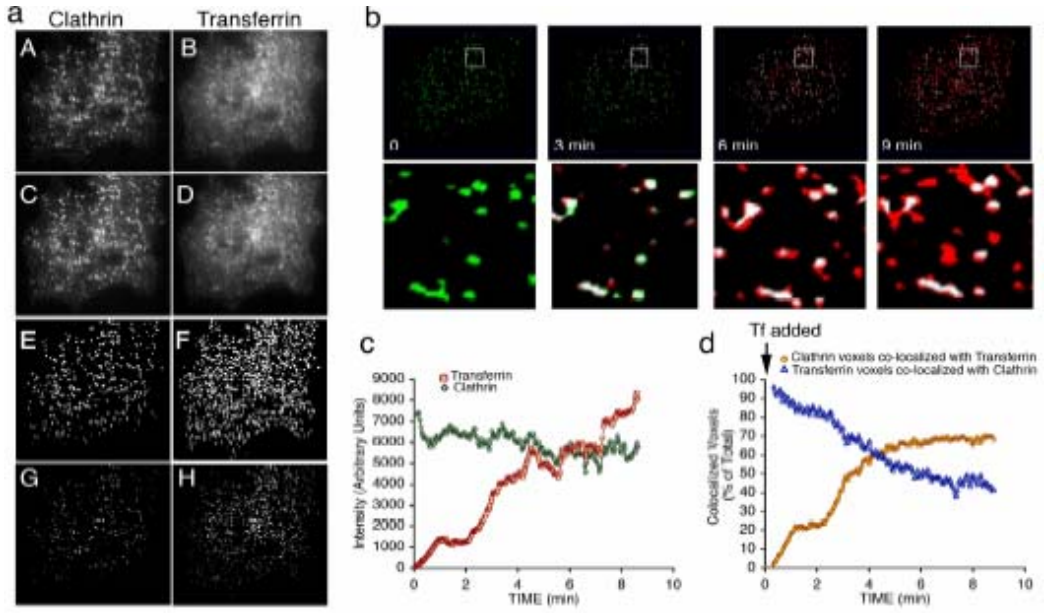

Figure 1. Transferrin binding to clathrin-coated membrane domains. *a)* A and B are TIRF images of COS-7 cells transfected with GFP-clathrin obtained after 10 minutes of incubation with Alexa^{568}-Tf, with only the background signal outside the cell has been removed; C and D are running averages of 3 image sets of a 4 sec interval (average of images corresponding to 9 min 56 sec, 9 min 58 sec, and 10 min); E and F are binary masks of C and D; G and H are the product of the binary masks and the original images. *b)* Overlapped masked images of GFP-clathrin *(green)* and Alexa^{568}-Tf *(red)*, with overlapped voxels depicted in white at time points after Tf addition in the lower left corner of each panel. Lower panels represent the areas within the rectangle indicated in the upper panels. *c)* Quantification of the total voxel intensity within masked images of clathrin (*green trace)* and Tf *(red trace)* over time. *d)* Percent of total clathrin voxels co-localized with Tf voxels *(gold trace)* and of total Tf voxels co-localized with clathrin voxels *(blue trace)* in the masked image sets over time.